



Planetary Science from Directed Aerial Robot Explorers (DARE)

Phase I Final Report

Global Aerospace Corporation

2 December 2002

Universities Space Research Association Research Grant No.: 07600-099

GAC Report 510-09911-003

Global Aerospace
Corporation

711 W. Woodbury Road, Suite H
Altadena, CA 91001-5327 USA
Telephones: +1 (626) 345-1200
(626) 303-9500, Fax (626) 296-0929
Email: global@gaerospace.com
Web: <http://www.gaerospace.com>

Abstract

Global Aerospace Corporation (GAC) is developing a revolutionary system architecture for exploration of planetary atmospheres and surfaces from atmospheric altitudes. This innovative system architecture relies upon the use of Directed Aerial Robot Explorers (DARE), which essentially are long-duration-flight autonomous balloons with trajectory control capabilities that can deploy swarms of miniature probes over multiple target areas. The balloons will serve a dual purpose as independent explorers and as microprobes (MIPs) delivery systems for targeted observations. Trajectory control capabilities will offer unprecedented opportunities in high-resolution targeted observations of both atmospheric and surface phenomena. Multifunctional micro probes will be deployed from the balloons over the target areas, and perform a multitude of functions, such as atmospheric profiling (Jupiter, Saturn), or surface exploration (Mars, Venus, Titan), relaying data back to the balloons or to an orbiter. This architecture will enable low-cost, low-energy, long-term global exploration of planetary atmospheres and surfaces. This proposed effort addresses several objectives of the NASA Enterprise for Human Exploration and Development of Space (HEDS) and of the NASA Space Science Enterprise (SSE), namely: (1) Understand the formation and evolution of the solar system and the Earth within it (SSE); (2) Probe the evolution of life on Earth, and determine if life exists elsewhere in the solar system (SSE); (3) Investigate the composition, evolution, and resources of Mars, the Moon, and small bodies (SSE); (4) Acquire new technical approaches and capabilities; validate new technologies in space (SSE); (5) Help create 21st century scientific and technical workforce (SSE) and (6) Enable human exploration through collaborative robotic missions (HEDS).

Key elements of this new concept are:

- Low-cost, low-energy, long-duration autonomous balloon systems,
- Balloon trajectory control capability,
- Lightweight and efficient power generation and energy storage,
- Deployable micro sensors for *in situ* atmospheric profiling or surface exploration, and
- Communications relay orbiter.

Direct Aerial Robot Explorers will revolutionize exploration of the planets and moons of the solar system by providing targeted ultra-high-resolution surface coverage at a cost significantly less than satellite orbiters in addition to enabling global *in-situ* measurements.

Study Participants

Global Aerospace Corporation (GAC)

Dr. Kim M. Aaron

Keith M. Baker

Dr. Matthew K. Heun

Kerry T. Nock

Susan L. Nock

Dr. Alexey A. Pankine, Principal Investigator and NIAC Fellow

Stephen R. Schlaifer

Christopher J. Wyzkowski

California Institute of Technology (Caltech)

Prof. Andrew P. Ingersoll

Planetary Science Consultant

Dr. Ralph Lorenz

Planetary Balloon Concepts Technical Advisor

Dr. Jack Jones, Jet Propulsion Laboratory

Table of Contents

1	INTRODUCTION.....	9
1.1	PLANETARY SCIENCE FROM DIRECTED AERIAL ROBOT EXPLORERS (DARE).....	9
1.2	WHAT MAKES THIS CONCEPT REVOLUTIONARY?.....	11
1.3	CONCEPT OBJECTIVES.....	12
1.4	POTENTIAL SIGNIFICANCE TO NASA.....	13
1.4.1	<i>Significance to SEE.....</i>	<i>13</i>
1.4.2	<i>Significance to HEDS.....</i>	<i>14</i>
1.5	PAST, PRESENT AND FUTURE OF PLANETARY EXPLORATION.....	14
2	CONCEPT ARCHITECTURE DEVELOPMENT SUMMARY	16
2.1	SUMMARY OF PHASE I TASKS.....	16
2.1.1	<i>Task 1 Develop Application Scenarios.....</i>	<i>16</i>
2.1.2	<i>Task 2 Define Preliminary System Requirements.....</i>	<i>16</i>
2.1.3	<i>Task 3 Conceptual System Architecture Design.....</i>	<i>16</i>
2.1.4	<i>Task 4 Planning and Reporting.....</i>	<i>16</i>
2.2	SUMMARY OF WORK ACCOMPLISHED.....	16
2.2.1	<i>Task 1 Develop Application Scenarios.....</i>	<i>17</i>
2.2.2	<i>Task 2 Define Preliminary System Requirements.....</i>	<i>17</i>
2.2.3	<i>Task 3 Conceptual System Architecture Design.....</i>	<i>17</i>
2.2.4	<i>Task 4 Planning and Reporting.....</i>	<i>17</i>
3	ADVANCED TECHNOLOGIES AND SYSTEMS	18
3.1	INTRODUCTION.....	18
3.2	PLANETARY BALLOONS.....	18
3.2.1	<i>Past and Current Planetary Balloon Concepts.....</i>	<i>18</i>
3.2.1.1	VEGA.....	18
3.2.1.2	VAMS-VEVA.....	19
3.2.1.3	Venus Discovery.....	19
3.2.1.4	VGA.....	20
3.2.1.5	Venus Solar IR Montgolfier.....	20
3.2.1.6	Mars Solar Montgolfier.....	20
3.2.1.7	Mars 96 Aerostat.....	21
3.2.1.8	MABS-MGA.....	21
3.2.1.9	MAP.....	22
3.2.1.10	TAM.....	22
3.2.1.11	Titan RTG Montgolfier.....	22
3.2.1.12	TAS.....	22
3.2.1.13	Titan superpressure.....	22
3.2.1.14	Outer Planets Solar & IR Montgolfier (SIRMA).....	23
3.2.1.15	Summary.....	24
3.2.2	<i>Simplified Balloon Sizing Model.....</i>	<i>26</i>
3.2.2.1	<i>Balloon Design Model Options.....</i>	<i>26</i>
3.2.2.2	<i>Design Model Selection for DARE.....</i>	<i>27</i>
3.3	TRAJECTORY CONTROL SYSTEM (TCS).....	29
3.3.1	<i>StratoSail® TCS.....</i>	<i>29</i>
3.3.2	<i>Advanced TCS.....</i>	<i>31</i>
3.3.3	<i>TCS Modeling.....</i>	<i>32</i>
3.3.3.1	<i>Simple Model.....</i>	<i>32</i>
3.3.3.2	<i>Detailed Model.....</i>	<i>34</i>
3.3.4	<i>TC Capabilities Assessment: Venus.....</i>	<i>34</i>
3.3.4.1	<i>Atmospheric Structure.....</i>	<i>35</i>
3.3.4.2	<i>Atmospheric Winds.....</i>	<i>36</i>
3.3.4.3	<i>Flow Regime.....</i>	<i>39</i>
3.3.4.4	<i>Results.....</i>	<i>39</i>

3.3.5	<i>TC Capabilities Assessment: Titan</i>	44
3.3.5.1	Atmospheric Structure	44
3.3.5.2	Atmospheric Winds	46
3.3.5.3	Flow Regime	47
3.3.5.4	Results	47
3.3.6	<i>TC Capabilities Assessment: Jupiter</i>	49
3.3.6.1	Atmospheric structure	49
3.3.6.2	Atmospheric Winds	50
3.3.6.3	Flow Regime	51
3.3.6.4	Results	51
3.3.7	<i>TC Capabilities Assessment: Mars</i>	53
3.3.7.1	Atmospheric Structure	53
3.3.7.2	Flow Regime	57
3.3.7.3	Results	57
3.3.8	<i>Summary</i>	58
3.4	MICROPROBES	59
3.4.1	<i>Scope</i>	59
3.4.2	<i>Project architecture</i>	59
3.4.3	<i>Sensors</i>	59
3.4.3.1	Expendable sensors for water vapor profiling at Venus	60
3.4.4	<i>Subsystems</i>	62
3.4.5	<i>Vehicle Types</i>	62
3.4.5.1	Microprobes	62
3.4.5.2	Glider	62
3.4.5.3	Sycamore-seed ('seedwing')	63
3.4.5.4	Miniature Helicopters	64
3.4.5.5	Unconventional Vehicles	65
3.4.6	<i>Tracking of Microprobes</i>	66
3.4.6.1	Doppler Tracking	66
3.4.6.2	Ranging	67
3.4.6.3	Angle-Sensitive Links	67
3.4.6.4	VLBI	67
3.4.7	<i>Conclusions</i>	68
4	DARE ARCHITECTURE POTENTIAL APPLICATIONS	69
4.1	INTRODUCTION	69
4.2	VENUS	69
4.2.1	<i>Science Requirements and Priorities</i>	69
4.2.2	<i>Model Atmosphere</i>	70
4.2.3	<i>Potential Applications</i>	73
4.2.3.1	In Situ Atmospheric Sampling	73
4.2.3.2	Surface Seismological and Meteorological Station Network	73
4.2.3.3	Surface and Subsurface Probes	73
4.2.3.4	Potential Landing Site Reconnaissance	73
4.2.3.5	Monitoring Global Circulation	73
4.2.3.6	Monitoring Volcanic Activity	74
4.2.4	<i>Trajectories</i>	74
4.3	TITAN	76
4.3.1	<i>Science Requirements and Priorities</i>	76
4.3.2	<i>Model Atmosphere</i>	78
4.3.3	<i>Application Scenarios</i>	81
4.3.4	<i>Trajectories</i>	81
4.4	JUPITER	83
4.4.1	<i>Science Requirements and Priorities</i>	83
4.4.2	<i>Model Atmosphere</i>	84
4.4.3	<i>Application Scenarios</i>	85
4.4.3.1	Deployment of Dropsondes at three Locations	85
4.4.4	<i>Trajectories</i>	85
4.5	MARS	88

4.5.1	<i>Science Requirements and Priorities</i>	88
4.5.2	<i>Model Atmosphere</i>	88
4.5.3	<i>Application Scenarios</i>	89
4.5.3.1	Monitoring Dust Storm Activity	89
4.5.4	<i>Trajectories</i>	89
4.6	VENUS IS CHOSEN FOR DESIGN ANALYSIS	95
5	KEY CONCEPTUAL DESIGN REQUIREMENTS	97
5.1	PERFORMANCE REQUIREMENTS	97
5.1.1	<i>Flight duration</i>	97
5.1.2	<i>Flight altitude</i>	97
5.1.3	<i>Suspended mass</i>	97
5.1.4	<i>TCS Tether</i>	97
5.1.5	<i>Trajectory control capabilities</i>	97
5.1.6	<i>Materials longevity</i>	97
5.1.7	<i>Balloon envelope stress</i>	97
5.1.8	<i>Communications</i>	98
5.1.9	<i>Data storage</i>	98
5.1.10	<i>Power generation and storage</i>	98
5.1.11	<i>Navigation</i>	98
5.1.12	<i>Dropsonde measurements</i>	98
5.1.13	<i>Dropsonde lifetime</i>	98
5.1.14	<i>Dropsonde power</i>	98
5.2	TECHNOLOGY REQUIREMENTS	98
5.2.1	<i>Balloon material</i>	98
5.2.2	<i>Dropsonde thermal control</i>	98
5.2.3	<i>Deployable instruments</i>	98
5.2.4	<i>High temperature electronics</i>	99
5.2.5	<i>Balloon thermal control</i>	99
5.2.6	<i>Power storage</i>	99
5.2.7	<i>Lightweight inflation systems</i>	99
5.2.8	<i>Venus Balloon TCS</i>	99
6	VENUS DARE CONCEPTUAL ARCHITECTURE DESIGN DESCRIPTION	100
6.1	INTRODUCTION	100
6.2	CONCEPTUAL ARCHITECTURE DESCRIPTION	100
6.2.1	<i>DARE Venus System Parameters and Components</i>	100
6.2.2	<i>Balloon</i>	101
6.2.3	<i>Gondola</i>	103
6.2.4	<i>Trajectory Control System</i>	104
6.2.5	<i>Dropsonde</i>	105
7	FUTURE WORK	110
7.1	INTRODUCTION	110
7.2	DARE ARCHITECTURE PERFORMANCE ADVANTAGES	110
7.3	TRAJECTORY CONTROL AND OBSERVATIONAL TECHNIQUES	110
7.4	DEPLOYABLE MICROSONDES CONCEPTS	110
7.5	BALLOON CONCEPTS	111
7.6	DARE ARCHITECTURE ENGINEERING COST ANALYSIS	111
7.7	PATHWAYS TO DARE ARCHITECTURE DEVELOPMENT	111
8	SUMMARY	113
9	ACRONYMS	114

List of Figures

FIGURE 1-1 CONCEPTUAL DRAWING OF DARE PLATFORM AT VENUS	9
FIGURE 1-2 PLANETARY TARGETS FOR DARE – VENUS (NASA), MARS (NASA), JUPITER (HST), TITAN (HST)	10
FIGURE 1-3 DARE VISION	11
FIGURE 3-1 VEGA BALLOON DURING TESTING AT EARTH.....	19
FIGURE 3-2 ARTIST'S CONCEPT OF A BALLOON ON MARS (NASA).....	21
FIGURE 3-3 SIRMA BALLOON AT JUPITER (J. JONES).....	23
FIGURE 3-4 DARE BALLOON DESIGN MODEL SCREENSHOT	28
FIGURE 3-5 FIRST GENERATION STRATO SAIL® TCS	29
FIGURE 3-6 TCS FORCES VECTOR DIAGRAM – TOP VIEW	30
FIGURE 3-7 ADVANCED TRAJECTORY CONTROL SYSTEM (ATCS)	31
FIGURE 3-8 DRAG COEFFICIENT FOR TWO-DIMENSIONAL BODIES.....	33
FIGURE 3-9 DRAG COEFFICIENT FOR AXIALLY-SYMMETRIC BODIES	33
FIGURE 3-10 TEMPERATURE STRUCTURE OF THE LOWER ATMOSPHERE OF VENUS FROM THE PIONEER VENUS PROBE AND THE VEGA-2 LANDER	35
FIGURE 3-11 VENUS ATMOSPHERIC DENSITY PROFILE.....	36
FIGURE 3-12 OBSERVED VERTICAL PROFILES OF ZONAL WINDS FROM VENERA AND PIONEER PROBES.	37
FIGURE 3-13 VENUS ZONAL AND MERIDIONAL VELOCITIES AT CLOUD TOP	38
FIGURE 3-14 MERIDIONAL VELOCITY PROFILES FOR THE PIONEER VENUS PROBES.....	39
FIGURE 3-15 VENUS TCS PERFORMANCE	40
FIGURE 3-16 VENUS TCS PERFORMANCE	41
FIGURE 3-17 VENUS TCS PERFORMANCE	41
FIGURE 3-18 VENUS TCS PERFORMANCE VS. WING MASS AND AREA.....	42
FIGURE 3-19 VENUS TCS PERFORMANCE VS. TETHER LENGTH AND WING AREA	43
FIGURE 3-20 TITAN ATMOSPHERIC TEMPERATURE	45
FIGURE 3-21 TITAN ATMOSPHERIC PRESSURE	45
FIGURE 3-22 TITAN ATMOSPHERIC DENSITY	46
FIGURE 3-23 ZONAL WIND STRUCTURE ON TITAN (FROM FLASAR ET AL, 1997)	47
FIGURE 3-24 TITAN TCS PERFORMANCE, $Z_B=50$ KM.....	48
FIGURE 3-25 TITAN TCS PERFORMANCE, $Z_B=60$ KM.....	48
FIGURE 3-26 TITAN TCS PERFORMANCE, $Z_B=70$ KM.....	48
FIGURE 3-27 TITAN TCS PERFORMANCE, $Z_B=80$ KM.....	49
FIGURE 3-28 JUPITER ATMOSPHERIC TEMPERATURE	50
FIGURE 3-29 JUPITER UPPER TROPOSPHERE THERMAL WIND SHEAR COMPARED WITH CLOUD TRACER WIND VELOCITIES.	51
FIGURE 3-30 JUPITER TCS PERFORMANCE, $P_B=0.1$ BAR	52
FIGURE 3-31 JUPITER TCS PERFORMANCE, $P_B=0.2$ BAR	52
FIGURE 3-32 MARTIAN TOPOGRAPHY FROM MOLA DATA	53
FIGURE 3-33 MARS TIME- AND ZONALLY-AVERAGED ZONAL WINDS (M/S), $L_s=270^\circ$, WINTER SOLSTICE.....	54
FIGURE 3-34 MARS TIME-MEAN TEMPERATURES AND HORIZONTAL WINDS AT 3 MBAR, $L_s=270^\circ$, WINTER SOLSTICE.....	55
FIGURE 3-35 MARS TIME- AND ZONALLY-AVERAGED ZONAL WINDS (M/S), $L_s=180^\circ$, AUTUMN EQUINOX.....	56
FIGURE 3-36 MARS TIME-MEAN TEMPERATURES AND HORIZONTAL WINDS AT 3 MBAR, $L_s=180^\circ$, AUTUMN EQUINOX.....	56
FIGURE 3-37 MARS TCS PERFORMANCE, NORTHERN WINTER	57
FIGURE 3-38 VENERA SPECTRA OF SCATTERED SOLAR RADIATION	60
FIGURE 3-39 WATER IN THE VENUSIAN ATMOSPHERE	61
FIGURE 3-40 CAPACITIVE POLYMER SENSORS.....	61
FIGURE 3-41 BIOMORPHIC EXPLORERS.....	64
FIGURE 3-42 MINIATURE HELICOPTER PIXEL 2000	65
FIGURE 3-43 ENTOMOPTER VEHICLE (A. COLOZZA, NORTHLAND SCIENTIFIC/OHIO AEROSPACE INSTITUTE)	65
FIGURE 4-1 TIME AVERAGE VELOCITY FIELDS (M/S) IN SOLAR-FIXED REFERENCE FRAME, AT CLOUD TOP (FROM GIERASCH ET AL, 1997).....	70
FIGURE 4-2 MODEL VENUS ZONAL WINDS AT 60 KM (M/S) ON A LATITUDE-LONGITUDE GRID.....	71
FIGURE 4-3 MODEL VENUS MERIDIONAL WINDS AT 60 KM (M/S) ON A LATITUDE-LONGITUDE GRID.....	72
FIGURE 4-4 TRAJECTORIES OF 2 UNCONTROLLED BALLOONS AT 60 KM AT VENUS.....	74

FIGURE 4-5 VENUS DARE BALLOON TRAJECTORY AT 55 KM	75
FIGURE 4-6 VENUS DARE MULTIPLE TARGET OVERFLY	76
FIGURE 4-7 MODEL TITAN ZONAL WINDS	79
FIGURE 4-8 MODEL TITAN WINDS AT 40 KM	80
FIGURE 4-9 TITAN WINDS AT 40 KM FROM TN	80
FIGURE 4-10 VERTICAL PROFILE OF THE LONGITUDINAL AMPLITUDE OF ZONAL AND MERIDIONAL WIND AT 60° N SIMULATED BY THE GCM (FROM TAKANO AND NEUBAUER, 2002).....	81
FIGURE 4-11 UNCONTROLLED BALLOON AT TITAN	82
FIGURE 4-12 TITAN DARE TRAJECTORY AT 60 KM	82
FIGURE 4-13 DARE TRAJECTORIES AT JUPITER	86
FIGURE 4-14 DARE TRAJECTORY SPIRALING INTO GRS.....	87
FIGURE 4-15 DARE SPIRALING INTO GRS PLOTTED ON THE JUPITER DISC.....	87
FIGURE 4-16 COMPARISON OF 5-DAY TRAJECTORIES OF THE FREE-FLOATING AND CONTROLLED BALLOON ON MARS.....	90
FIGURE 4-17 MARS FREE-FLOATING BALLOON IN SOUTHERN HEMISPHERE, Ls=0°	91
FIGURE 4-18 MARS DARE BALLOON IN SOUTHERN HEMISPHERE, Ls=0°	91
FIGURE 4-19 HISTOGRAM OF THE MARS BALLOON LOCATIONS	92
FIGURE 4-20 MARS FREE-FLOATING BALLOON IN NORTHERN HEMISPHERE, Ls=90°	93
FIGURE 4-21 MARS DARE BALLOON IN NORTHERN HEMISPHERE, Ls=90°	93
FIGURE 4-22 MARS DARE CROSS EQUATORIAL TRAJECTORY	94
FIGURE 6-1 CONCEPTUAL DRAWING OF THE DEPLOYED VENUS DARE PLATFORM	102
FIGURE 6-2 CONCEPTUAL DRAWING OF THE VENUS DARE GONDOLA WITH DROPSONDE MAGAZINE	103
FIGURE 6-3 CONCEPTUAL DRAWING OF THE DEPLOYED VENUS DARE TCS.....	104
FIGURE 6-4 POTENTIAL TCS WING ASSEMBLY FOLDINGS	105
FIGURE 6-5 CONCEPTUAL DRAWING OF THE VENUS DROPSONDE.....	106
FIGURE 6-6 VENUS DROPSONDE PARAMETERS	108

List of Tables

TABLE 3-1 PLANETARY BALLOONS REFERENCE DESIGNS	25
TABLE 3-2 VISCOSITY OF VENUS ATMOSPHERE	36
TABLE 3-3 VENUS DARE FLOW REGIME	39
TABLE 3-4 VISCOSITY OF TITAN ATMOSPHERE	46
TABLE 3-5 TITAN DARE FLOW REGIME.....	47
TABLE 3-6 VISCOSITY OF JUPITER ATMOSPHERE.....	50
TABLE 3-7 JUPITER DARE FLOW REGIME	51
TABLE 3-8 MARS DARE FLOW REGIMES	57
TABLE 3-9 ESTIMATED TCS LIMITS	58
TABLE 6-1 PRELIMINARY DARE SYSTEM PARAMETERS	101
TABLE 6-2 ALTITUDE VISIBILITY FACTOR DEPENDENCE.....	107

1 Introduction

In this section we summarize the Planetary Science from the DARE concept, its objectives, and what makes it revolutionary; describe the potential significance of the concept to NASA and to the World, and discuss past, present and future of planetary exploration.

1.1 Planetary Science from Directed Aerial Robot Explorers (DARE)

Due to their relatively low cost and low power consumption balloons represent a very attractive platform for planetary exploration. Indeed, the successful Venera-Vega Project demonstrated technical feasibility of deploying a balloon on another planet and a wealth of opportunities presented by a balloon platform for atmospheric and surface studies. Concepts and technologies enabling planetary balloon exploration of Mars, Venus, Titan and the Outer Planets have been developed. The DARE architecture advances these concepts to the next level of utility and universality by integrating the balloon platform with the innovative lightweight Trajectory Control System (TCS) and Micro Probes (MIPs) into a revolutionary architecture for planetary exploration (see Figure 1-1, background image D. P. Anderson, Southern Methodist University). This architecture would greatly expand the planetary exploration capabilities allowing high-resolution targeted observations, and augmenting observations at atmospheric altitudes with *in situ* surface observations.

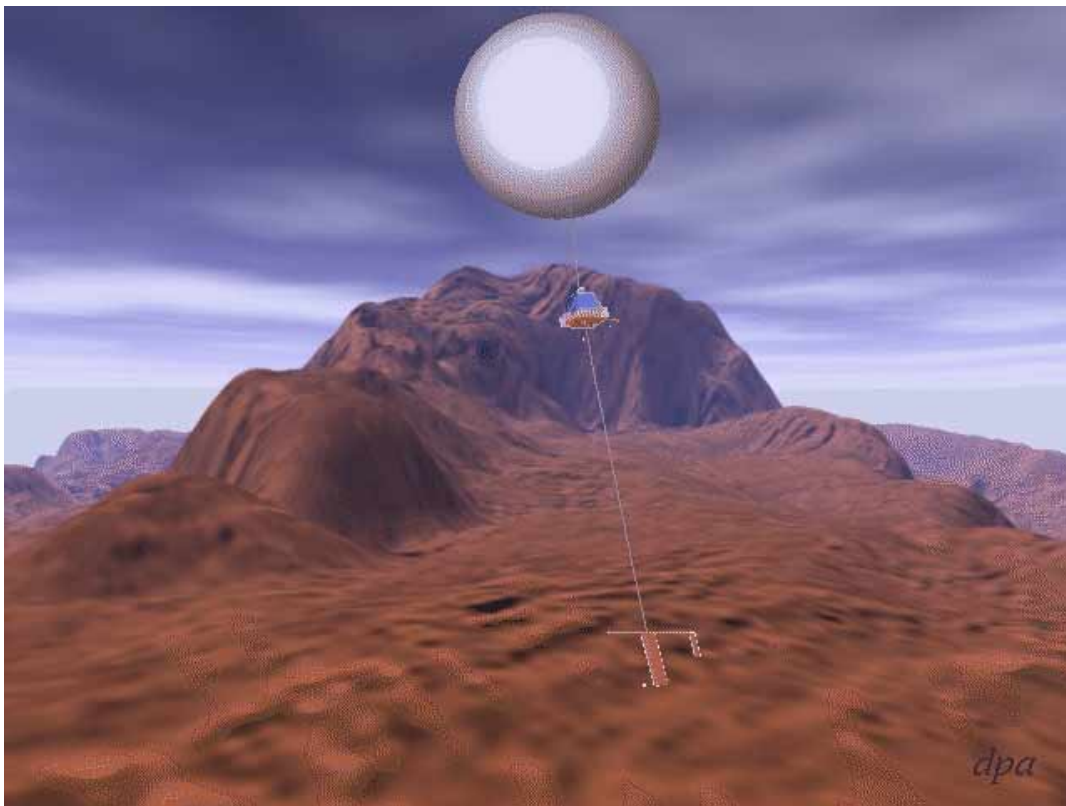


Figure 1-1 Conceptual drawing of DARE platform at Venus

The Directed Aerial Robot Explorer (DARE) would represent a highly adaptive observational platform capable of observing planetary atmospheres and surfaces over long periods of time without consuming much power. DARE would orbit the planet using winds to adapt their trajectory according to observational objectives. Studies of the atmospheric dynamics, atmospheric chemical, and radiative processes on other planets would become possible at an advanced level. MIPs would be deployed over the target areas and perform a multitude of tasks at the surface or while descending, such as chemical, biological, meteorological, or thermal analyses, high-resolution imaging, measuring seismic activity, etc. The data would be relayed in real time to the overflying DARE, processed or temporarily stored onboard, and then relayed to the orbiter. Some MIPs would be capable of descending to the surface, “grabbing” a sample of the surface material and then ascending back to the altitude of the DARE platform to rendezvous with the platform and transfer the sample for geochemical analysis onboard the platform.



Figure 1-2 Planetary targets for DARE – Venus (NASA), Mars (NASA), Jupiter (HST), Titan (HST)

On Mars, DARE would visit Polar Regions to closely observe sublimation of polar caps during the spring and the genesis of local dust storms, and then migrate towards tropical regions to observe formation of the dust devils and evolution of topographic winds during summer, or to monitor the changing concentration of atmospheric water vapor. DARE would release ice penetrators to study ice sheet crosssections while over the polar cap, miniature weather and geophysical stations and rovers while overflying highlands and lowlands, and subsurface penetrators over the areas where subsurface ice could be present. Small imaging probes would be deployed over potential landing sites to provide close up images of the surfaces. The platform can carry multiple magnetometers to study enigmatic magnetic crustal anomalies.

On Venus, DARE would drop small probes capable of imaging the surface below the dense cloud cover during descent and deploy miniature networks of seismological and meteorological surface stations. The platform could be repositioned to provide wind speed measurements in the different regions of the atmosphere, on the day and night sides of the planet and to deploy small meteorological probes to study the lowest part of the atmosphere.

On Titan, flying below the dense atmospheric haze, DARE could be maneuvered to look for methane lakes and seas, deploy biochemical analyzers, rovers and floaters.

On the Outer Planets, a DARE platform would study atmospheric circulation and composition above and below cloud decks inside the zones and bands of zonal winds. The TCS would allow targeted observations of localized regions of interest, such as “hot spots” (like the one

encountered by the Galileo probe), thunderstorm formation regions (on Jupiter), and large vortices (like the Great Red Spot on Jupiter or Great Dark Spot on Neptune).

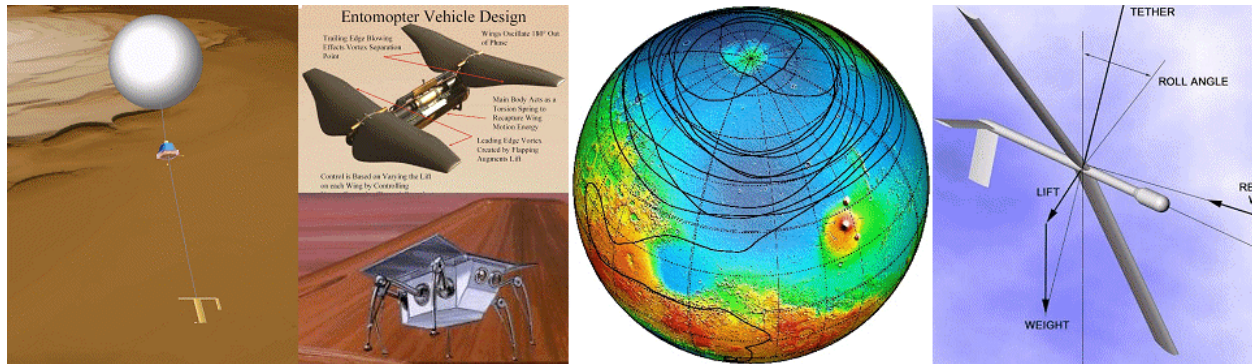


Figure 1-3 DARE vision

Figure 1-3 illustrates the DARE architecture vision. It shows (from left to right) the conceptual drawing of the DARE platform at Mars with the oblique view of the North polar cap (background image from NASA/Goddard Space Flight Center Scientific Visualization Studio); examples of the deployable vehicles, that can be released by a DARE platform – an “entomopter” (A. Colozza, Northland Scientific/Ohio Aerospace Institute) and a “hexobot”; an example of equator-crossing DARE trajectories at Mars (background image is NASA MOLA topography); and the Advances TCS.

The key elements of the overall DARE architecture are listed below:

- Long-duration planetary balloon
- Balloon trajectory control
- Lightweight and efficient power generation and energy storage
- Micro Probes
- Communication relay orbiter

The innovative design architecture proposed by Global Aerospace Corporation departs from the existing approaches to planetary exploration in several fundamental ways, and these are described below.

1.2 What Makes This Concept Revolutionary?

A combination of several factors makes this concept revolutionary:

First, flight path guidance of the planetary balloons enormously expands the capabilities of the balloon platforms and takes them to a higher level of utility. A balloon platform can now be used as an active observational tool rather than a passive winds tracer. Together with low power consumption and long flight duration the path control capability opens up possibilities for continuous long term monitoring of the planetary environments, targeted observations and near global coverage not possible with any other platform.

Second, the use of multiple deployable low-cost targeted micro in situ packages allows to reach a level of sampling of the atmospheres and surfaces that previously could not be achieved. Deployment of packages from atmospheric altitudes and slow moving platforms would allow to drastically reduce the mass of the packages, so that many microprobes can be carried by a single platform, and improve targeting. New measuring techniques would become possible involving networks of sensors. Multiple locations could be sampled with a single DARE platform providing a comprehensive picture of the composition and processes in the atmosphere and on the surface.

These significant divergences from traditional approaches promise to reduce cost and increase scientific return for planetary exploration, advance our understanding of the Solar System and bring human planetary exploration closer to reality.

1.3 Concept Objectives

The objectives of this concept are to:

1. Enable low-cost, high-performance and targeted in situ and remote sensing of planetary atmospheres and surfaces,
2. Exploit electronics and sensor miniaturization technology to enable new measurements,
3. Instigate new observational techniques by planetary scientists, and
4. Facilitate NASA meeting objectives of SSE and HEDS by offering a new observational vantage point from which to explore other planets.

The primary objective of this concept is to enable low-cost, high-performance and targeted in situ and remote sensing of planetary atmospheres and surfaces through the utilization of the new planetary exploration architecture incorporating balloon platforms with trajectory control capabilities, miniature deployable probes and orbiters. Such architecture would enable unique measurements and observations not feasible with any other means, would greatly expand our knowledge about the Solar System and provide reconnaissance means for future human planetary exploration.

Advances in technology now allow for unprecedented miniaturization of sensors and electronics. This miniaturization enables radically new measurements, such as multiple soundings of the atmospheres with small densely packed sondes equipped with multiple sensors, or positioning of the multiple light probes along the balloon-carried tether for atmospheric profiling. The reduction of mass would allow for carrying more instruments onboard the observational platform for the same payload mass, which would enable more comprehensive observations. The microprobe concepts developed as part of this study can be implemented outside the DARE concept.

The proposed DARE architecture offers a new approach to performing in situ and remote sensing observations in planetary environments. The unique features of the DARE architecture (long mission duration combined with low observing altitudes, targeted observations and possibilities for combined surface/atmosphere measurements) were never exploited together before. Collaborative efforts of the planetary science community are needed to develop new

observational techniques and methodologies that would allow maximizing the return from the DARE architecture implementation.

The development of the DARE architecture concept facilitates NASA meeting objectives of SSE and HEDS (as outlined in Section 1.4) by providing a new observational vantage point from which to explore other planets and a new reconnaissance robotic platform to assist human exploration, and by providing ways to establish partnership between space science and educational communities.

1.4 Potential Significance to NASA

A number of objectives outlined by NASA Strategic Plan for the Space Science Enterprise and Enterprise for the Human Exploration and Development of Space are addressed by the proposed concept, namely:

1.4.1 Significance to SEE

Five goals of the NASA Space Science Enterprise (SSE) are supported by this concept, namely:

- Understand the formation and evolution of the solar system and the Earth within it,
- Probe the evolution of life on Earth, and determine if life exists elsewhere in the solar system,
- Investigate the composition, evolution, and resources of Mars, the Moon, and small bodies,
- Acquire new technical approaches and capabilities, validate new technologies in space, and
- Help create a 21st century scientific and technical workforce.

The proposed concept supports the first SSE goal by providing a unique scientific observational platform to study, through various *in situ* and remote sensing means, the changes that the surfaces and atmospheres of the planetary bodies have experienced over eons.

The second SSE goal is supported by providing up-close observations of geological features on the surfaces of other planets and looking for evidences of water or other life-sustaining conditions now or in the past. *In situ* analysis of the chemical make up of the atmospheres and surfaces by *in situ* sensors will also provide means to determine if life exists or has existed on the other planets.

The third SSE goal is supported by enabling a systematic guided search for resources from atmospheric altitudes and targeted deployment of micro analyzers that would determine the composition of surface and subsurface layers, and thus provide clues to planetary evolution.

The fourth goal is supported by the development of new technologies and capabilities, such as lightweight power generation and storage systems, new communication approaches, the TCS, and the microprobes.

The fifth goal is supported by potential future involvement of university students in the development of the microprobes. A microprobe is a small enough project that a university group

involving students could build one. This would be a way to involve many students in the project even if the one that students built won't be flown (there could be a competition between the groups and only the best design flown). The fact that students can build something of the same size and similar function is very appealing.

In addition, the recently published Solar System Exploration Survey ("New Frontier in the Solar System", National Research Council, 2002) makes a detailed exploration and study of the composition of Venus' atmosphere and surface, including sample return, the highest priority for inner planets. In fact, the Survey outlines a combined lander/balloon Venus mission – VISE (Venus In Situ Explorer) as the highest ranked mission for Inner Planet exploration for the next decade. The DARE architecture for Venus atmosphere and surface exploration fits very well into Venus exploration strategy. The DARE Venus concept supports Venus exploration by developing new options for Venus balloon mobility, atmospheric and surface measurements, and by developing concepts for Venus microprobes.

1.4.2 Significance to HEDS

At least one goal of the NASA Human Exploration and Development of Space Enterprise (HEDS) is supported by this concept, namely:

- Enable human exploration through collaborative robotic missions.

The HEDS goal is supported by providing robotic reconnaissance agents (DARE with MIPs) that would search for resources that can be used by humans in the course of planetary exploration and colonization, and for safe landing sites for landers.

1.5 Past, Present and Future of Planetary Exploration

Current approach to planetary exploration relies on the Earth-based remote observations, spacecraft flybys, the use of orbiters, entry probes, surface landers, and rovers. Only in one instance planetary balloons were used to study the atmosphere of other planet (VEGA, 1984).

The current approach allows for global coverage of a planetary system with orbiters, sampling in situ and at a closer range with the probes, surface landers and rovers. However, orbiters are too removed from the surface and atmosphere and cannot sample them directly, or with the ultra-high resolution needed to resolve scientific questions or to locate safe landing sites for landers and ultimately – humans. Orbital configuration of spacecraft often limit observations of specific regions on the surface or in the atmosphere to particular times of the day, thus limiting our knowledge of the dynamics of the observed phenomena. The probes and landers are able to sample atmospheres and surfaces in situ, but are limited in coverage to a few sites. Deployment of multiple probes from space is impractical, because a large proportion of the probe mass would be wasted on entry thermal shielding and surface impact survivability systems, and not used for scientific experiments. Only large regions of a planet can be targeted with any certainty. The surface rovers have a certain degree of mobility on the surface and can perform in situ sampling, but their range is limited to several kilometers at best – like on the Moon, - but more often the range is limited to just several meters - as in the case of the Mars Sojourner.

Planetary exploration has now reached the stage when global in situ coverage, high-resolution surface imaging and targeted observations are required to advance our knowledge about the Solar System. These observations cannot be made by orbiters or landers alone. In situ sampling missions and sample return missions for Mars and Venus are now viewed as the highest priority by the experts in the field (“New Frontier in the Solar System”, National Research Council, 2002). The new goals and objectives require a new approach to planetary exploration.

There are a number of advantages to basing the new approach on a balloon-based observational platform. The balloons can be made of lightweight materials and, while potentially being relatively inexpensive themselves, also bring down the launch costs. They can examine large areas with higher resolution than would be available from an orbiter. In addition, some observations, such as *in situ* atmospheric chemistry can only be done from a balloon. Some critical observations, such as magnetic field measurements or subsurface water search on Mars, can be better done from an atmospheric platform. Due to the dense cloud coverage, the Venus surface is only observable from space with radio and some infrared wavelengths, making a balloon-based platform a more practical option. Deployment of landers or entry vehicles from orbiters present numerous challenges, including targeting, thermal shielding during entry, survivability of impact, etc., while the low speed of the balloon system reduces the severity of these problems. In some instances, for example, on the Outer Planets, the balloons could provide the necessary communication link between deep atmospheric probes and orbiters.

The DARE concept developed in this NIAC Phase I effort advances the new approach to planetary exploration. It combines long-duration guided balloons, deployable microprobes and orbiting spacecraft into the new planetary exploration architecture that has capabilities to perform breakthrough in situ and remote observations of the planetary atmospheres and surfaces. The features of the DARE architecture are discussed in the following sections.

2 Concept Architecture Development Summary

2.1 Summary of Phase I Tasks

The primary technical objective of the Phase I of the Planetary Science from Directed Aerial Robot Explorers (DARE) concept development was:

- Demonstrate the validity of the proposed system architecture for long-term exploration of planetary atmospheres and surfaces, which focuses on long-duration balloons low-energy trajectory control technology, and the use of small deployable probes.

Phase I of the DARE Concept Development included the following tasks as originally planned and described.

2.1.1 Task 1 Develop Application Scenarios

A preliminary study of potential scientific and reconnaissance applications utilizing adaptive characteristics of the proposed architecture for every planet will be developed. A detailed numerical study of the most promising mission for one planet will be produced.

2.1.2 Task 2 Define Preliminary System Requirements

The preliminary DARE system architecture design requirements will be defined by analyzing the applications objectives and determining the derived system requirements for the most promising planet and balloon concept.

2.1.3 Task 3 Conceptual System Architecture Design

The conceptual system architecture design will be developed establishing interrelationships between key components, systems and subsystems, their functionality, and mass and power constraints for one chosen planet and application.

2.1.4 Task 4 Planning and Reporting

A detail Phase I plan will be generated. Two interim status reports and a final report shall be written. We shall participate in the NIAC Fellows Conference in Houston TX in June of 2002 and participate and present a report at the NIAC Fellows Conference in October 2002 in Atlanta, GA.

2.2 Summary of Work Accomplished

This section provides a short summary of the work accomplished during the Phase I effort. A more detailed description follows in later sections.

2.2.1 Task 1 Develop Application Scenarios

Potential applications for the DARE architecture at Venus, Titan, Mars and Jupiter were studied. Detailed numerical study of the most promising mission - Venus Global Circulation Study - was developed. The development of the potential applications proceeded in the following way: the existing planetary balloon concepts and designs were identified and used as a reference designs in the identification of the Trajectory Control System (TCS) limits and in the definition of the DARE balloon vehicle. A simple model was developed to calculate the increased size of the balloon in the reference design corresponding to the increased suspended mass due to the addition of the TCS and microprobes. A numerical model to calculate the available trajectory control for each planet was developed. Planetary atmospheres data were compiled for the use with the TC limits modeling. The science and engineering objectives for each planet were then identified. Application scenarios that would address the science objectives were conceived and analyzed to determine the most promising application – Venus General Circulation Study (VGCS). DARE VGCS application was chosen as a context for the preliminary conceptual design development in Task 3.

2.2.2 Task 2 Define Preliminary System Requirements

Preliminary performance requirements for the DARE planetary exploration architecture and its systems components were identified. These requirements are discussed in Section 5.

2.2.3 Task 3 Conceptual System Architecture Design

A first order conceptual planetary exploration architecture design for the DARE VGCS application was developed, focusing on the Balloon, Gondola, Dropsonde and the TCS systems.

2.2.4 Task 4 Planning and Reporting

A detailed Phase I plan was generated. Two status reports and a final report were written. We attended and gave a poster presentation at the Annual NIAC Meeting June 11-12, LPI, Houston, TX, and participated and presented a report at the NIAC Fellows Conference in October 23-24, 2002 at NIAC HQ in Atlanta, GA.

We also issued a press release describing the DARE planetary exploration architecture work, which generated significant public interest and resulted in a publication of several articles on the World Wide Web that can be found at:

http://www.space.com/business/technology/technology/venus_dare_021113.html

http://beyond2000.com/news/Nov_02/story_1401.html

<http://einstein.stcloudstate.edu:81/Dome/2002/11/13>

<http://www.spacedaily.com/news/balloon-02b.html>

3 Advanced Technologies and Systems

3.1 Introduction

A number of advanced technologies, systems and methods relevant to the development of the DARE planetary exploration architecture have been studied during Phase I. These included planetary balloon concepts, TCS performance, models of planetary atmospheres and the microprobe options. The application scenarios for the DARE architecture were studied and conclusions regarding the use of the proposed TCS on each planet were made. Venus DARE architecture was chosen for the preliminary design analysis. Preliminary requirements on the DARE performance and technologies were established and preliminary design for the Venus DARE developed. These subjects are all discussed in detail in the following sections.

3.2 Planetary Balloons

Long duration flight planetary balloons are at the center of the DARE planetary exploration architecture. Below we review past and current planetary balloon concepts and the balloon sizing model that allows us to extend previous concepts to accommodate the larger weight of the TCS and microprobes.

3.2.1 Past and Current Planetary Balloon Concepts

We identified existing planetary balloon concepts and designs to serve as reference designs in the identification of the TCS limits and in the development of the DARE Balloon Vehicle.

3.2.1.1 VEGA

The only planetary balloon mission to date was the successful deployment of the two Venus superpressure balloons in 1984 during the French-Russian-US VEGA Project (Sagdeev, R.Z., et al., "Overview of the VEGA Venus balloon in situ meteorological measurements", *Science* **231**, 1411-1422, 1986).

Figure 3-1 shows the VEGA balloon during testing in the Earth's atmosphere. The two balloons were inserted at the night side of the planet near the terminator. The balloon floated at about 55 km for almost two days (46.5 hours) returning meteorological data. The lifetime of the balloons was limited by the battery life. The balloon envelope was made from Teflon fabric resistant to the sulfuric acid. The balloons probably survived longer than the 2 days, after which communication contact was lost due to the battery's limited life time - the balloons lost less than 5% of the buoyant gas (He) during the mission. The VEGA mission successfully demonstrated several key technologies - the planetary balloon operation, communications, deployment and inflation. Additional technical information is summarized in Table 3-1.



Figure 3-1 VEGA balloon during testing at Earth

3.2.1.2 VAMS-VEVA

NASA JPL developed a Venus Aerobot Multisonde (VAMS) concept that envisioned a superpressure balloon floating in the upper atmosphere (above 50 km) above the Venus clouds (Cutts, J.A., et al., Venus Aerobot Multisonde Mission, AIAA Balloon Tech. Conference, 1-10, 1999). The balloon would carry four probes that would be dropped over surface targets. The data from the sondes would be relayed directly to Earth. The Aerobot itself would perform various observations, including observations of the magnetic field and *in situ* atmospheric measurements. The VAMS concept was relatively low-cost and did not require development of fundamentally new technology. The concept was used in the development of the Venus Exploration of Volcanoes and Atmospheres (VIVA) Discovery mission proposal. Additional technical information is summarized in Table 3-1.

3.2.1.3 Venus Discovery

The Venus superpressure balloon concept was developed by JPL in 1997 under the Discovery Program for launch in 2002. The concept envisioned three helium balloon probes delivered by a single spacecraft. The balloons would be deployed at 55 km altitude at three different latitudes for a 30 to 100 day mission. Each balloon would carry a 34 kg gondola and 4 dropsondes weighing 2.5 kg each. The concept envisioned direct communication with Earth via X-band antenna. Additional technical information is summarized in Table 3-1.

3.2.1.4 VGA

NASA JPL Venus Geoscience Aerobot (VGA) concept envisioned a relatively large phase-change fluid altitude control system with helium and water as the working substances (K. Nock et al, "Venus Geoscience Aerobot Study", JPL Presentation, July 28, 1997; A. Bachelder, et al., "Venus Geoscience Aerobot Study", AIAA paper 99-3856, AIAA International Balloon Technology Conference, June 28-July 1, 1999, Norfolk, VA). Water, by itself, condenses at 42 km altitude on Venus (130°C, 2.7 bar); however, with helium added, peak altitudes can reach 64 km (-20°C, 0.15 bar). The balloon would be able to descend and sample the surface, and then ascend again to higher altitudes to cool down. VGA concept faces a number of technological challenges, such as developing a balloon envelope that can withstand the high pressures and temperatures on the surface of Venus (up to 480° C), as well as passage through sulfuric acid clouds. Prototype balloon envelopes have been fabricated from polybenzoxazole (PBO), a polymer that exhibits high strength, resistance to heat, and low leakage for light gases. A gold coating is applied to allow the polymer film to resist corrosion from acid clouds. A prototype VGA gondola weighing about 30 kilograms has also been developed and tested. The gondola is based on a concentric sphere design. The instruments are contained inside the pressure vessel with an outer shell of titanium, an inner shell of stainless steel, and xenon-filled fiberglass insulation between the two shells. The gondola contains a solid-state camera and other instruments, as well as communications and flight control systems. The advanced design of the gondola would maintain internal temperatures below 30° C even on the surface of Venus and withstand pressures of up to a hundred atmospheres. Additional technical information is summarized in Table 3-1.

3.2.1.5 Venus Solar IR Montgolfier

A concept for a Solar IR Montgolfier balloon at Venus was developed in 1997 (J. A. Jones and M. K. Heun, "Montgolfier Balloon Aerobots for Planetary Atmospheres," AIAA, Paper No. 97-1445, 1997). A 22 m balloon would be fabricated from PBO and weight 20 kg and use ambient gas heated by the sun and the heat from the hot Venus atmosphere for floatation. During the night the balloon would float in the upper clouds using the IR heat from the planet. During the day it could be possible to briefly descend to the surface by venting some of the gas. Additional technical information is summarized in Table 3-1.

3.2.1.6 Mars Solar Montgolfier

NASA JPL has considered Mongolfier balloons for use on Mars (http://www.jpl.nasa.gov/adv_tech/balloons/mars.htm, also J. Jones and J. Wu, "Solar Montgolfier Balloons for Mars", AIAA paper 99-3852, 1999). The novel venting mechanism for altitude control developed by JPL would allow multiple descents to the surface where the balloon would deploy science instruments. The required balloon mass for a 1 kg gondola at Mars is just 4 kg and the balloon can tolerate gas loss, because the gas is replenished from the ambient atmosphere and reheated by the sun. Additional technical information is summarized in Table 3-1.

3.2.1.7 Mars 96 Aerostat

The Russian/French Mars Aerostat concept (C. Tarrieu, Status of the Mars 96 Aerostat Development, Paper IAF-93-Q.3.399, 44th Congress of the International Astronautical Federation, 1993) was developed after the success of the Venera/VEGA projects. Early versions of this concept employed a "dual balloon" system, with a light-gas balloon (helium or hydrogen filled) attached with a tether to a solar Montgolfier. The light-gas balloon would keep the Montgolfier off the ground at night, while during the day the balloon assembly would rise due to the solar heating of the Montgolfier balloon. Later the "dual balloon" solution was abandoned and the concept featured a cylindrical, sealed helium balloon made of Mylar with a volume of 5,500 cubic meters. The balloon would rise when heated during the day and sink as it cooled at night. The balloon would carry an imaging system and drop a guide rope to drag along the Mars' surface, acquiring chemical samples and taking physical measurements. Total mass of the balloon assembly was 65 kilograms, with a 15-kilogram gondola and a 13.5 kilogram instrumented guiderope. The balloon was expected to operate for ten days. Additional technical information is summarized in Table 3-1.

3.2.1.8 MABS-MGA

NASA JPL Mars Aerobot/Balloon System (MABS) or Mars Geoscience Aerobot (MGA) was envisioned as a large superpressure balloon (Nock, K.T. *et al.*, Overview of a Mars 2001 Aerobot/Balloon System. 12th AIAA Lighter-Than-Air Technology Conference, San Francisco, 1997). The payload mass of the MGA would be 15-30 kg, and the balloon would remain operational for up to three months. During that time MGA would circle Mars more than 25 times and cover over 500,000 km of ground. MGA would carry sophisticated equipment, including an ultrahigh resolution stereo imager, instruments for weather and atmospheric observations, radar for subsurface water detection, and an infrared spectroscopy system to study surface mineral composition. Additional technical information is summarized in Table 3-1.

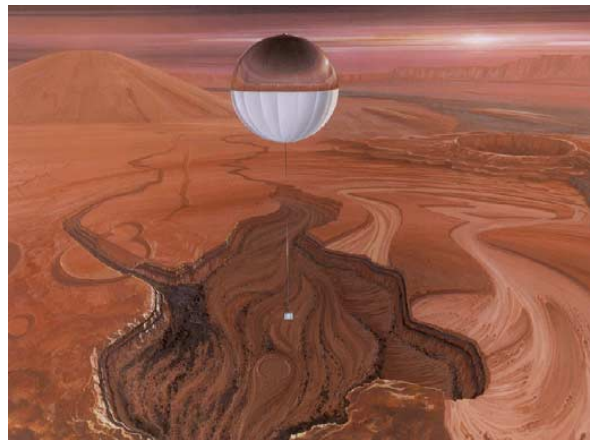


Figure 3-2 Artist's concept of a balloon on Mars (NASA)

3.2.1.9 MAP

In 1994 a Mars Aerial Platform (MAP) mission was proposed under the NASA Discovery Program (Greeley, R., et al., “The Mars Aerial Platform Mission Concept”, AIAA paper 96-0335, 34th Aerospace Science Meeting, Reno, NV, January 1996). The design included a superpressure hydrogen balloon and a small (7 kg) gondola. The balloon was designed to float at a constant density level 6 km above mean Martian elevation. Three balloons were proposed to be deployed simultaneously in different regions of the planet, together with small surface meteorological stations. The mission duration was 100 Martian days (sols). The payload consisted of the imaging system, thermal emission spectrometer and neutron spectrometer. Additional technical information is summarized in Table 3-1.

3.2.1.10 TAM

NASA JPL Titan Aerobot Multisite (TAM) concept employs an argon-filled PCF balloon that would be able to explore multiple surface sites by performing multiple descents and ascents from high altitude to the surface of Titan and back (<http://robotics.jpl.nasa.gov/tasks/aerobot/studies/tadps.html>). (See also Jones J. A., “Balloon altitude and temperature control”, JPL Notice of New Technology, NPO#19223, JPL, Pasadena, CA, May 13, 1993). Additional technical information is summarized in Table 3-1.

3.2.1.11 Titan RTG Montgolfier

A Montgolfier balloon heated by Radioisotope Thermoelectric Generator (RTG) can (theoretically) be flown on Titan (M. Hinada, “Titan Buoyant Station”, JPL). The system mass for a 100 kg payload would vary from 142 kg for a 5 km floating altitude to 236 kg for 50 km floating altitude. Additional technical information is summarized in Table 3-1.

3.2.1.12 TAS

NASA JPL Titan Aerobot Singlesite (TAS) concept strategy is the opposite from that of TAM (<http://robotics.jpl.nasa.gov/tasks/aerobot/studies/tadps.html>). The concept employs a superpressure balloon that would descend to a single site, release much of its gas, and then explore the chosen site in great detail.

3.2.1.13 Titan superpressure

Analysis of a superpressure balloon performance at Titan has been performed by JPL (M. Hinada, “Titan Buoyant Station”, JPL). In this analysis the floating altitude of the balloon vs. mass of buoyant station was performed and options for gas storage were investigated. Additional technical information is summarized in Table 3-1.

3.2.1.14 Outer Planets Solar & IR Montgolfier (SIRMA)

Solar Infrared Montgolfier Aerobots (SIRMAs) are Montgolfier balloons that use planetary infrared heating during the night and solar heating during the day to remain afloat (J. A. Jones and M. K. Heun, "Montgolfier Balloon Aerobots for Planetary Atmospheres," AIAA, Paper No. 97-1445, 1997). Current studies of SIRMA use on Jupiter indicate that by using isentropic compression heating it is possible to slow the nightly descent rates, so that the balloon floats at about 0.1 bar during the day and descends to about 0.2 bar at night. Total floating mass of 112 kg would be required to suspend a ten-kg payload. The total mass of the balloon assembly in this case would be an order of magnitude lighter than that of the comparable light-gas (pure hydrogen) balloon system at Jupiter. At Saturn a similar SIRMA system would have a mass of about 220 kg, although this weight could be reduced in half if the SIRMA is flown during summer at a Saturn pole. Figure 3-3 illustrates operation of the SIRMA balloon at Jupiter.

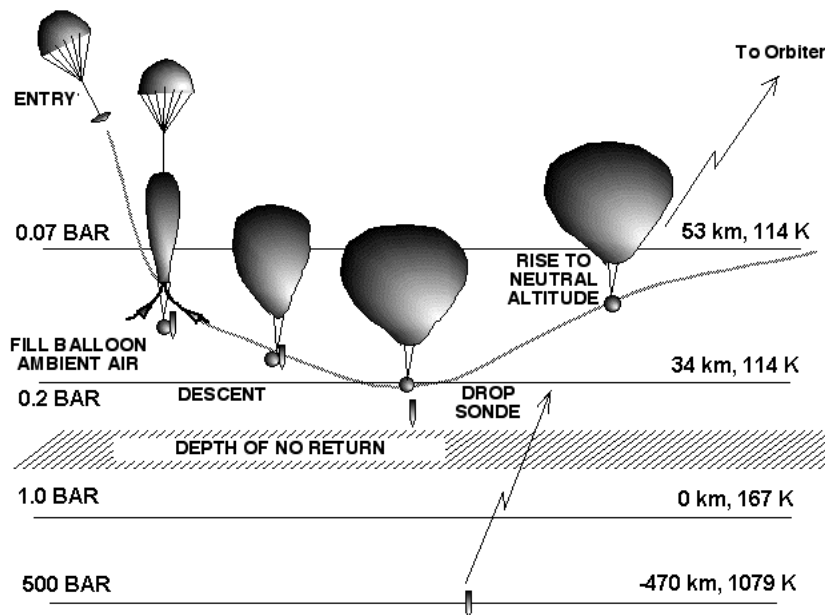


Figure 3-3 SIRMA balloon at Jupiter (J. Jones)

Uranus and Neptune are too far from the Sun, so there is not enough solar heat for a viable Montgolfier balloon. However, a unique concept has been proposed for these planets that envisions filling a balloon with light, methane-free, stratospheric gas to provide buoyancy in and below the cold methane clouds (J. A. Jones, "Inflatable Robotics for Planetary Applications", 6th International Symposium on Artificial Intelligence, Robotics, and Automation in Space" 2001). Detailed analysis shows that a relatively small balloon (15 kg) filled with upper atmospheric gas can support a 50-kg payload in the troposphere. Additional technical information is summarized in Table 3-1.

3.2.1.15 Summary

Table 3-1 lists key features of various planetary balloon designs. The designs are grouped into columns according to the planet and the type of balloon (solar Montgolfier, superpressure, etc.). Names of the designs are also given, where available (Mars 96, MABS, etc.). The rows of the table give design parameters, such as flight altitude, flight duration, floating mass, etc. The parameters vary between the balloon types and illustrate the advantages and disadvantages of different balloon types. All of these parameters can potentially affect our decision in choosing the most appropriate design for more detailed study. For example, flight altitude parameter determines the strength of atmospheric winds and vertical wind shear. These in turn determine the amount of spatial coverage that can be achieved (the higher the winds – the further the DARE will travel and the greater would be the coverage) and affects the available control force created by the TCS (the higher the wind shear – the more control force is there available to maneuver the DARE platform).

Only two planetary balloon missions have actually flown to date, the Venus balloons in the French-Russian-US VEGA Project. For other design concepts the parameter values are estimates based on detail design analysis – as for MAP and MABS, and others. Some designs are just emerging so that only preliminary estimates are available – such as Jupiter and Outer planets SIRMA.

Table 3-1 Planetary Balloons Reference Designs

	Mars				Venus					Titan			Jupiter, Saturn, Uranus, Neptune
	Solar Montgolfier	Light-gas (0 pressure)	Superpressure		Phase-change (PCF)	Solar IR Montgolfier	Superpressure			Phase-change (PCF)	RTG Montgolfier	Superpressure	Solar & IR Montgolfier
		Mars 96	MABS-MGA	MAP	VGA		VAMS (VEVA)	Venus Discovery	Venera-VEGA	TAM			
Flight altitude, km	0-3	0.05-3	6.5-12	6-7.7	0-60	60-70	60	55	53-55	0-8	5	50	0.1-0.2 bar (all)
Working Gas	ambient	He	He	H ₂	He-H ₂ O	ambient	H ₂	He	He	Ar-He	ambient	H ₂	ambient
Flight duration, d		10	90	100	> 100		7 (limited by battery life)	30-100	2 (limited by battery life)	> 100			
Entry probe Mass (kg)			212	80.9	224		94	110.8	115	67		296	
Floating Mass (kg)		65	80.2	24.3	108	45	63	68.6	21	20	142	127	112 (J), 220 (S), 280 (U), 840 (N)
balloon mass, kg (diameter, m)	16 (20)	24.5 (cylindrical, 18 equiv. sphere)	55 (27)	15.3 (18)	29 (3.5)	20 (22)	20 (~ 6.4)	29.7 (~5.6)	10.5 (3.4)	1.5	15.7 (8.7)	12 (8.2)	(60 J), (86 S), (97 U), (172 N)
gas mass, kg		6	12	1.9	28(water)+5(He)=33		~3.2	6.7	2	6 (Ar)+3 (He)=9		10	
suspended mass, kg	10	28.5 (15 gondola+13.5 guidrope)	13.2	7.1	31	25	41	32	6.7	9.5 (6.5 gondola + 3 "snake")	100	100	10 (all)
science mass, kg			5	3.5	4.6			10	1.3			20	
engineering mass, kg			8.2	3.6	26.4			22	6.4			80	

3.2.2 Simplified Balloon Sizing Model

The objective of the DARE balloon design model is to estimate the size of the buoyant system required for balloon flight at various planets. Inputs to a design model could be very sparse or very detailed, depending on the level of modeling fidelity desired. There are several options for levels of detail for balloon design models. The following subsections describe a characterization of these options.

3.2.2.1 Balloon Design Model Options

3.2.2.1.1 First-Order Model

In a first-order model, balloon size is calculated assuming

- a fixed areal density for the balloon material and
- that the balloon gas is at the same temperature as the atmosphere
- that heat transfer has a negligible effect on balloon gas temperature (and therefore volume).

Inputs to a first-order model include

- Temperature profile
- Pressure profile
- Atmospheric molecular weight
- Buoyant gas molecular weight

3.2.2.1.2 Basic Radiative Model

A basic radiative model is more sophisticated than the first-order model, and it includes radiative heat transfer effects to obtain an estimate of balloon film and buoyant gas temperatures. This temperature correction has a second-order effect on balloon size. The effect that these volume changes have on material strength requirements for superpressure balloon systems is neglected in this model. With a radiative model, balloon size is estimated assuming

- fixed areal density for the balloon material and
- negligible convective heat transfer (good for a stratospheric environment)

Inputs to the basic radiative model include all the inputs to the First-Order model and

- Solar flux
- Floor temperature (upwelling IR flux) at the flight altitude
- Canopy temperature (downwelling IR flux) at the flight altitude

- Effective albedo (reflected solar flux) at the flight altitude
- Balloon material solar absorptivity (α) and IR emissivity (ϵ)

3.2.2.1.3 Basic Convective Model

A basic convective model also includes convective heat transfer effects on the temperature of the balloon and the buoyant gas. With a basic convective model, balloon size is estimated assuming

- fixed areal density for the balloon material

Inputs to the basic convective model include all the inputs to the basic radiative model and

- Atmospheric viscosity
- Atmospheric specific heat
- Atmospheric thermal conductivity

3.2.2.1.4 Sophisticated Model

None of the above models address the relationship between material areal density and strength of the balloon material for a superpressure balloon. A sophisticated model will include this effect when sizing the balloon. For example, if higher-strength material is needed, the areal density (and therefore the mass) of the balloon material will increase. This change requires a larger balloon to provide additional buoyancy to carry the additional mass of the balloon film.

A sophisticated model requires all the inputs of the Basic Convective Model or the Basic Radiative Model and

- Material strength as a function of areal density for all material options

3.2.2.2 Design Model Selection for DARE

For DARE, we decided to utilize a First-Order Model to estimate balloon envelope sizes. This decision is appropriate for the initial evaluation of balloon design concepts at various planets during Phase I. For material areal density and strength information, we rely on previous concept studies and planetary balloon flights.

3.2.2.2.1 First-Order Model for DARE

We developed an Excel-based first-order model for DARE. Figure 3-4 shows a screen shot of the model.

Input Parameters

Atmosphere		
MW_atm	44	kg/kmol
T_atm	206	K
P_atm	305	Pa
Balloon		
rho_areal	0.023	kg/m ²
MW_gas	4	kg/kmol
Supertemperature	40	K
Superpressure	240	Pa
Payload		
m_pay	15	kg

Constants

R_bar	8314.4	kJ/kmol-K
-------	--------	-----------

Iterated Parameter

Vol	9677.5	m ³
-----	--------	----------------

Calculated Parameters

T_gas	246	K
P_gas	545	Pa
rho_gas	0.00107	kg/m ³
rho_atm	0.00784	kg/m ³
m_gas	10.315	kg
m_envelope	50.512	kg
m_tot	75.826	kg
m_dry	65.512	kg
Diameter	26.4	m
S	2196	m ²
Weight/gravity	75.826	kg
Buoyancy/gravity	75.826	kg
Diff	-5.4E-06	kg

Assumptions

- * Spherical balloon for S/Vol ratio
- * All non-envelope dry mass included in m_pay

Figure 3-4 DARE Balloon Design Model screenshot

The input parameters to our first-order model included super temperature (buoyant gas temperature in excess of the ambient temperature) and superpressure (buoyant gas pressure in excess of the ambient pressure).

Calculated parameters include the diameter and surface area of the balloon (assumed to be a sphere).

The DARE model operates by adjusting the volume of the balloon until the weight and buoyancy forces are equal.

This model was benchmarked against the balloon designs from MABS and shown to give correct results.

3.3 Trajectory Control System (TCS)

The TCS of the DARE platforms consists of a wing hanging on its side below the balloon on a very long (several km) tether. Due to the difference in winds between the altitudes of the balloon and the wing, the wing experiences relative winds, that create a sideways lifting force, that can be used “to drag” the balloon across the winds. Because the density of the atmosphere is higher at the wing altitude, the wing can be much smaller than the balloon. Figure 3-5 and Figure 3-7 show the first generation StratoSail® TCS and the advanced TCS currently being developed by GAC, respectively. The advanced system increases the amount of control force (compared to the StratoSail® TCS) that can be exerted on a balloon.

3.3.1 StratoSail® TCS

The StratoSail® trajectory control system (Figure 3-5) provides a horizontal force component that can be used to alter the flight path of a free-floating balloon. This system was developed for operation in the earth’s stratosphere, hence the name, but the method is applicable at any celestial body with a significant atmosphere with wind differences at different altitudes.

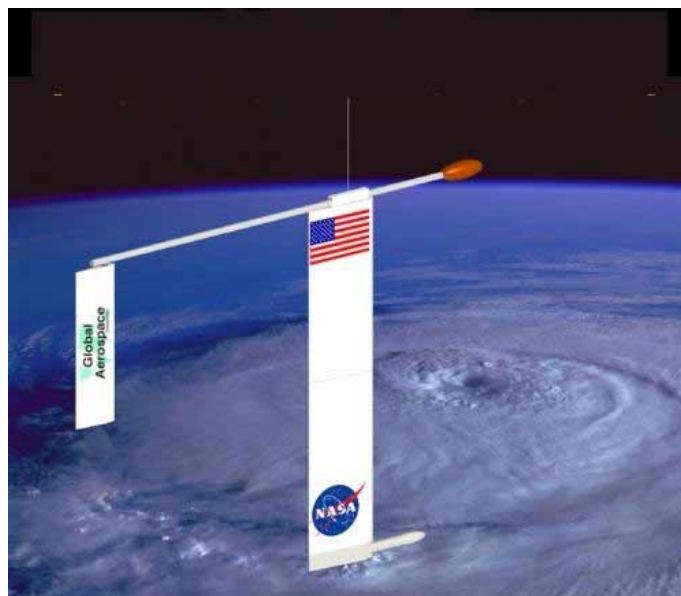


Figure 3-5 First generation StratoSail® TCS

Due to the large size of the balloon, the system is forced to move at very close to the wind speed at the altitude of the balloon. The TCS Wing Assembly (TWA) is suspended on a long tether

well below the balloon. Because the TWA is attached to the balloon via the tether, the wing is forced to move at the same velocity as the balloon. Therefore, it is dragged through the air and experiences a relative airflow. The wing is oriented with an angle-of-attack with respect to this relative wind by use of a rudder. The wing produces a net lift force, which is directed mostly horizontally. This force is transmitted up the tether to the balloon, and causes the balloon to have a small drift velocity with respect to the wind at the balloon's altitude. This small bias velocity is the useful effect produced by the system. By controlling the direction and magnitude of the lift force (by adjusting the wing angle-of-attack) the balloon's flight path can be altered over a small range. This small change in trajectory can integrate to substantial changes in the end point. This is precisely the effect that is exploited by the system to enable useful exploration of celestial bodies.

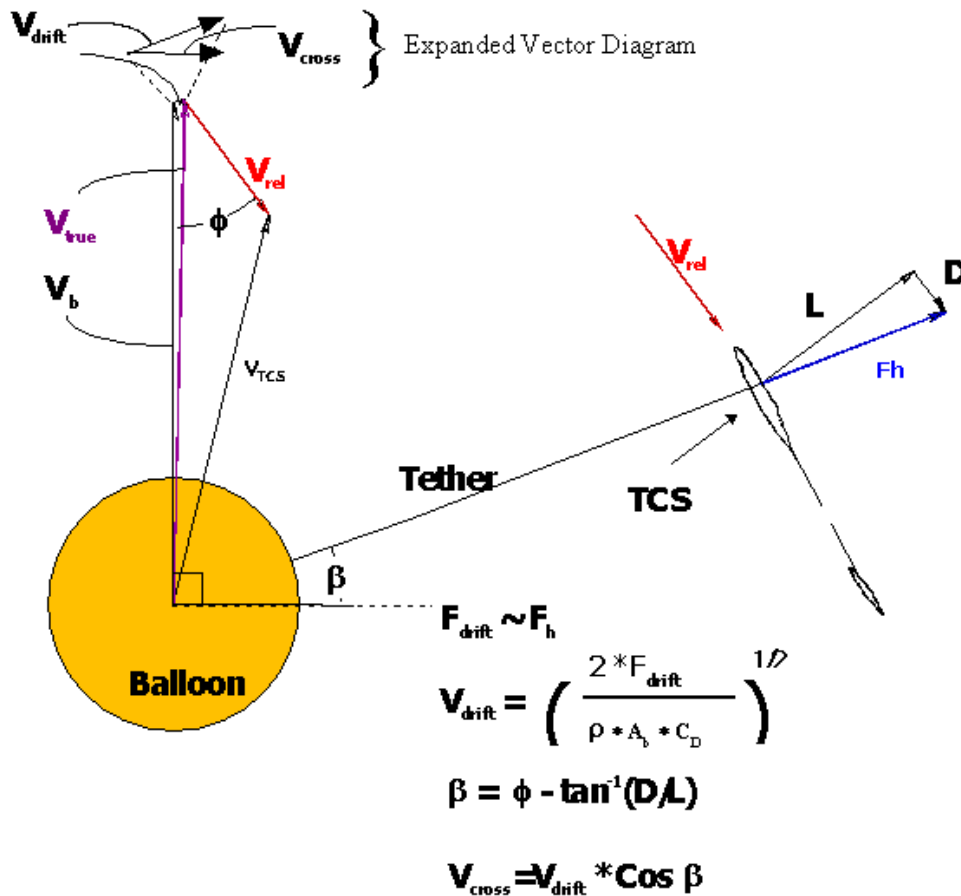


Figure 3-6 TCS forces vector diagram – top view

Figure 3-6 shows the balance of forces involved in the operation of the trajectory control system. Although the winds at the balloon and at the wing are usually in the same direction, a small difference in angle is shown in the diagram as well as a difference in magnitude. V_b is the wind velocity at the balloon, and V_{TCS} is the wind at the TWA. V_{true} shows the true velocity of the system (both the balloon and the TWA). This velocity is very close to the wind vector at the balloon. The vector difference between V_{true} and V_b is the small drift of the system and is shown expanded towards the top of the figure. This drift velocity is parallel to the horizontal component of the tension force in the tether where it attaches to the balloon. The vector difference between

the true velocity of the system and the wind at the TWA is labeled V_{rel} . This is the relative wind at the TWA and can be used to generate a lift force, L . This force is proportional to the dynamic pressure due to the relative airflow, $\frac{1}{2}\rho V_{rel}^2$, to the wing area, and to the lift coefficient of the TWA. This lift coefficient is essentially proportional to rudder angle up to point at which the wing stalls, and can not produce more lift. Because the wing is hanging close to vertically, the lift force is mostly horizontal, as desired. The drag force, being perpendicular to the lift, mostly acts to slow down the balloon, whereas the lift force contributes most strongly to the lateral component of the drift velocity. This sideways (cross-track) component of the drift velocity is labeled V_{cross} in the expanded vector diagram at the top of the figure. There are some simplifying assumptions in this figure, but it illustrates the general operating principle of the trajectory control system.

3.3.2 Advanced TCS

The first generation TWA was developed assuming that the weight would greatly exceed the lift force ($L/W > \sim 5$). After some design and development effort, we found that we could design the wing to be lighter and we also learned that the wind differences could be stronger than we first expected. At times, it is possible for the maximum lift to exceed the weight of the TWA. With the first generation TWA, this means that the wing will swing far up to one side. This reduces its effectiveness for several reasons. First, the wing is in lower density air, so the maximum force is reduced. Second, the wind speed difference is reduced because the wing is operating at a higher altitude closer to the balloon's altitude. Third, the lift force is directed more upwards and less to the side. It would be possible to overcome these problems in a brute force manner by simply adding weight to the TWA. For a lighter-than-air system, this is a very unattractive solution. Furthermore, the balloon size would have to be larger to support the additional mass. Instead, we chose to use aerodynamic forces to hold the TWA down in the atmosphere.

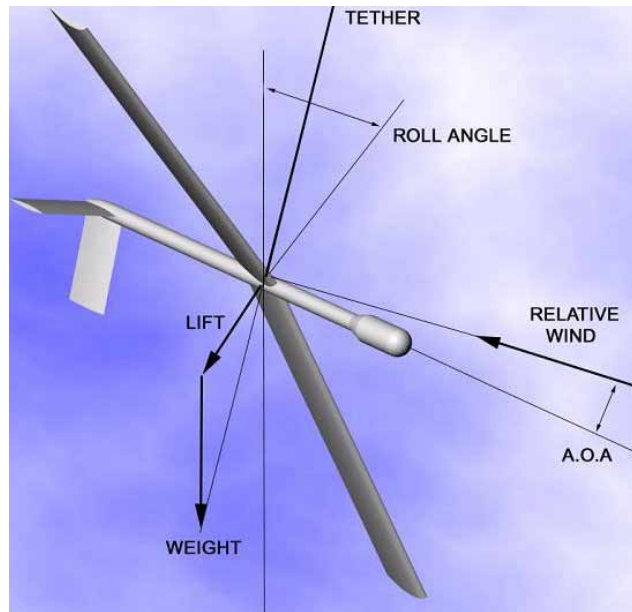


Figure 3-7 Advanced Trajectory Control System (ATCS)

Figure 3-7 shows the advanced TCS, or ATCS, which resembles a glider hanging upside-down. By rolling the TWA using ailerons on the wing tips, the lift force can be made to have a downward component in addition to the desired horizontal component. This downward component prevents the TWA from swinging too far to the side and climbing into air with significantly lower density. There is an optimum roll angle that produces the maximum sideways component of lift force (which then gives the greatest sideways component of drift velocity at the balloon). The peak in the performance is very broad, so it is not very critical to control the roll angle very precisely.

3.3.3 TCS Modeling

A detailed numerical model of the first generation StratoSail® TCS aerodynamic behavior in the planetary atmospheres was developed. The ATCS model will be developed in Phase II of the study.

3.3.3.1 Simple Model

Before developing a detailed numerical model of the TCS aerodynamic performance, it is beneficial to consider a simpler model that would describe the behavior of the system qualitatively. A first order estimate of the available TC can be made with such a simple model. The model is based on a simple assumption that the lift force, created by the TCS, is balanced by the drag forces on the system that arise when the balloon is “dragged” across the wind by the TCS. The drag forces are due to the balloon, wing and tether drag. Previous experience with the Earth StratoSail® indicates that the tether drag can be approximated by the drag of the lowest 10% of the tether length. The wing drag is negligible compared to the balloon and tether drag, because the wing is thin and its cross-sectional area is small (compared to the tether’s and balloon’s cross-sectional areas). A simple formula then gives the cross-track velocity u that is due to the TCS action – the velocity with which balloon is dragged across the wind:

$$u \approx V_{rel} \left[\frac{C_L \rho_w A_w}{C_{Db} \rho_b A_b + C_{Dt} \rho_t A_t} \right]^{1/2},$$

where

V_{rel} is the relative velocity between the balloon and the wing;

ρ_w , ρ_b and ρ_t are the densities of the air at the wing, balloon and tether altitudes, respectively; ρ_t is equal to ρ_w , since only the lowest part of the tether efficiently contributes to drag;

A_w , A_b and A_t are the wing area, the balloon cross-sectional area, and the effective cross-sectional area of the tether (10% of the total cross-sectional area), respectively;

C_L , C_{Db} and C_{Dt} are the wing lift coefficient and the balloon and tether drag coefficients, respectively. In this simplified analysis it can be assumed that $C_L = 1$, thus providing maximum lift. The drag coefficients are determined from the experimental data relating drag to the flow regime (Reynolds number). For the balloon and tether the drag coefficients for a sphere and a

cylinder are used, respectively. The graphs showing the C_D dependence on Reynolds number for cylindrical and spherical bodies are shown on Figure 3-8 and Figure 3-9 (reproduced from B. S. Massey, "Mechanics of Fluids", 3rd Ed., Van Nostrand Reinhold Company, 1976).

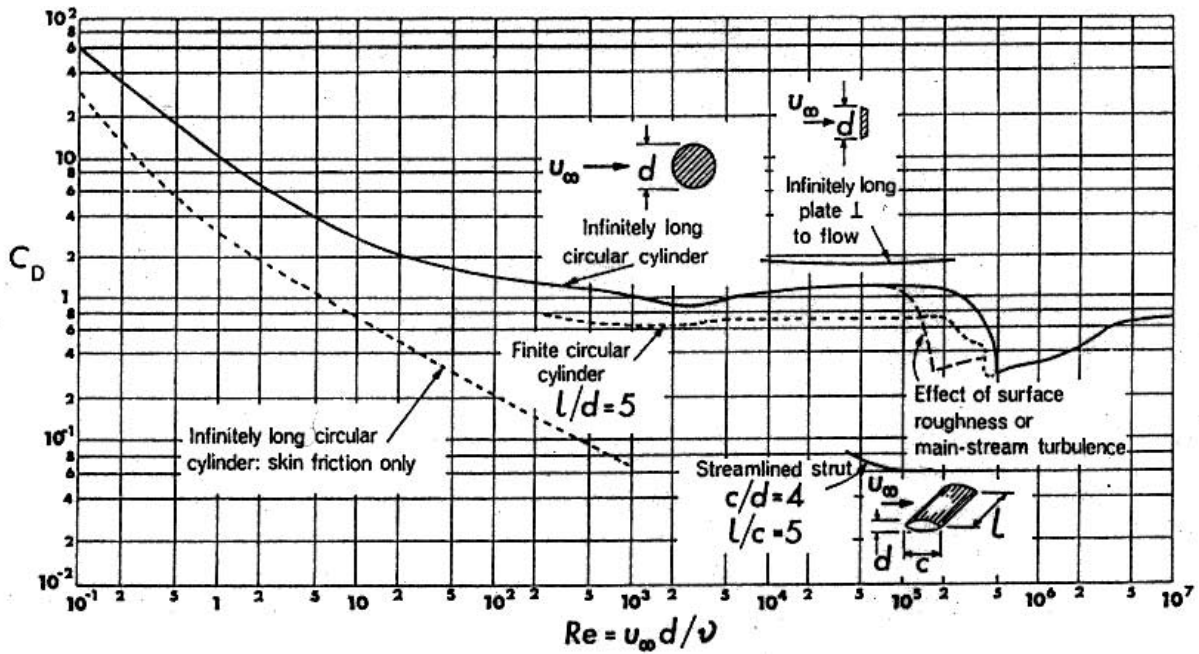


Figure 3-8 Drag coefficient for two-dimensional bodies

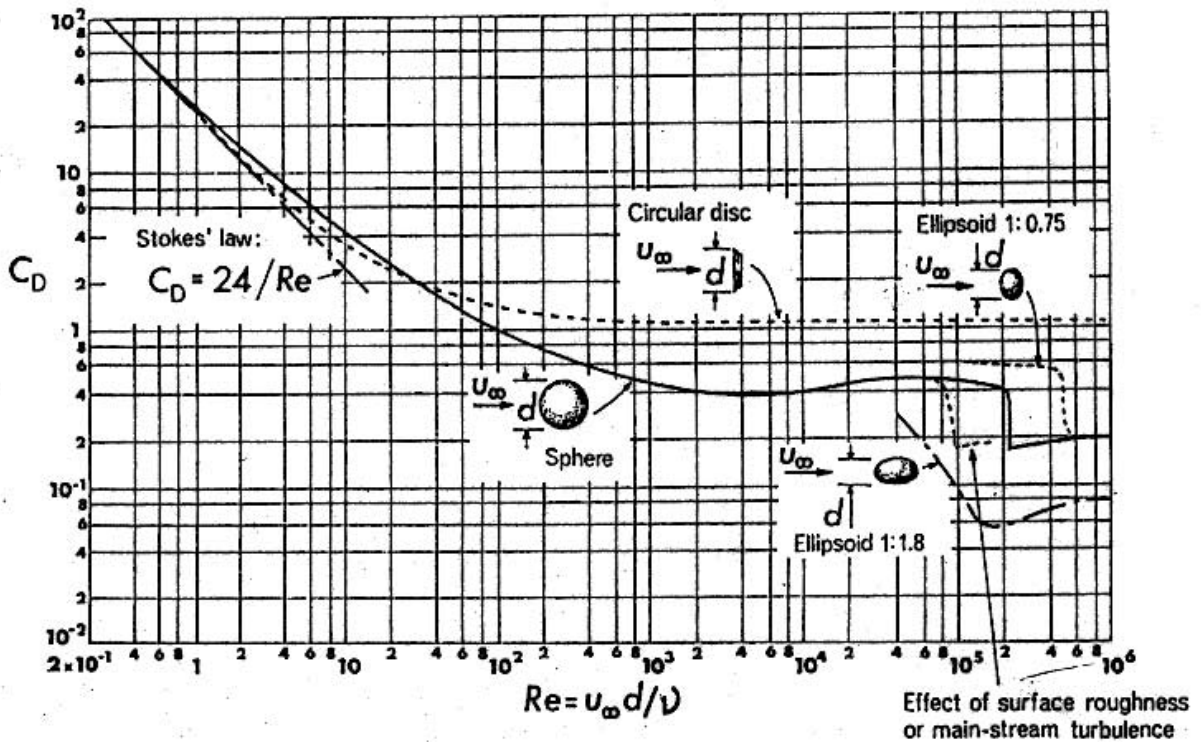


Figure 3-9 Drag coefficient for axially-symmetric bodies

The simplified formula provides for a better understanding of the factors that affect the TCS performance. For example, it follows from the formula that u is linearly dependant on V_{rel} , thus increasing the tether length (and V_{rel}) is an efficient way to increase u . At the same time, the formula predicts that increasing the wing area A_w is a less efficient way to increase u , since u is proportional to the square root of A_w .

This simplified view ignores many factors that affect the behavior of the TCS, however, it is acceptable as a first step in a detailed analysis. The detailed model is discussed in the next section.

3.3.3.2 Detailed Model

The detailed numerical model accounts for the change of the wing orientation in 3 dimensions due to the lift and drag forces. The model equations cannot be solved analytically. The model equations are iterated numerically until the solution is found. The model takes into account changes of the atmospheric density and the zonal winds with altitude. The model input parameters are:

- Balloon altitude
- Tether length and diameter
- Wing area and aspect ratio
- Wing weight
- Planetary gravity
- Balloon and tether drag coefficients
- Wing lift coefficient
- The angle between the winds at the balloon and wing altitudes
- Atmospheric density profile
- Zonal winds vertical profile

The outputs of the model are the cross-track and along-track velocities due to the TCS action, as well as the angles that define the TCS position in space.

3.3.4 TC Capabilities Assessment: Venus

Data on planetary environments include temperature, pressure, density, viscosity and zonal and meridional winds profiles. These data are needed to estimate the TCS limits, to assess feasibility of mission scenarios and to characterize operational environments. The sections below describe the atmospheric winds, the general structure of the atmosphere, the estimated flow regime and TCS performance modeling results.

3.3.4.1 Atmospheric Structure

The atmosphere of Venus has been studied by probes and by remote sensing instruments. The surface of the Venus is hidden below a cover of thick sulfuric acid clouds. The cloud deck extends from 45 to 70 km with extended regions of haze above and below. The CO₂ atmosphere is very hot and dense, with the surface temperature reaching 740 K and surface pressure of 96 bars. The vertical temperature profile of the Venus atmosphere measured by Pioneer and Vega probes is shown on Figure 3-10 (reproduced from D. Crisp and D. Titov, "Thermal balance of the Venus atmosphere", in *Venus II*, The University of Arizona Press, 1997).

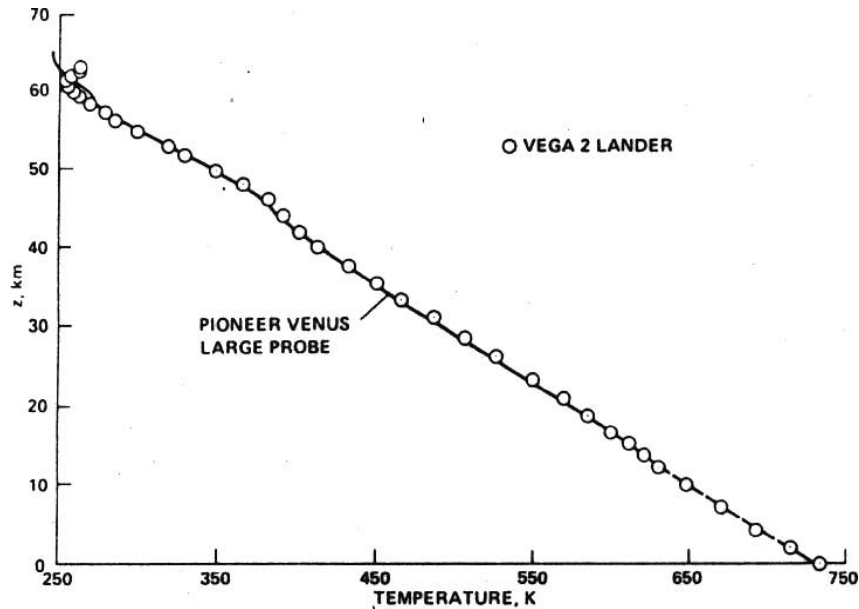


Figure 3-10 Temperature structure of the lower atmosphere of Venus from the Pioneer Venus probe and the Vega-2 lander

As can be seen from the figure, the temperature profile of the Venus atmosphere is remarkably unvaried below 60 km.

Figure 3-11 show the density profile in Venus atmosphere for latitudes below 40° from the model based on the available observation data (A. Seiff, "Models of Venus atmospheric structure", in *Venus*, The University of Arizona Press, 1983). The difference with the density profile for higher latitudes is less than 1%.

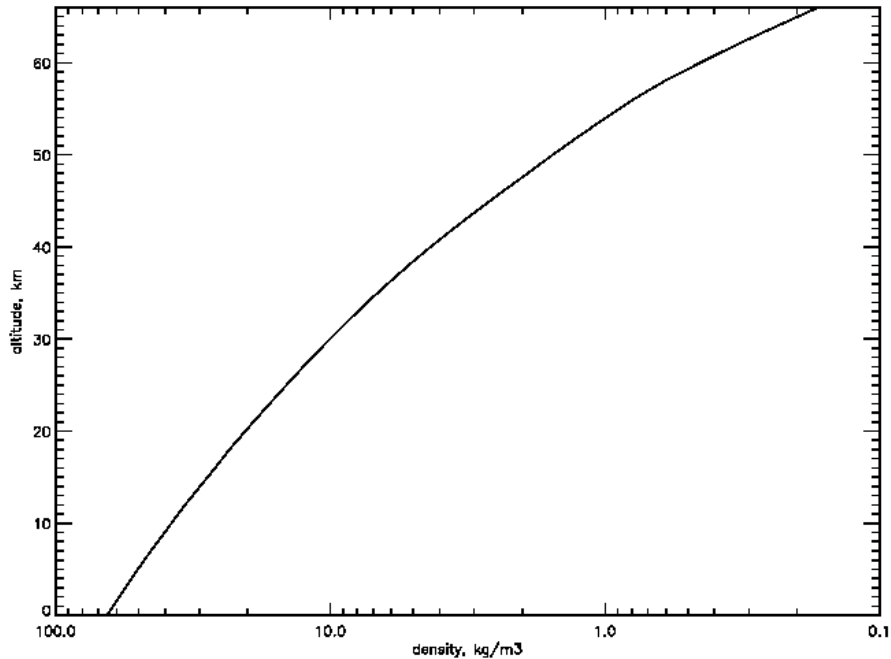


Figure 3-11 Venus atmospheric density profile

Another parameter that is needed to define the flow regimes (i.e. Reynolds numbers) and drag coefficients for the balloon and the tether - are atmospheric viscosity. Assuming purely CO₂ atmosphere, the viscosity of Venus atmosphere changes with temperature as described in Table 3-2 (from CRC Handbook of Chemistry and Physics, 71st edition, 6-140).

Table 3-2 Viscosity of Venus atmosphere

T, (K)	200	300	400	500	600
v, (μPa s)	10.0	15.0	19.7	24.0	28.0

3.3.4.2 Atmospheric Winds

The data on atmospheric winds are limited to observations of cloud movements and to a few descent profiles.

The data on Figure 3-12 show observed vertical profiles of zonal winds from Venera and Pioneer probes. The horizontal axis is wind speed in m/s and the vertical axis is altitude above the surface.

As can be seen from the figure the zonal wind velocities increase with height with a similar rate for observed locations. The wind speed increase may be stronger above 50 km, as indicated by a single Venera 8 profile. At the altitude of 60 km the winds reach speeds of 80 m/s. These observations are confirmed by the observations of the winds at cloud tops (Figure 3-13).

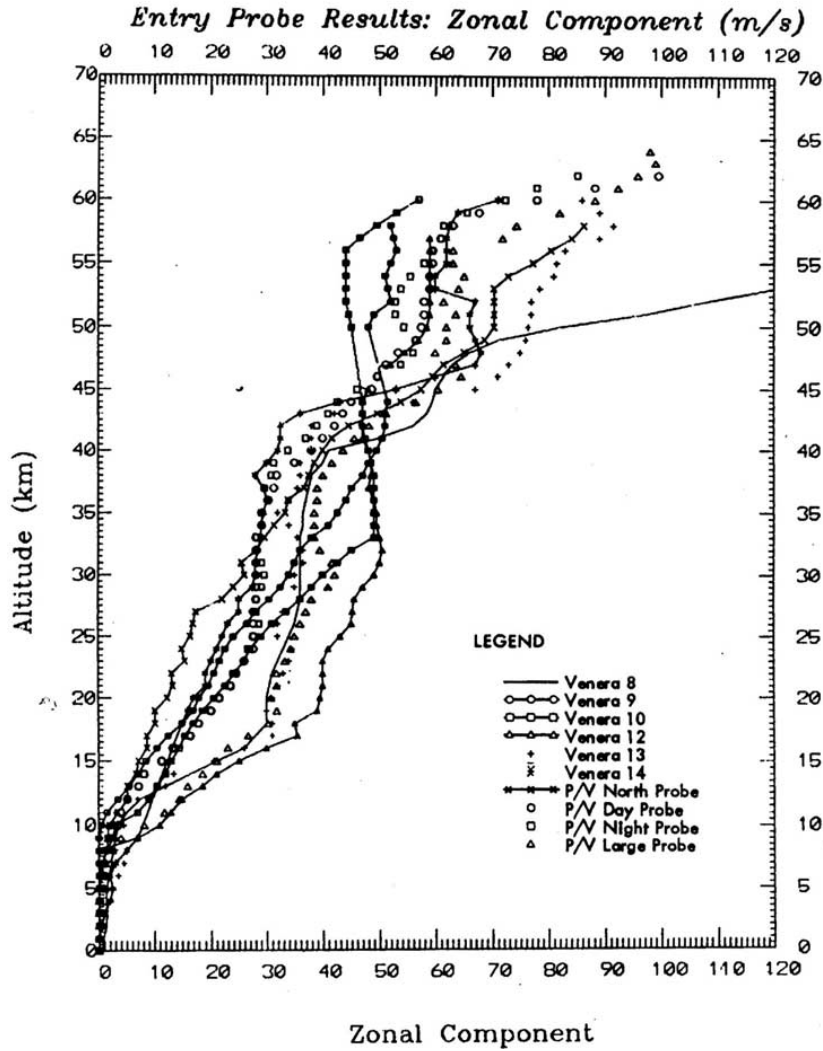


Figure 3-12 Observed vertical profiles of zonal winds from Venera and Pioneer probes.

The strong atmospheric rotation (“superrotation”) of the slowly rotating Venus is one of the unexplained enigmas of the Venus. It is currently believed that momentum transfer in the lower 10-15 km of the atmosphere is responsible for maintaining the superrotation.

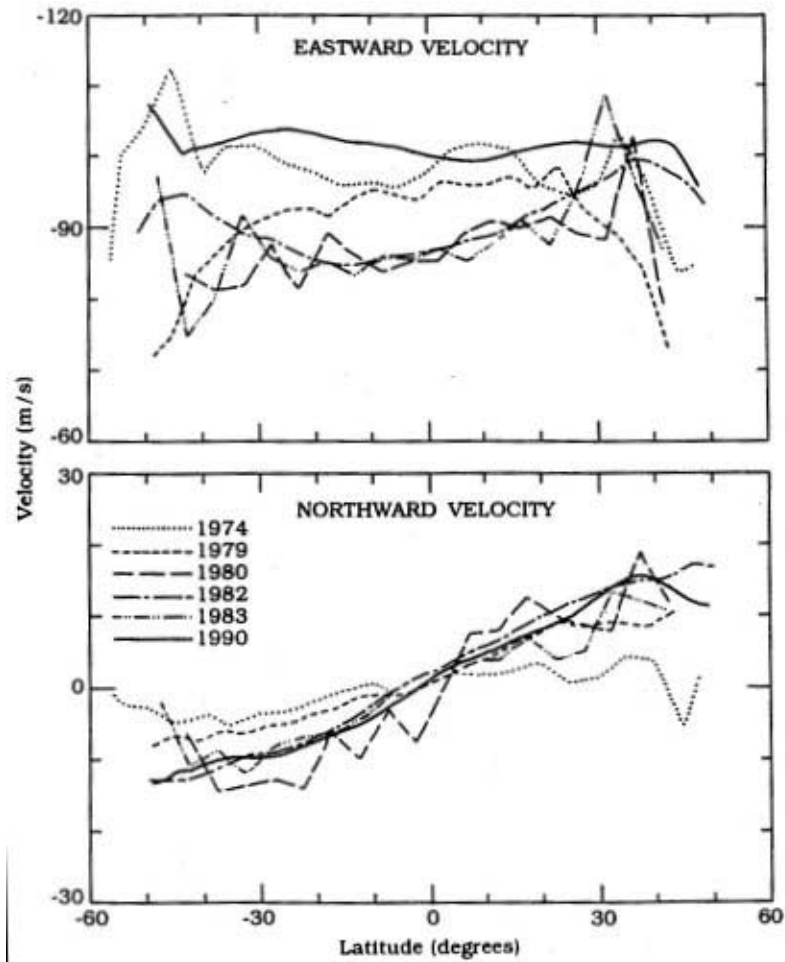


Figure 3-13 Venus zonal and meridional velocities at cloud top

Figure 3-13 shows the velocities of cloud features (reproduced from P. Gierasch et al., “Circulation of the Venus atmosphere”, in *Venus II*, The University of Arizona Press, 1997). These are averages over the illuminated portion of the Venus disc. Horizontal axis is latitude; vertical axis indicates velocity in m/s. The upper panel shows the zonal (eastward) velocity, the lower panel shows meridional (northward) velocity. Apparently, the cloud features move with the winds at 60-65 km altitudes.

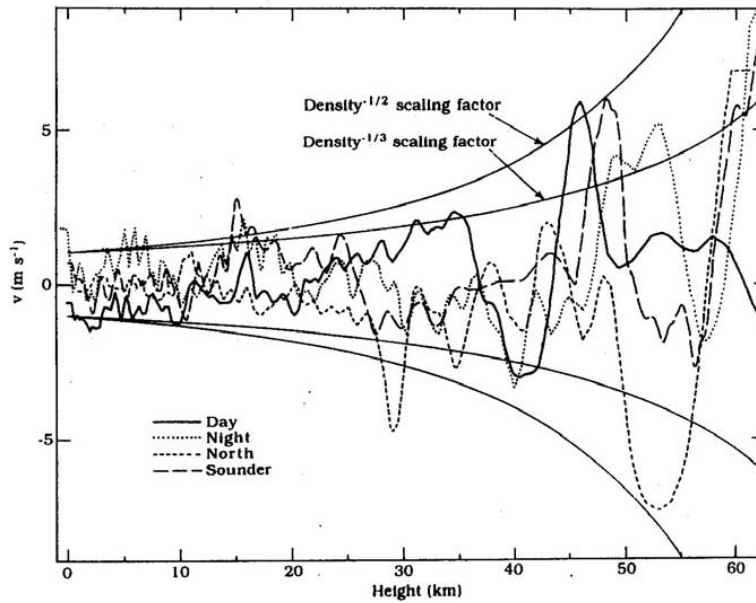


Figure 3-14 Meridional velocity profiles for the Pioneer Venus probes.

The meridional velocity profiles measured by the Pioneer Venus probes are shown on Figure 3-14 (reproduced from P. Gierasch et al., “Circulation of the Venus atmosphere”, in *Venus II*, The University of Arizona Press, 1997). Meridional winds exhibit the same tendency as the zonal winds, increasing with the height.

3.3.4.3 Flow Regime

Using the viscosity data from Table 3-2 and assuming relative winds of the order of 1 m/s for balloon (due to the action of the TCS) and of the order of 10 m/s for the wing and tether (due primarily to the wind change with altitude), the flow regime defining Reynolds numbers (Re) and drag coefficients (C_D) are given in Table 3-3.

Table 3-3 Venus DARE flow regime

	Reynolds number, Re	Drag coefficient, C_D
Balloon at 55-60 km	From $3.6 \cdot 10^5$ to $2.6 \cdot 10^5$	0.2
Tether at 45-55 km	1400-600	1.0-1.1

3.3.4.4 Results

Figure 3-15 shows results of the TCS performance simulations for the balloon at the altitude of 54 km and 10 kg wing with the area of 1 m^2 at the end of the 10 km long tether. Tether diameter is 1 mm. This is the configuration that was chosen for the preliminary architecture design study (see Section 6). The balloon diameter is 7.6 m and the vertical wind gradient is 1.6 m/s/km. The winds at balloon and wing altitudes are parallel.

The figure shows the variations of the cross-track velocity u (solid line) and the along-track velocity v (dashed line) for the lift coefficient C_L varying from 0 to 1. The y-axis indicates the values of the velocities, while the x-axis indicates the values of the lift coefficient. The change in lift coefficient is achieved by changing the angle of the rudder. Z_B is balloon altitude, M_W is the mass of the wing, A_W is the wing area, L_t is the tether length and α is the angle between the wind vectors at the balloon and wing altitudes. Angle α equal to 0° corresponds to wind vectors at both altitudes being parallel to each other.

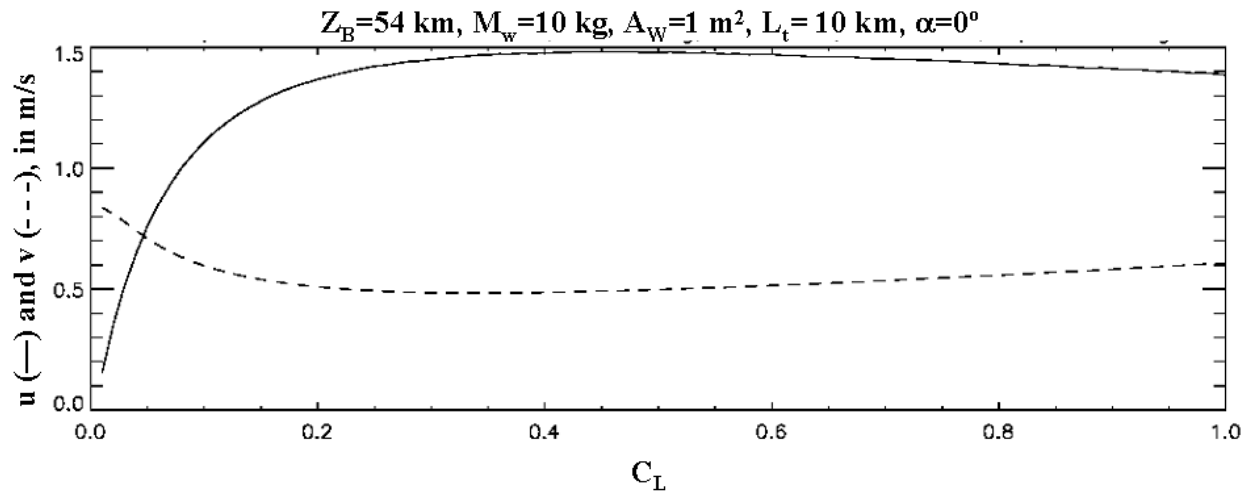


Figure 3-15 Venus TCS performance

As can be seen from the Figure 3-15, there is a preferential value for the lift coefficient C_L (about 0.45) at which the cross-track velocity u reaches its maximum of about 1.5 m/s. The cross-track velocity is close to its maximum value for a wide range of the values of the lift coefficient (from about 0.2 to 1). This means that it will not be necessary to control the rudder angle very precisely to achieve the maximum cross-track velocity.

The cross-track velocity is in the direction of the meridional winds at the balloon altitude (54 km in this case) and its value is comparable to the value of the meridional winds (see Figure 3-14). The along-track velocity is in the direction of the zonal winds at the balloon altitude and is much smaller than the zonal winds (compare to Figure 3-13). Similar situation is observed for TCS analysis on other planets, thus the effects of the along-track velocity are ignored in this analysis.

As can be seen, the cross-track velocity u increases rapidly for increasing lift coefficient, but then “levels off” for $C_L > 0.2$. This happens because the lift forces become stronger than the weight of the wing. The wing swings far up to one side, as described in 3.3.2. For $C_L = 1$ the wing raises by almost 4 km above the altitude of 10 km below the balloon. The horizontal projection of the lift force also becomes smaller, so that the cross-track velocity does not increase with the increasing lifting force.

The situation with the parallel winds at the balloon and the wing altitudes is idealistic, especially on Venus, where variations of meridional winds with altitudes are seen in the data (Figure 3-14). We estimate that the angle between the wind vectors could be up to about 10° for a balloon and a wing separated by a 10 km tether. As can be seen from the Figure 3-16 and Figure 3-17 the

cross-track velocity u decreases with the increasing angle between the wind vectors, while the along-track velocity v increases.

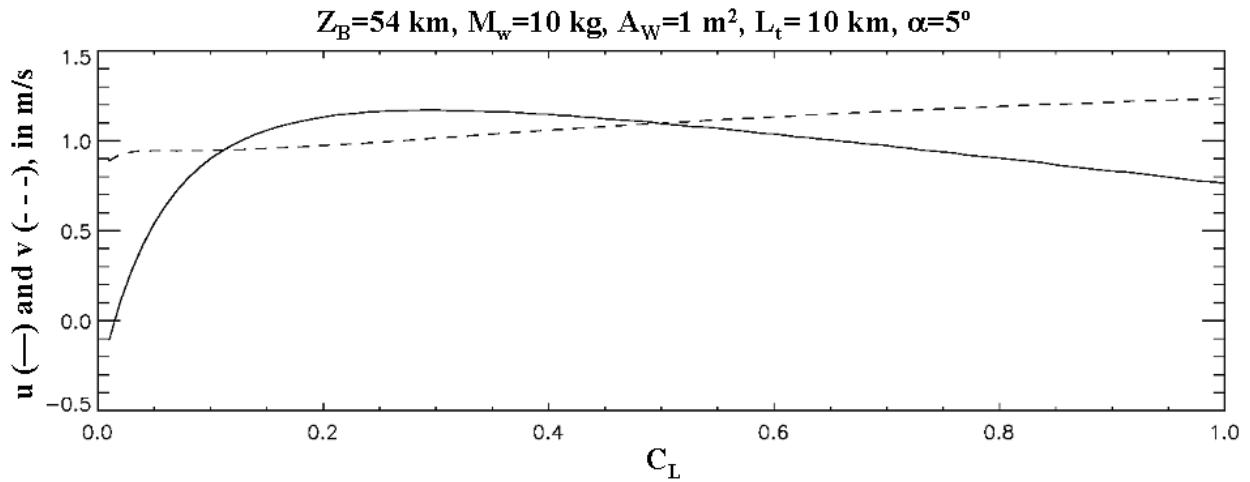


Figure 3-16 Venus TCS performance

Figure 3-16 shows the analysis for the same configuration, as Figure 3-15, but with the angle α equal to 5° .

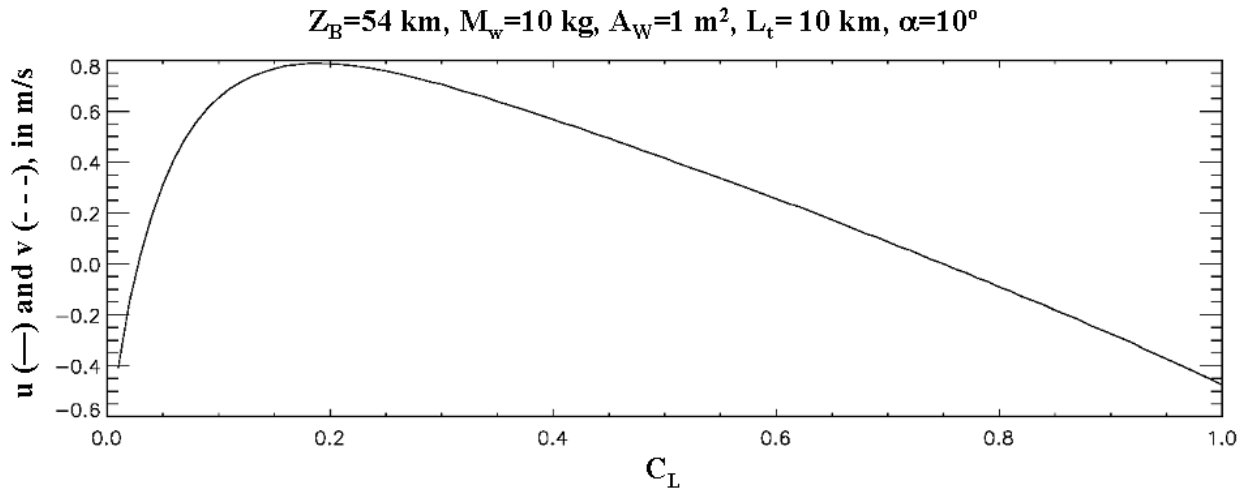


Figure 3-17 Venus TCS performance

Figure 3-17 shows the analysis for the same configuration, as Figure 3-15, but with the angle α equal to 10° . The along-track velocity in this case is stronger than the cross-track velocity and is not seen on the plot.

Figure 3-18 shows the changes in the TCS performance with changing wing mass and area. The curves of different colors represent TCS wings of different area, in m^2 . The y-axis gives the maximum cross-track velocity u in m/s , the x-axis gives the mass of the wing. The maximum cross-track velocity is given for the optimum C_L .

The figure shows that increasing the wing mass increases the cross-track control velocity. The weight increase improves performance because it allows to keep the wing lower in the atmosphere. The weight increase can be accomplished by placing useful payload inside the wing. However, it seems more beneficial to exploit the strong lifting force with the Advanced TCS. Employing the ATCS will significantly increase the maximum cross-track velocity. The analysis of the TC capabilities with ATCS can be done in Phase II of the study.

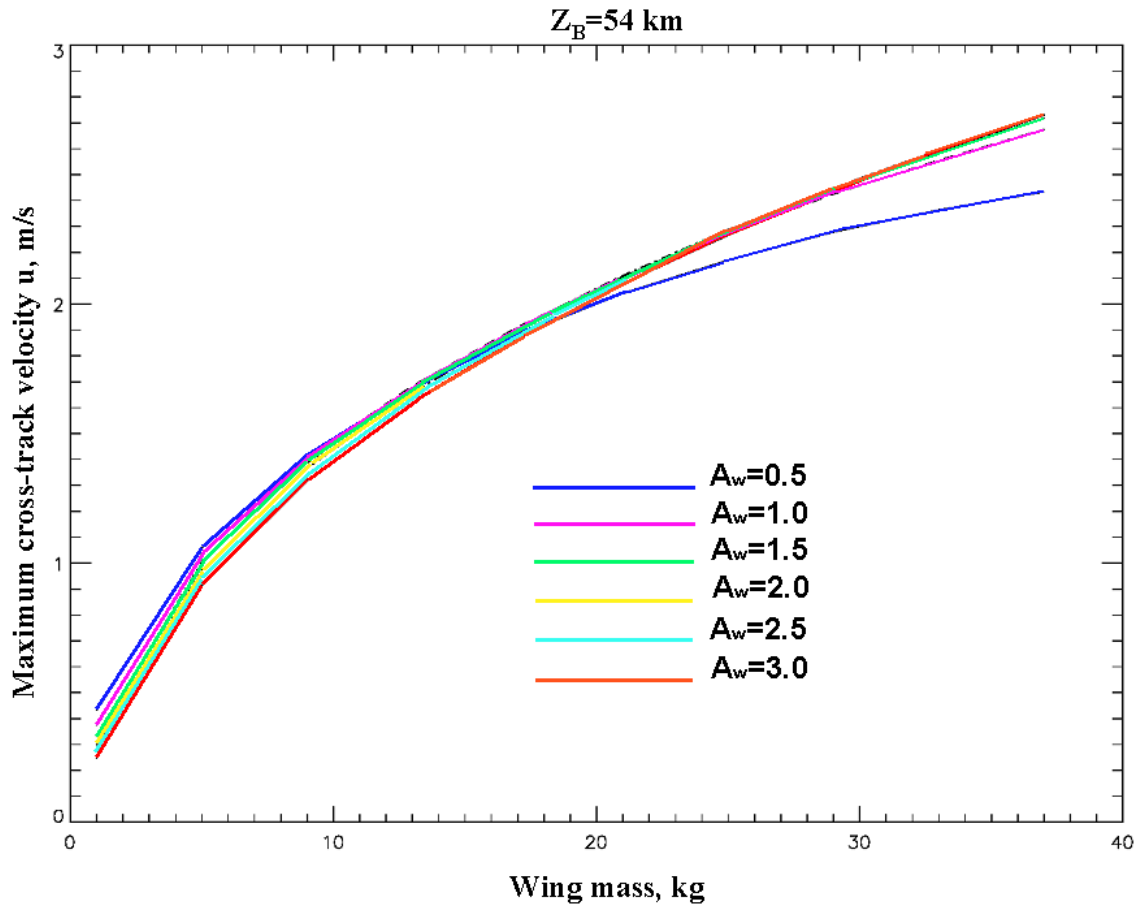


Figure 3-18 Venus TCS performance vs. Wing mass and area

The increase in wing area does not always lead to the increase in the maximum cross-track velocity. For a light wing (mass below 10 kg), the smaller wing ($A_w = 0.5 \text{ m}^2$, blue curve) gives a better performance than the larger wing ($A_w = 3 \text{ m}^2$, red curve), because the bigger proportion of the lift generated by the larger wing goes into lifting up the wing, rather than creating a sideways force.

When the lifting force becomes stronger than the weight of the wing, further increase in the wing area does not lead to a significant increase in the cross-track velocity, as can be seen from overlapping curves for wing masses larger than 15 kg and wing areas larger than 0.5 m^2 . Performance worsens significantly for small wing sizes for heavy wings ($A_w = 0.5$, wing mass larger than 20 kg). The performance of smaller wings ($A_w < 0.5 \text{ m}^2$, not shown) does not improve significantly with increasing wing mass for wing masses larger than 10 kg. This analysis

confirms that a better way to improve the TCS performance is to employ the ATCS, rather than the First Generation StratoSail® TCS.

We also performed preliminary analysis of the effects of the tether length on the TCS performance. For this analysis we keep the total weight of the TCS system (the wing and the tether) constant and vary the tether length. The changes in the tether mass are added to the mass of the wing and its area is recalculated in accordance with a simple scaling relationship. The scaling relationship assumes a small density for the wing ($\rho=50 \text{ kg/m}^3$, from the Earth StratoSail® analog) and a certain wing shape (height to width ratio of 5 and width to thickness ratio of 4).

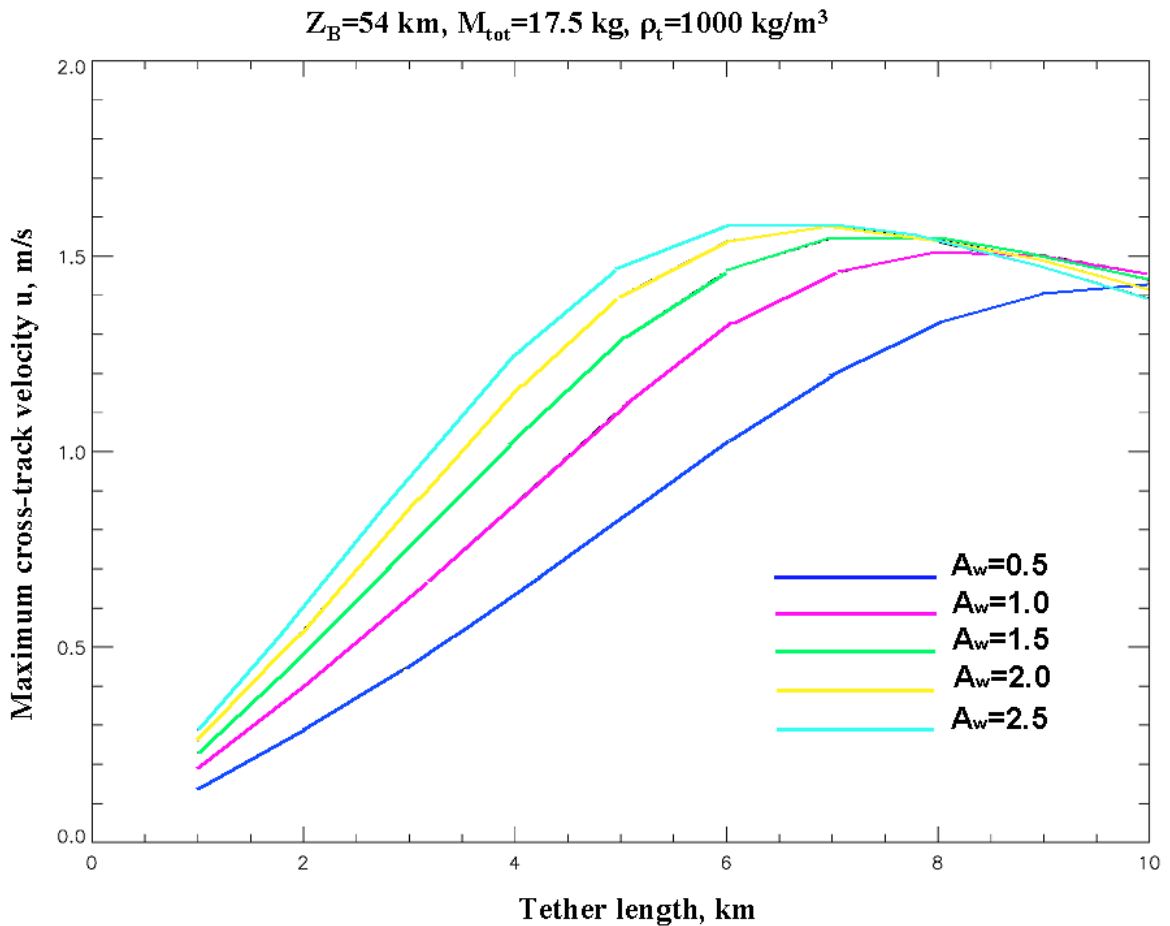


Figure 3-19 Venus TCS performance vs. Tether length and Wing area

Figure 3-19 illustrates this analysis. The curves of different colors represent TCS wings of different area, in m^2 . The y-axis gives the maximum cross-track velocity u in m/s , the x-axis gives the length of the tether. The maximum cross-track velocity is given for the optimum C_L . The tether density is $\rho_t=1000 \text{ kg/m}^3$ and the total mass of the TCS is 17.5 kg . This gives the wing mass of about 10 kg for the 10 km tether. The point on the purple curve ($A_w=1 \text{ m}^2$) for the tether length of 10 km corresponds to the wing analyzed on Figure 3-15.

The plot shows that for larger wings the optimal tether length (giving the highest TCS performance) shortens (to about 6 km for $A_w=2.5 \text{ m}^2$) from 10 km for $A_w=0.5 \text{ m}^2$. The

improvement comes from the additional mass, saved from the tether mass, going into the wing mass and increasing the wing area. The increase in lift due to the area increase is larger than the decrease in lift due to the reduction of the relative wind speed and density at the wing altitude for some range of tether lengths. For small wings ($A_w=0.5 \text{ m}^2$ and smaller – not shown) the reduction in tether length worsens the TCS performance.

The effect of optimal tether length depends on the tether density. For a less dense tether the effect would be less pronounced or will disappear, because less wing area can be gained with the tether shortening.

This analysis can be used to establish the preferred length of the tether for the given wing area and given total mass of the TCS when different elements of the TCS (tether, wing) are better defined (in Phase II). It may be useful to decrease the tether length and to sacrifice some TCS performance if this places the wing into a higher altitude and a less harsh environment.

3.3.5 TC Capabilities Assessment: Titan

The sections below describe the atmospheric winds, the general structure of the atmosphere, the estimated flow regime and TCS performance modeling results.

3.3.5.1 Atmospheric Structure

Our knowledge of Titan environment is limited to results of Voyager flybys, stellar occultation data and numerical modeling. Dense haze in the upper part of the atmosphere (above 80 km) hides the surface of the planet and lower and middle atmosphere from Earth observer.

The figures below show the altitudinal profiles of temperature, pressure and density in the atmosphere of Titan. The atmospheric profiles for Titan are from the model by R. V. Yelle, D. F. Strobell, E. Lellouch and D. Gautier, “The Yelle Titan Atmosphere Engineering Models” in Huygens: Science Payload and Mission, (A. Wilson, Ed.), ESA SP-1177, European Space Agency, Noordwijk, The Netherlands, 1997.

Figure 3-20 shows the vertical profile of the Titan atmospheric temperatures. As can be seen the temperatures are the lowest (about 70 K) at the tropopause at the altitude of about 50 km. Temperatures in the troposphere are within about 5 K of the condensation temperature of the major constituent of the Titan atmosphere – N_2 . Thus, it is not likely that N_2 clouds will form in the troposphere. However, condensation of methane and cloud formation can occur at altitudes from 0 to 30 km above the surface.

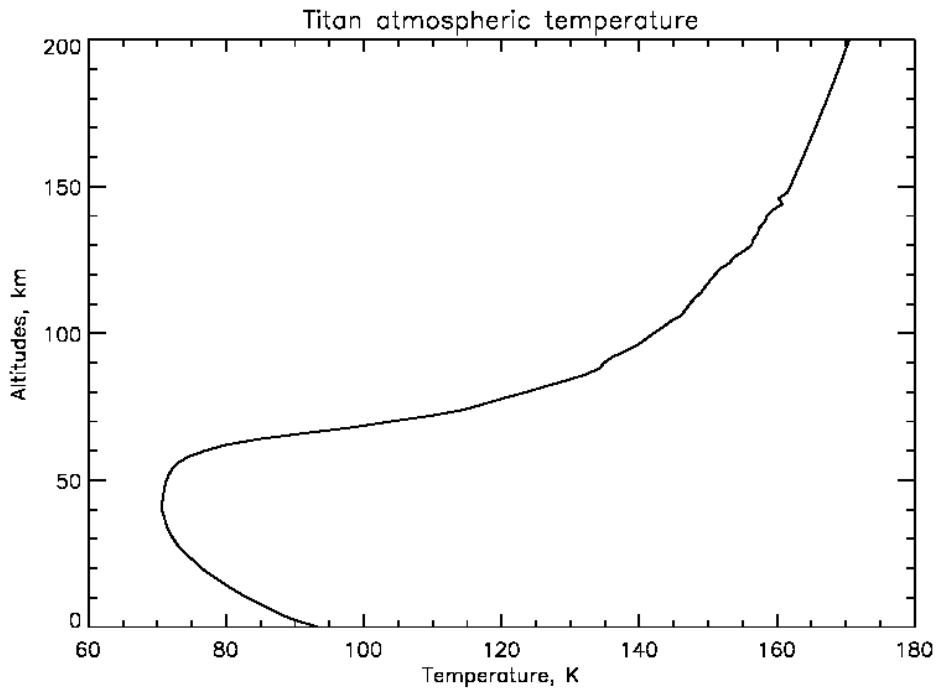


Figure 3-20 Titan atmospheric temperature

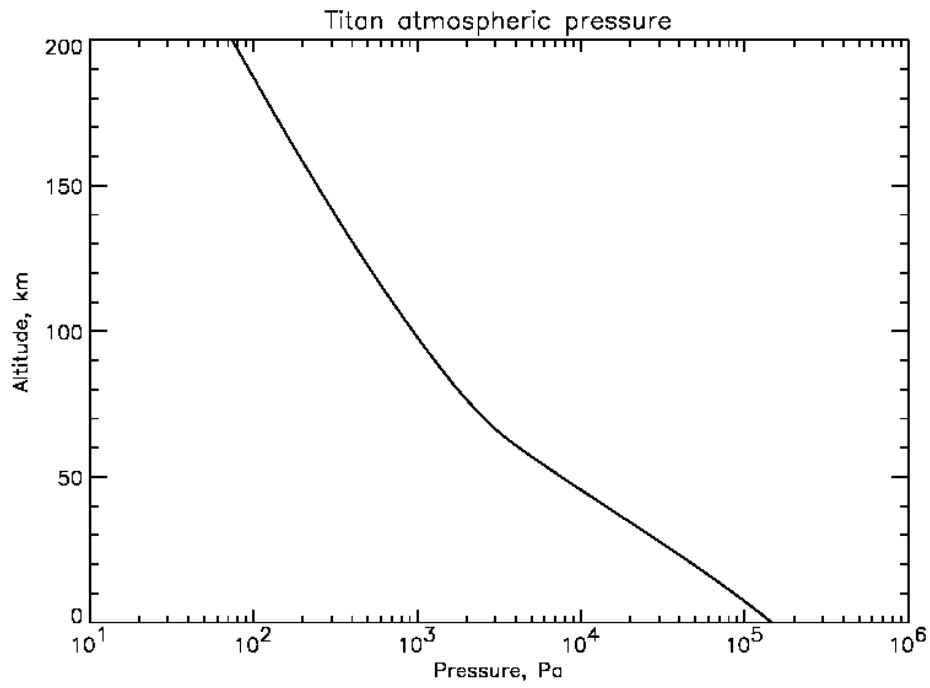


Figure 3-21 Titan atmospheric pressure

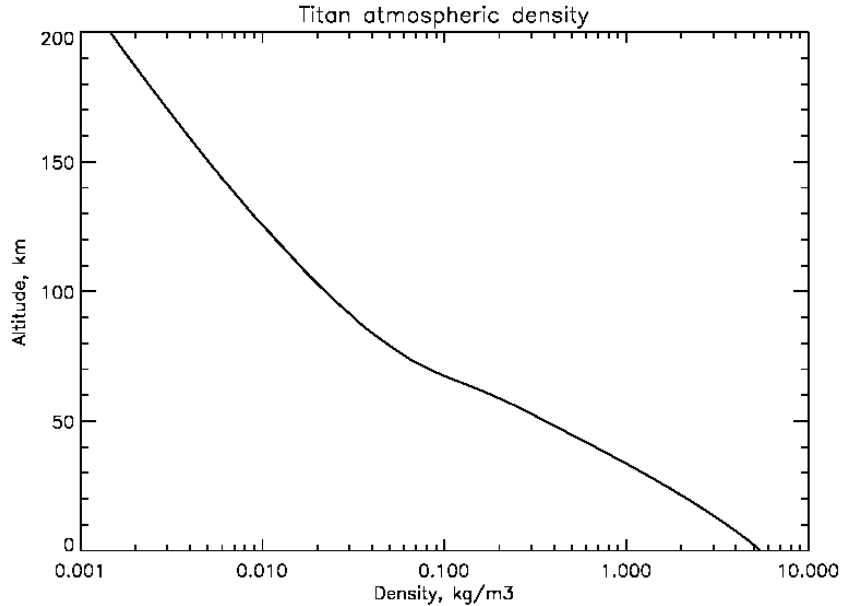


Figure 3-22 Titan atmospheric density

Figure 3-21 and Figure 3-22 show the vertical profiles of pressure and density, respectively. Titan atmosphere is quite dense and is well suited for balloon flight – the surface pressure 1.5 times larger than Earth surface pressure.

Another parameter that is needed to define the flow regimes (i.e. Reynolds numbers) and drag coefficients for the balloon and the tether – is viscosity. Assuming purely N₂ atmosphere, the viscosity of Titan atmosphere changes with temperature as described in Table 3-4 (adapted from the National Institute of Standards and Technology (NIST) web-site <http://properties.nist.gov/SemiProp/Gases/N2.html>).

Table 3-4 Viscosity of Titan atmosphere

T, (K)	77	80	85	90	95	100	110	120	130	120	125	130	135
ν , ($\mu\text{Pa s}$)	5.4	5.6	5.9	6.3	6.6	7.0	7.6	8.3	8.9	9.5	10.1	10.7	11.3

3.3.5.2 Atmospheric Winds

Figure 3-23 shows the meridional cross section of the zonal winds structure on Titan based on the model of Flasar et al., “Titan zonal wind model”, in Huygens: Science Payload and Mission, (A. Wilson, Ed.), ESA SP-1177, European Space Agency, Noordwijk, The Netherlands, 1997. The contours are envelopes of winds speeds (in m/s) calculated from the thermal wind equation assuming twice the observed horizontal temperature gradient. The wind directions are uncertain, so that the cross section can give eastward, as well as westward winds. Symmetry about the equator is assumed.

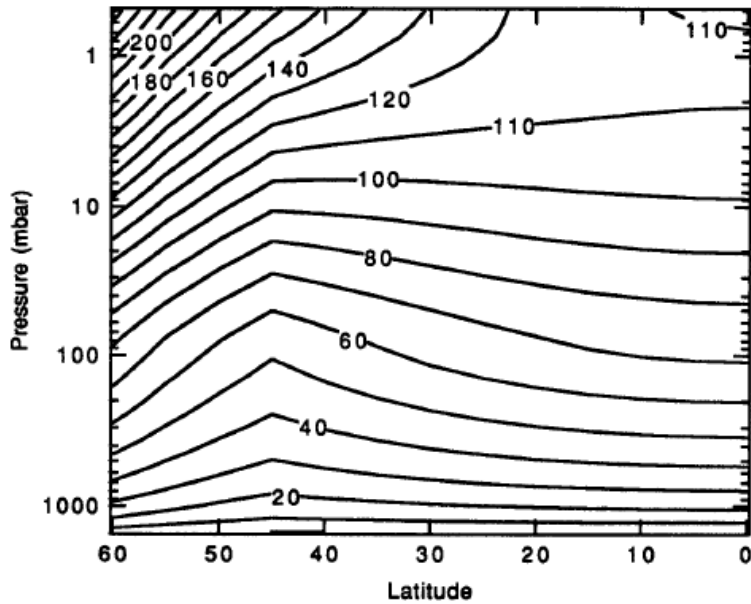


Figure 3-23 Zonal wind structure on Titan (from Flasar et al, 1997)

3.3.5.3 Flow Regime

Using the viscosity data from Table 3-4 and assuming relative winds of the order of 1 m/s for the balloon (due to the action of the TCS) and of the order of 10 m/s for the wing and tether (due primarily to the wind change with altitude), the flow regime defining Reynolds numbers (Re) and drag coefficients (C_D) are given in the table below.

Table 3-5 Titan DARE flow regime

	Reynolds number, Re	Drag coefficient, C_D
Balloon at 50-80 km	From $5.8 \cdot 10^5$ to $1.1 \cdot 10^5$	0.2-0.5
Tether at 40-70 km	1200-120	1.0-1.5

3.3.5.4 Results

Figures Figure 3-24 through Figure 3-27 compare TCS performance for different altitudes on Titan. The balloon system in all cases supports a 100 kg payload. The analysis takes into account the change of balloon size for different float altitudes. The vertical wind gradient is 1 m/s/km. The balloon diameters are 8.7, 11.2, 15.5 and 19.8 m for floating altitudes 50, 60, 70 and 80 km, respectively. In all cases the wing mass is 10 kg and its area is 1 m^2 . The tether is 10 km long and its diameter is 1 mm. The figures' notation is the same as in Section 3.3.4.2.

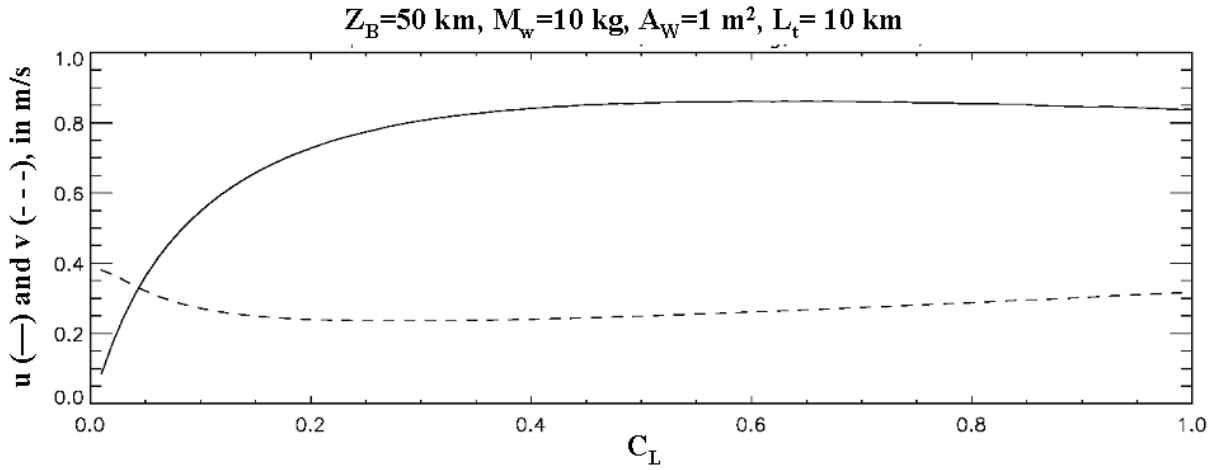


Figure 3-24 Titan TCS performance, $Z_B=50 \text{ km}$

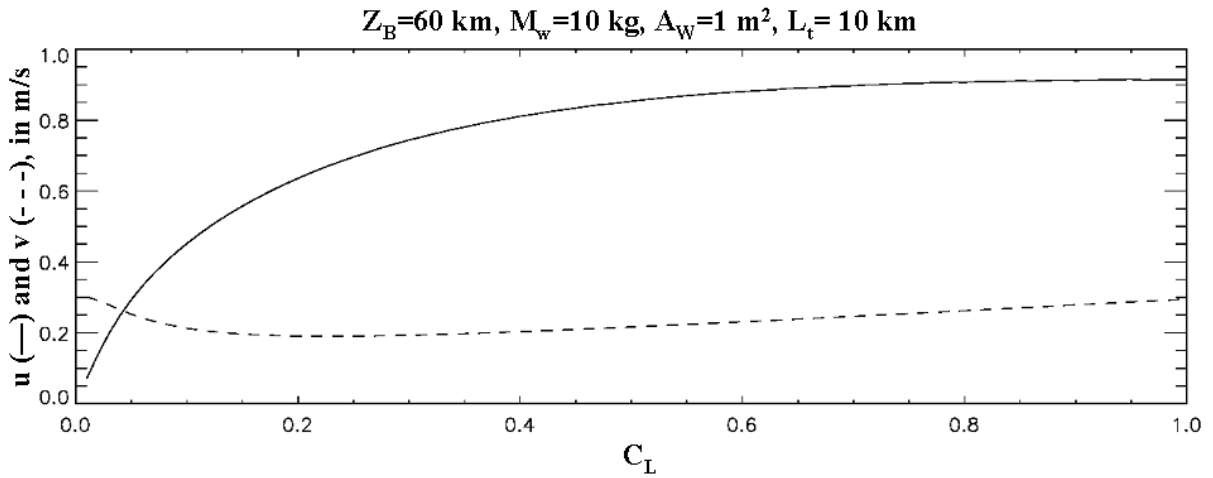


Figure 3-25 Titan TCS performance, $Z_B=60 \text{ km}$

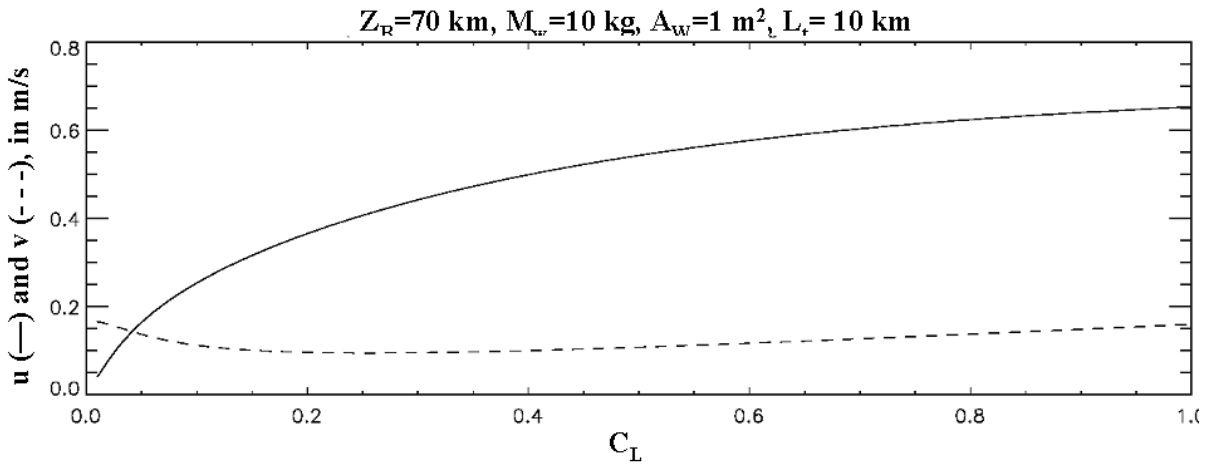


Figure 3-26 Titan TCS performance, $Z_B=70 \text{ km}$

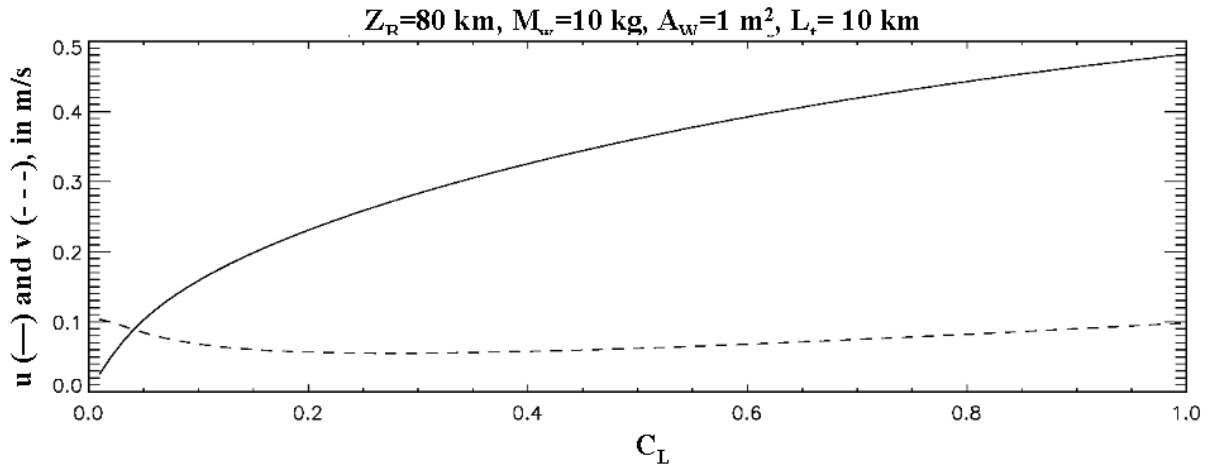


Figure 3-27 Titan TCS performance, $Z_B=80$ km

The figures show that the best floating altitude (from the point of view of the TCS performance) for a 100 kg payload system is 50-60 km. For higher altitudes the TCS performance rapidly worsens due to the increase in the balloon size.

The “leveling off” of the cross-track velocity curves for large lift coefficients on the 50 and 60 km floating altitude plots is due to the same effect of lift being larger than weight described in Section 3.3.4.2. The same conclusion can be reached here: the TCS performance can be significantly improved by employing the ATCS.

3.3.6 TC Capabilities Assessment: Jupiter

The sections below describe the atmospheric winds, the general structure of the atmosphere, the estimated flow regime and TCS performance modeling results.

3.3.6.1 Atmospheric structure

The atmosphere of Jupiter is thought to be representative of the atmospheres of the Outer Planets (Jupiter, Saturn, Uranus, Neptune) both chemically and dynamically.

Jupiter atmosphere consists primarily of hydrogen. Dense ammonia and methane clouds in the atmosphere prevent remote sensing of the deeper parts of the atmosphere. The upper boundary of the cloud cover is estimated to be at the altitude of 0.6-1 bar.

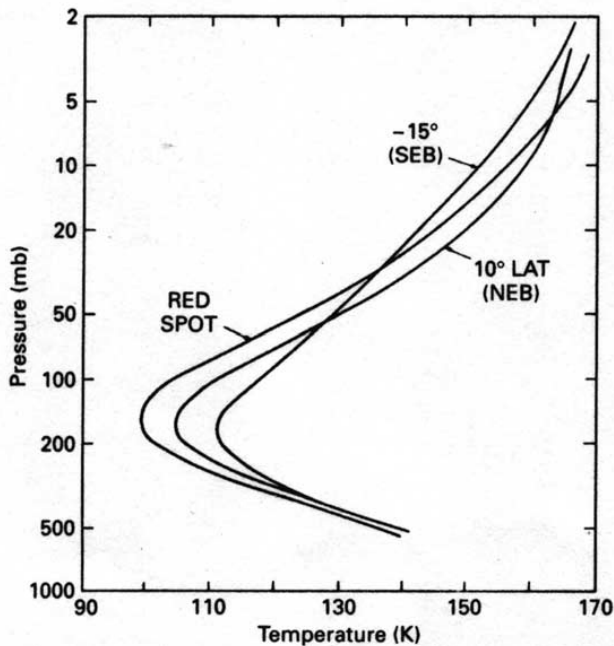


Figure 3-28 Jupiter atmospheric temperature

Figure 3-28 shows vertical profiles of temperature at three different locations across Jupiter (from Hanel, R., et al “Infrared observations of the Jovian system from Voyager 2”, *Science* **206** (4421), 1979). These profiles show the existence of the tropopause region between the 0.1-0.2 bar pressure levels. This data indicates that the temperature profiles look quite similar for the observed regions of the Jupiter, except maybe for the tropopause, where the temperature can vary by about 10 K.

Another parameter that is needed to define the flow regimes (i.e. Reynolds numbers) and drag coefficients for the balloon and the tether is viscosity. Assuming purely H₂ atmosphere, the viscosity of Jupiter atmosphere changes with temperature as described in Table 3-6 (adapted from CRC Handbook of Chemistry and Physics, 71st edition, 6-140).

Table 3-6 Viscosity of Jupiter atmosphere

T, (K)	100	200
ν , ($\mu\text{Pa s}$)	4.2	6.8

3.3.6.2 Atmospheric Winds

From the point of view of dynamics, characteristic features of the atmospheres of the Outer Planets include the zonal jets and giant vortices (the most famous being the Great Red Spot (GRS) of Jupiter). Figure 3-29 shows the observed structure of the zonal winds and calculated wind shear (vertical gradient of the wind) at the cloud top height (~1 bar pressure level) at Jupiter (from Limaye S. S., “Jupiter: New estimates of the mean zonal flow at the cloud level”, *Icarus* **65**, 1986).

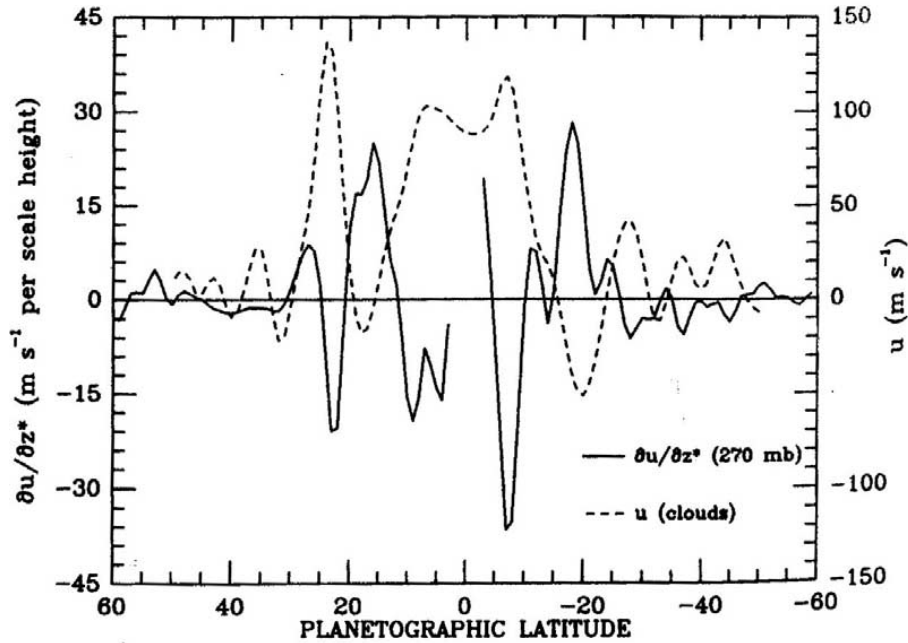


Figure 3-29 Jupiter upper troposphere thermal wind shear compared with cloud tracer wind velocities.

3.3.6.3 Flow Regime

Using the viscosity data from Table 3-6 and assuming relative winds of the order of 1 m/s for the balloon (due to the action of the TCS) and of the order of 10 m/s for the wing and tether (due primarily to the wind change with altitude), the flow regime defining Reynolds numbers (Re) and drag coefficients (C_D) are given in the table below.

Table 3-7 Jupiter DARE flow regime

	Reynolds number, Re	Drag coefficient, C_D
Balloon at 0.1-0.2 bars	From $3.5 \cdot 10^5$ to $7.0 \cdot 10^5$	0.2-0.2
Tether at 10 km below (0.17-0.33 bars)	300-600	1.2-1.1

3.3.6.4 Results

Figure 3-30 and Figure 3-31 show the results of the TCS performance analysis for the Jupiter SIRMA balloon. It is assumed that the balloon would float at $P=0.1$ bar level during the day, descending to the $P=0.2$ bar level during the night (as described in Section 18). The TCS consists of the 50 kg 10 m^2 wing on a 10 km long tether. The tether diameter was increased to 5 mm (from 1 mm for all other planets) to account for larger gravity of Jupiter and heavier wing. A 72 m diameter balloon is required to support a 10 kg payload and 60 kg TCS. The vertical wind gradient is 1.5 m/s/km.

The figure's notation is the same as in Section 3.3.4.2. The cross-track and along-track velocities shown in the figures are negative, because the vertical gradient of the wind is negative – the winds decay with altitude, as described in Section 3.3.6.2. Correspondingly, the relative wind vector at the wing altitude is from the opposite direction than in the case of Venus and Titan. Consequently, the wing lifting force vector would be also directed into the opposite direction (compared to Venus and Titan) for positive C_L . At any rate, we are only concerned with the magnitudes of the velocities, since the direction of the lifting force vector is controlled by the rudder angle and the wing performance is symmetric about the 0° rudder angle.

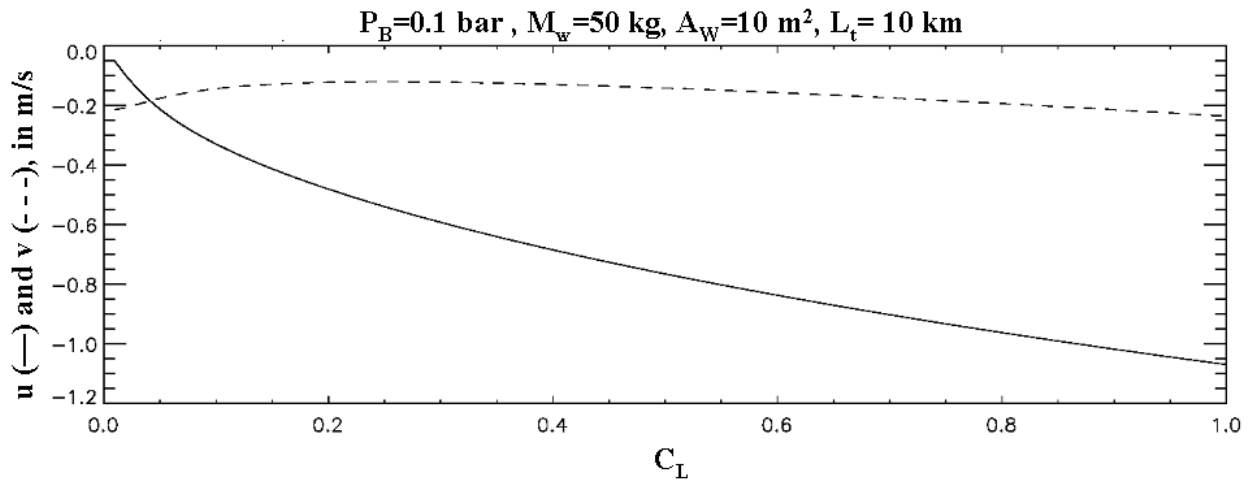


Figure 3-30 Jupiter TCS performance, $P_B=0.1 \text{ bar}$

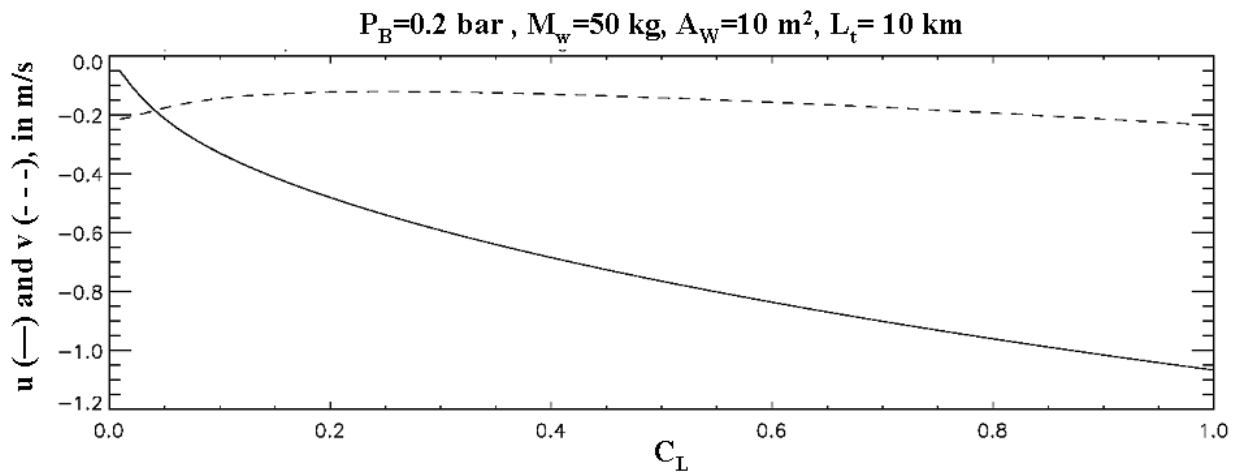


Figure 3-31 Jupiter TCS performance, $P_B=0.2 \text{ bar}$

Figure 3-30 and Figure 3-31 show that the TCS performance does not change significantly for the two pressure levels, and thus does not change significantly during the daytime and nighttime operation. In both cases the maximum cross-track velocity is for $C_L=1$ and is about 1.0 m/s. The lift created by the wing is smaller than the wing weight. The TCS performance can be improved

by increasing the tether length and by reducing the wing mass (leading to the balloon size and tether diameter reductions).

3.3.7 TC Capabilities Assessment: Mars

The sections below describe the atmospheric winds, the general structure of the atmosphere, the estimated flow regime and TCS performance modeling results.

3.3.7.1 Atmospheric Structure

A wealth of observational and modeling data is available for Mars. The winds, temperatures and atmospheric density on Mars vary considerably with the season and the amount of dust in the atmosphere. In addition, the surface of Mars exhibits considerable topographic variations that may need to be taken into account for analysis of balloon performance. In our simulations we rely on the published results of the Mars General Circulation Model (MGCM) for the analysis of DARE trajectories on Mars. We are using Run 98.04 of the MGCM. MGCM is a well-developed model and its results represent the observations fairly well.

The TCS performance analysis here is based on the MABS-MGA-like balloon with the added TCS. The balloon would float at the density level of about 0.008 kg/m^3 . The pressure level of the floating altitude is between 2.4 and 3.4 mbars. The altitude of the balloon system above the surface would vary depending on geography and season from 6 km (summer over Southern highlands) to 12 km (winter over Northern lowlands). Thus, topography must be considered in describing the operational balloon environment.

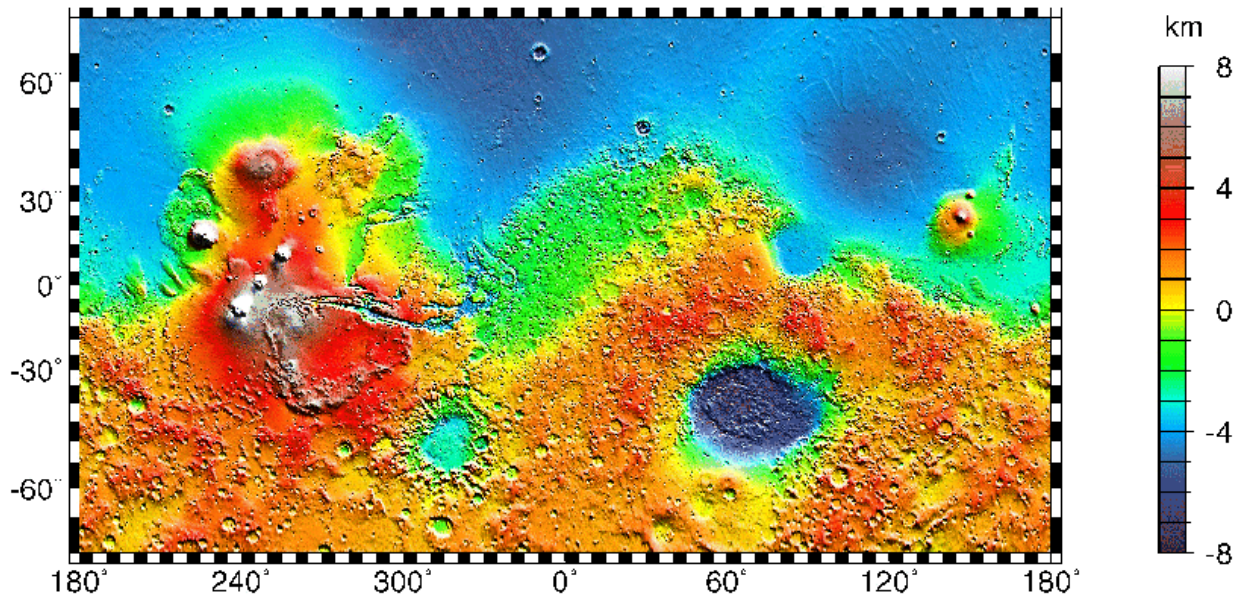


Figure 3-32 Martian topography from MOLA data

Figure 3-32 shows the Martian topography as measured by Mars Orbital Laser Altimeter (MOLA) onboard the Mars Global Surveyor (MGS). The Tharsis volcano-tectonic province is centered near the equator in the longitude range 220° E to 300° E and contains the vast east-west trending Valles Marineris canyon system and several major volcanic shields including Olympus

Mons (18° N, 225° E), Alba Patera (42° N, 252° E), Ascræus Mons (12° N, 248° E), Pavonis Mons (0°, 247° E), and Arsia Mons (9° S, 239° E). Other prominent regions and structures include Solis Planum (25° S, 270° E), Lunae Planum (10° N, 290° E), and Claritas Fossae (30° S, 255° E). Major impact basins include Hellas (45° S, 70° E), Argyre (50° S, 320° E), Isidis (12° N, 88° E), and Utopia (45° N, 110° E). The low floating Martian balloon would be in danger of impacting high topography in the equatorial region (Tharsis bulge).

The figures below give examples of the Mars environment (from MGCM web-site <http://humbabe.arc.nasa.gov/mcc/CC.html>).

Figure 3-33 and Figure 3-34 show Martian zonal winds and horizontal temperatures and winds, respectively, for one season. The season is winter solstice (the start of astronomical winter in the Northern hemisphere). It is customary in planetary science to measure seasons in terms of the L_s parameter, which is a subsolar longitude, measured in degrees. For winter solstice $L_s=270^\circ$. At vernal equinox $L_s=0^\circ$, at summer solstice $L_s=90^\circ$ and at autumn equinox $L_s=180^\circ$.

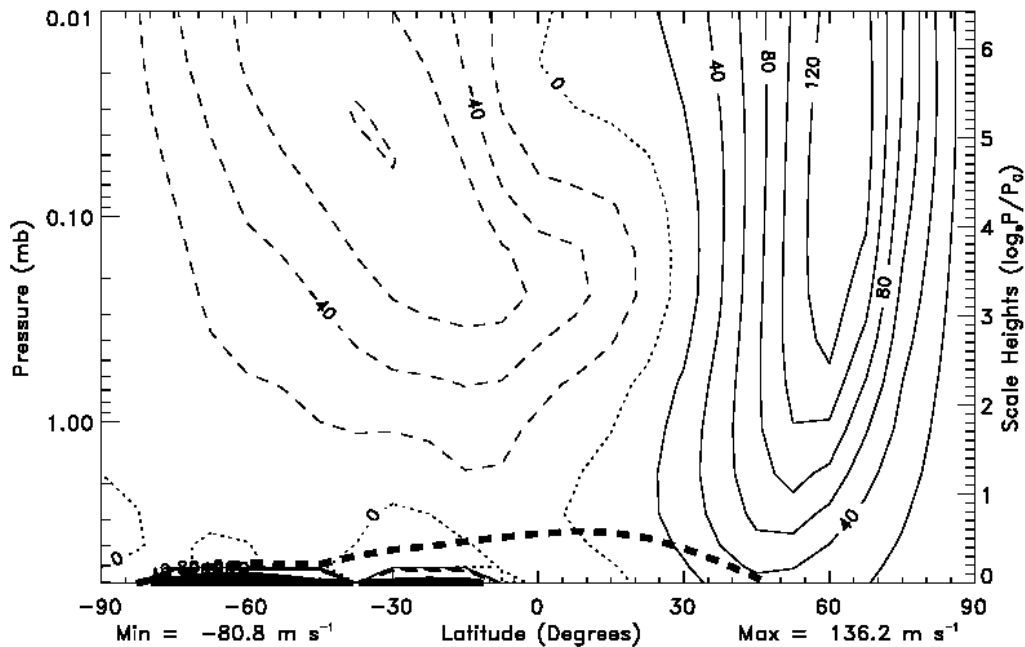


Figure 3-33 Mars time- and zonally-averaged zonal winds (m/s), $L_s=270^\circ$, Winter Solstice

Figure 3-33 shows time- and zonally-averaged zonal winds. The vertical axis is pressure (altitude) and the horizontal axis is latitude. The winds are shown as contours. Solid contours correspond to the winds blowing in the direction of the East, while dashed contours represent the winds blowing towards West.

A strong atmospheric flow develops during this season in the Polar Regions in the Northern hemisphere. This region exhibits highest vertical wind gradients (5 to 10 m/s/km), which is beneficial for the TCS operation. The rest of the planet shows weak vertical zonal wind gradients (about 1 m/s/km). The zonally averaged meridional winds are of the order of 1 m/s in the lower atmosphere.

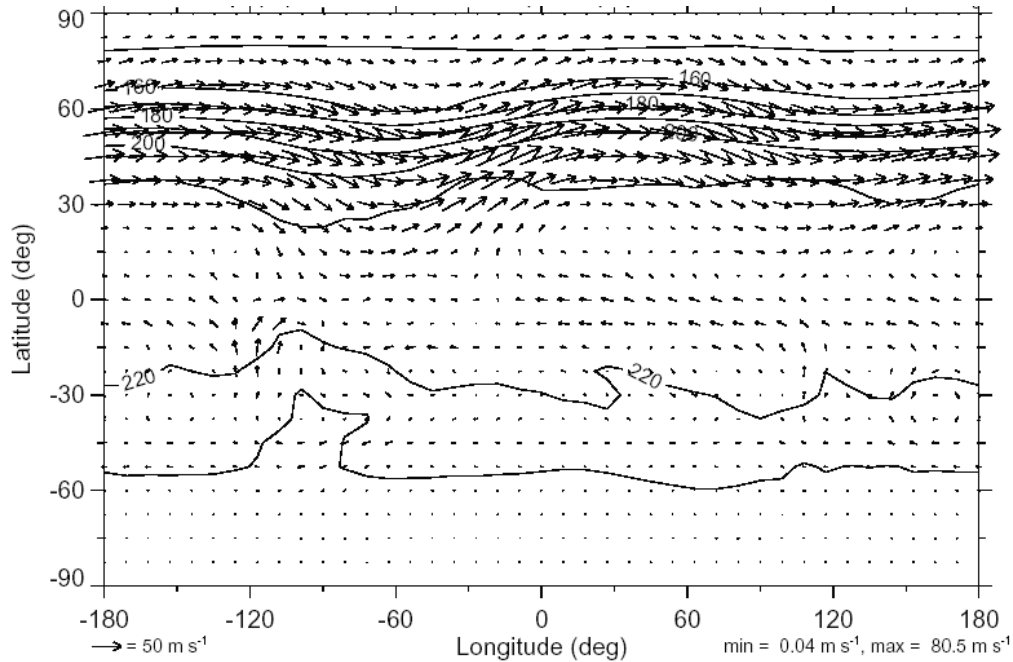


Figure 3-34 Mars time-mean temperatures and horizontal winds at 3 mbar, $L_s=270^\circ$, Winter Solstice

Figure 3-34 shows time-mean temperatures and horizontal winds at 3 mbars (300 Pa), the level close to where the Mars balloon would float. The horizontal axis is longitude and the vertical axis is longitude. The winds are shown as arrows and the temperatures are shown as labeled contours.

The lowest temperatures (160 K) during this season are found in the northern Polar Regions. A strong atmospheric flow is also seen in northern Polar Regions (maximum winds 80 m/s). In contrast, the rest of the planet exhibits very moderate winds. The topography is seen to be influencing the circulation in the vicinity of the Tharsis bulge (-60° to -120° longitude, latitudes from 30° to -30°). A strong cross-equatorial flow is also observed.

The state of the Martian atmosphere during the summer solstice ($L_s=90^\circ$, the start of astronomical summer in the Northern hemisphere) is similar to that during the winter solstice except that the strong atmospheric flow and lowest temperatures are found in the southern Polar Regions.

Figure 3-35 and Figure 3-36 illustrate the state of the Martian atmosphere during the autumn equinox ($L_s=180^\circ$, the start of astronomical autumn in the Northern hemisphere). The state of the atmosphere would be similar to that during the vernal equinox ($L_s=0^\circ$, the start of astronomical spring in the Northern hemisphere). The winds and temperatures are more symmetric about the equator, than during solstices. The strongest winds are also about half as strong as the strongest winds during the solstices.

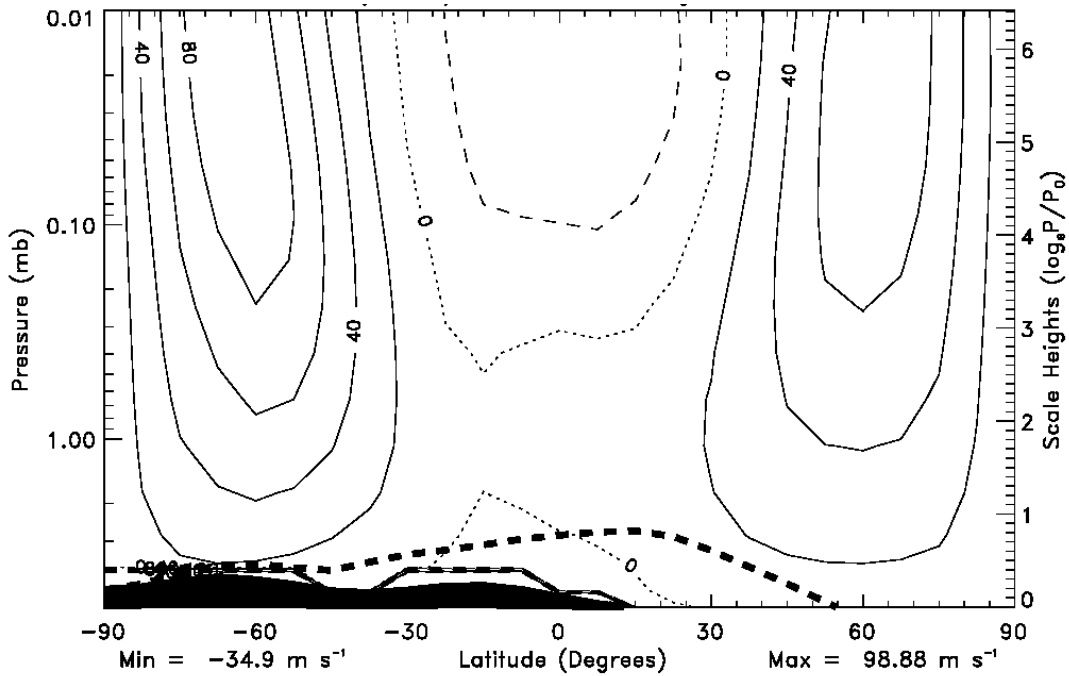


Figure 3-35 Mars time- and zonally-averaged zonal winds (m/s), $L_s=180^\circ$, Autumn Equinox

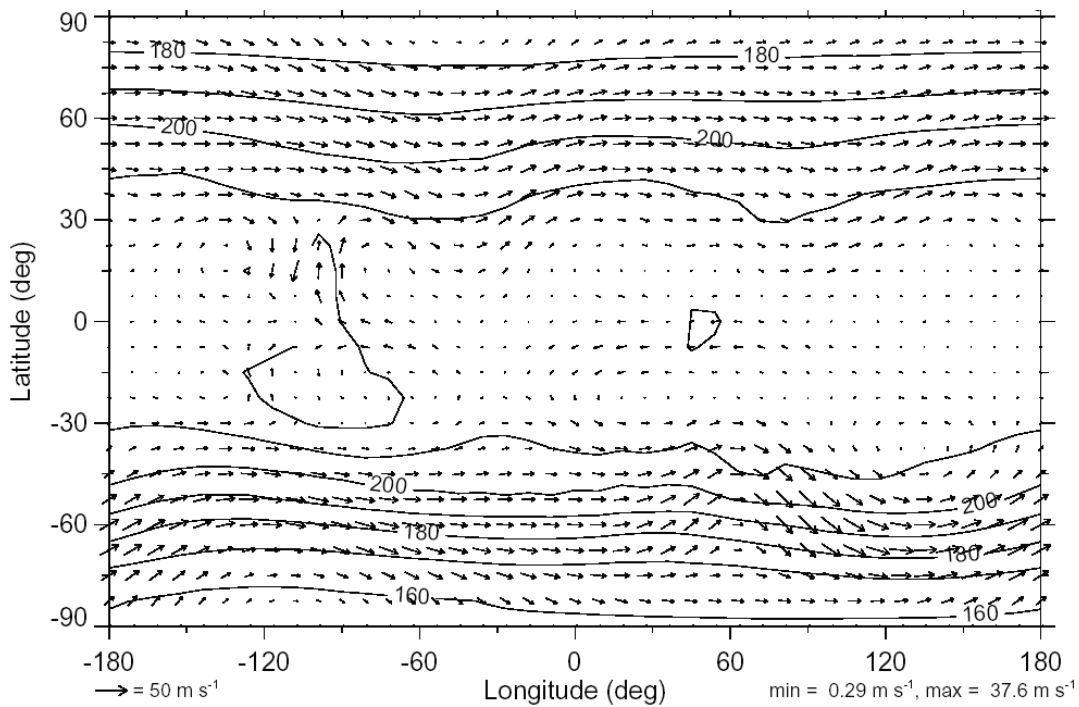


Figure 3-36 Mars time-mean temperatures and horizontal winds at 3 mbar, $L_s=180^\circ$, Autumn Equinox

Assuming purely CO₂ atmosphere, the same data as in Table 3-2 can be used to assess the viscosity of the Martian atmosphere.

3.3.7.2 Flow Regime

Using the viscosity data from Table 3-2 and assuming relative winds of the order of 1 m/s for balloon (due to the action of the TCS) and of the order of 10 m/s for the wing and tether (due primarily to the wind change with altitude), the flow regime defining Reynolds numbers (Re) and drag coefficients (C_D) are given in the table below.

Table 3-8 Mars DARE flow regimes

	Reynolds number, Re	Drag coefficient, C_D
Balloon at $T=150-230$ K	From $2.6 \cdot 10^4$ to $2.0 \cdot 10^4$	0.4
Tether 3 to 6 km below	8-20	3-2

3.3.7.3 Results

The TCS performance analysis here is based on the MABS-MGA-like balloon with the added 10 kg TCS. The balloon is 30 m in diameter. The TCS for this analysis consists of the 5 kg 1 m² wing and a 3 to 6 km tether 1 mm in diameter. The mass of the tether for the Martian TCS is estimated at 2.5 to 5 kg because of the low gravity and lighter wing (compared to the Earth's analog).

We have considered four combinations of environments that can be encountered by a balloon on Mars, which limit the range of TCS performances. They are: winter over northern polar regions, summer over northern polar regions, winter over southern polar regions, summer over southern polar regions. These combinations of season and location span a range of vertical wind gradients, floating altitudes above topography and acceptable tether lengths.

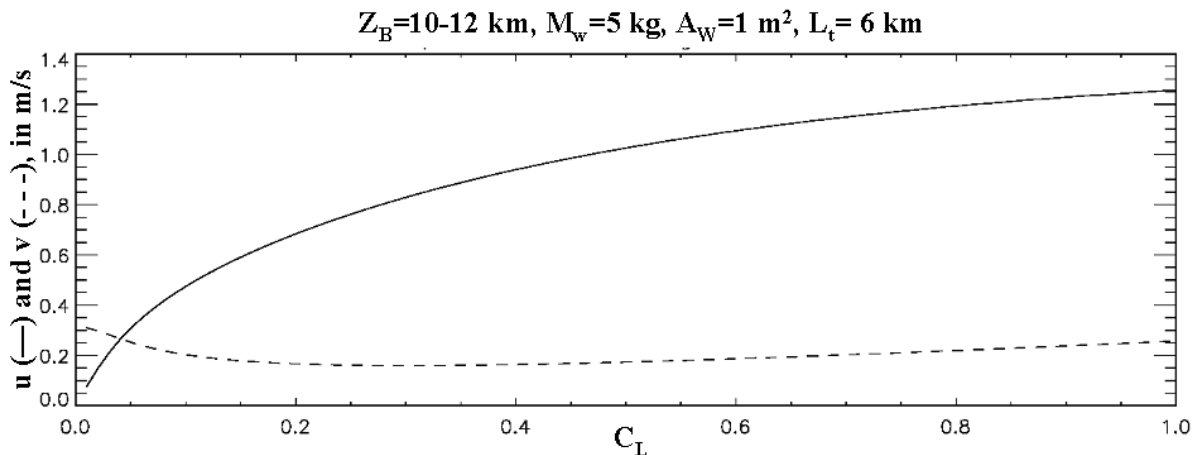


Figure 3-37 Mars TCS performance, Northern Winter

Figure 3-37 shows the TCS performance analysis for Northern Winter. The notation is the same as before. The balloon would be high (10-12 km) above the low topography of the Northern

Polar Regions (see Figure 3-32), which would allow for a relatively long 6 km tether. The vertical wind gradient is about 6 m/s/km (see Figure 3-33).

As can be seen from the figure, the maximum cross-track velocity (1.25 m/s) is reached for the maximum lift coefficient. This is the highest cross-track velocity seen in our Mars TCS analysis. The lift remains below the weight. The TCS performance can be improved by reducing the balloon size.

During the summer in the northern hemisphere, the balloon would float at about the same altitude, but the wind gradient would be much weaker – about 1 m/s/km. As a result, the maximum cross-track velocity that can be achieved is just 0.25 m/s.

In the southern hemisphere the balloon would be much closer to the surface, so that a shorter tether would need to be employed. For the case of the southern winter we consider a 3 km tether. The balloon altitude above topography would be about 6 to 7 km. The vertical wind gradient is about 9 m/s/km. Consequently, the maximum cross-track velocity is about 0.9 m/s in this case.

Finally, for the southern summer the vertical wind gradient is again about 1 m/s/km. The maximum cross-track velocity is about 0.2 m/s in this case.

3.3.8 Summary

Below we summarize the analysis of TCS performance in the Table 3-9.

Table 3-9 Estimated TCS limits

Planet	Mars	Venus	Titan	Jupiter
Balloon type	Super-pressure	Super-pressure	Super-pressure	SIRM
Balloon flight altitude	6-12 km	54 km	50-80 km	0.1-0.2 bar
Balloon diameter	30 m	7.6 m	8.7–19.8 m	72 m
Wing area	1 m ²	1 m ²	1 m ²	10 m ²
Tether length	3-6 km	10 km	10 km	10 km
Wing mass*	5 kg	10 kg	10 kg	50 kg
Tether mass**	2.5-5 kg	7.5 kg	5 kg	10 kg
Total floating mass	111 kg	202 kg	125-195 kg	208 kg
Wind shear	1-9 m/s/km	1.6 m/s/km	1 m/s/km	1.5 m/s/km
Cross-track velocity	0.2-1.25 m/s	1.5 m/s	0.5-0.9 m/s	1.0 m/s

* - preliminary estimate based on Earth StratoSail® TCS

** - preliminary estimate based on Earth analog

3.4 Microprobes

3.4.1 Scope

This section presents some thoughts on project architecture, sensor types, and vehicle design. The goal is to leverage measurements made by the balloon itself with measurements at other altitudes or on the surface, made by some deployable sensor package (“microprobe”). An important paradigm here is that these packages are at most a few hundred grams - requiring a significant divergence from conventional spacecraft thinking.

3.4.2 Project architecture

Of course, microprobes could be built by the prime contractor of the balloon vehicle itself. This is simplest, but misses some important programmatic opportunities.

Partnering, education and outreach on a mission of this type might be enhanced by outsourcing some or all, or parts of, the microprobes to, for example, various universities or international partners. At the risk of introducing some programmatic complexity, the political benefits could be substantial (by involving a wider geographical community in the project), and the technical risks ameliorated by soliciting more units than actually fly, - i.e. selecting the actual flight units competitively.

One possibility might be to design or provide a standard attach interface and telemetry system, but, subject to mass, volume, etc. constraints, permit the provider to introduce their own aerodynamic and/or payload design, with some probes falling quickly straight down, others falling slowly and yet others gliding some horizontal distance.

3.4.3 Sensors

Any sensor that is available on a wristwatch should be flyable - pressure, temperature sensors, radio receivers, magnetometers, UV flux sensors, simple cameras, etc. Corresponding sensor masses should be less than 10 grams. (Note that camera here means something like a webcam - fixed optics, no filter wheels, etc. - everything solid-state).

Suitable solid-state integration of dispersive optics (i.e. a fiber optic spectrometer) should be possible at this scale.

Conventional gas composition measurements (GCMS etc) will not be applicable. However, “E-nose” chemical-specific electrodes and fiber-optic sensors (for example, the MOX experiment on Mars-96 and MAUS on Beagle-2) would be attractive. Similarly, there are rapid ongoing developments in “GC-on-a-chip” microfluidics, such that, profiling of abundances of a small number of predesignated chemical species may be possible even with sensor masses of 10 s of grams. Solid-state water humidity sensors also come into this category.

Active sensors (radars, sonars, etc.) are unlikely to be appropriate.

3.4.3.1 Expendable sensors for water vapor profiling at Venus

The water vapor profile in the Venus atmosphere is of considerable scientific interest, yet there are significant discrepancies between prior measurements. Profiles at multiple locations could be obtained by balloons with altitude control or expendable microprobes (perhaps using parachutes or even wings to retard their descent) to resolve this issue. Sensor masses need be only a few grams.

Simple upward-looking photodiodes with interference filters could isolate flux at relevant parts of the optical spectrum – specifically, the strong water band at 940 nm, and continuum wavelengths on either side. The ratio of the in-band signal to the adjacent ones yields an estimate of the column mass (when convolved with the appropriate curve-of-growth, scattering effects etc) of water vapor above the sensor. Although one could equally envisage a fiber optic spectrometer or similar device (a large spectrophotometer on a Venera probe produced the data shown on Figure 3-38), the key information is contained in only a few wavelengths, so a simple solid-state 3-channel photometer lends itself to this application, and could be made little larger than a fingertip.

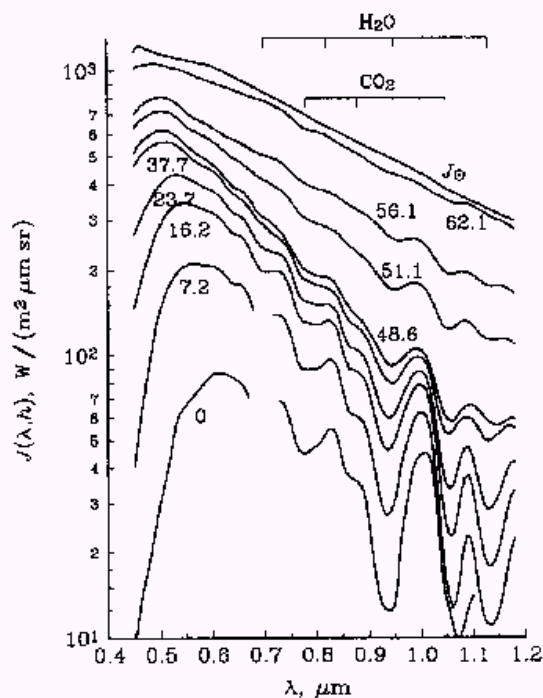


Fig. 1. Examples of the Venera 11 spectra of solar radiation scattered in the Venus atmosphere at some altitudes h (numbers near curves) above the ground

Figure 3-38 Venera spectra of scattered solar radiation

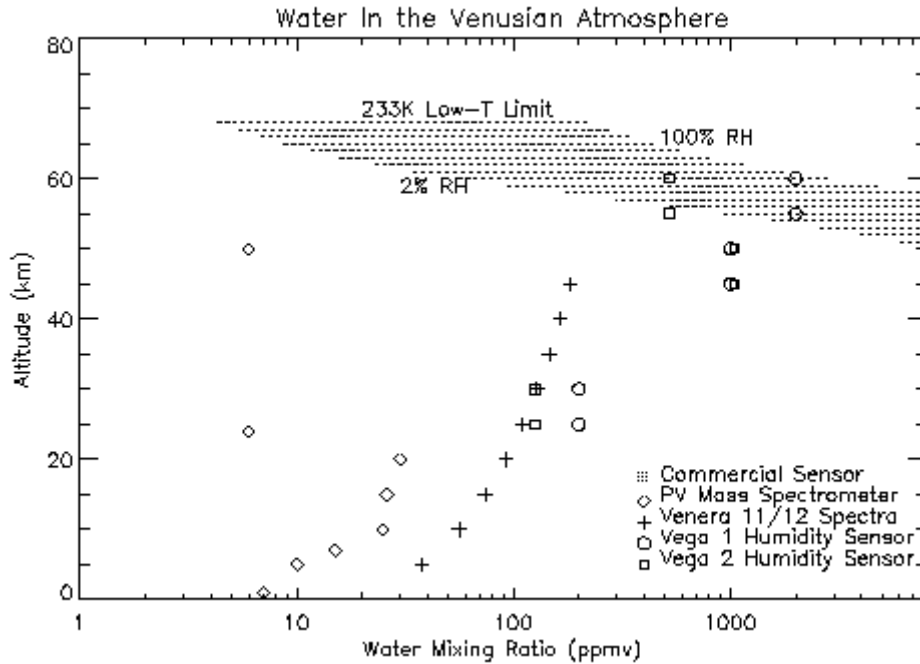


Figure 3-39 Water in the Venusian atmosphere

Another approach is to sense the local water vapor directly. Figure 3-39 (compiled from results in Donohue, et al.) shows the wide disparity in estimates of the water content of the Venusian atmosphere. The VEGA humidity sensors were fairly primitive (>1 kg) phosphorous pentoxide devices. The stippled region illustrates where modern capacitive polymer sensors should operate (these devices are about 5 mm in diameter and length – much like a typical LED or transistor – see Figure 3-40). Although they are limited by their temperature range to altitudes above about 50 km, such a sensor would be very easy to incorporate into an expendable probe, and would usefully complement the optical technique described earlier.

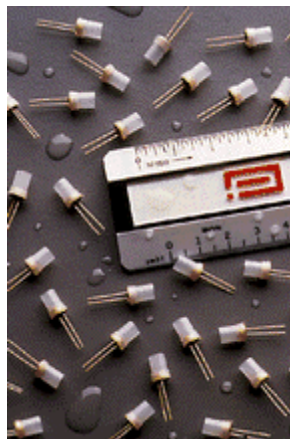


Figure 3-40 Capacitive polymer sensors

3.4.4 Subsystems

Since these are deployable sensors, the subsystems may be limited simply to power and data handling. However, mobility, guidance and possibly thermal control may also be involved. Note, however, that the small size means large surface-to-volume ratios, and thus the thermal time constant is very short - it is not possible to insulate the vehicle from its environment - it must instead be designed to tolerate it (an important consideration perhaps more for hot locations like Jupiter and Venus than for cold locations like Mars and Titan)

Since the duration of the expendable probe life is expected to be short, battery power is logical, and developments in cell phone power (specifically polymer-electrolyte, flat-pack batteries) are very pertinent. In some locations solar power may be attractive since for modest mission durations the energy per unit mass for a solar cell may become competitive with that for a battery, and the temperature limits for a solar cell may be more forgiving than those for a battery, when the vehicle is so small that it warms or cools to the ambient temperature rapidly.

As for communications, a modern cell phone is again a good benchmark - with low DC power levels, these can transmit digitally encoded audio, (several kbps) to ranges of several km. A microprobe could perform comparably over hundreds of km. (As a comparison, the DS-2 probes were, with a couple of watts, able to transmit 8 kbps).

Note that it may make sense to transmit in a burst mode, e.g., if solar power is used, the solar cell can trickle-charge a capacitor which is used to transmit, for example, one second out of every ten. Such circuits ("solar engines") are popular with the hobby robotics community since useful power can be applied to actuators - intermittently - even with very low power supply levels.

A timing transponder could be used to measure the range between balloon and microprobe, and suitable direction-finding antennas on the balloon would constrain their relative motion.

3.4.5 Vehicle Types

3.4.5.1 *Microprobes*

This is simply a scaled-down version of a conventional planetary probe (see R. Lorenz, Design Considerations for Venus Microprobes *Journal of Spacecraft and Rockets*, vol.35, 228-230, 1998) with perhaps an attempt to streamline the vehicle to enable a rapid descent, and to insulate it (for deep measurements at Venus or Jupiter)

3.4.5.2 *Glider*

A glider could simply be released to fly freely, with no directional control. It may therefore deviate significantly from a linear flight path, even without considering wind drift. A meandering or circling trajectory will not achieve as large a horizontal displacement from the balloon (presumably the goal of using a glider in the first place) than if it were actively held to a constant heading.

On hobby model gliders on Earth, this type of guidance used to be common before radio control systems became more widespread, compact and affordable. The method employed there was a

direct mechanical linkage between a magnet (acting as a high-torque compass needle) and the rudder.

Broadly similar schemes can be envisaged for other bodies. Magnetic control might be possible on Mars (although with the present knowledge of the magnetic anomalies, might be deterministic in terms of the direction actually flown - since the small-scale structure of the anomalies is not well-known, a glider locked to the field might fly in a constant, but arbitrary, direction)

Perhaps more promising is solar guidance - a simple photodiode sensor could be used to sense the bearing of the sun to generate an error signal with which to control that bearing to a specified value. The net heading will depend on the latitude and longitude of the glider and the sun, e.g., with both on the equator during afternoon, a commanded 90 deg azimuth will result in the glider pointing due south.

Another approach would simply be to maintain an inertial heading, i.e., use a gyro to sense heading. Very low mass gyros are available for model aircraft applications (S. Thakoor, C. Miralles and coauthors, "Cooperative mission concepts using biomorphic explorers", LPL XXX, paper 2029.).

NB NASA Ames has conducted 100,000 feet drop tests of gliders for Mars applications

3.4.5.3 *Sycamore-seed ('seedwing')*

When no particular horizontal direction is intended - only a retarded descent - an approach that has been proposed (with some merit, in this author's opinion) is a seedwing design. This is essentially an autorotating wing-body, patterned around nature's seedwings: these spin as they descend, generating lift to force descent at a reduced rate (S. Thakoor, C. Miralles and coauthors. "Cooperative mission concepts using biomorphic explorers", LPL XXX, paper 2029).

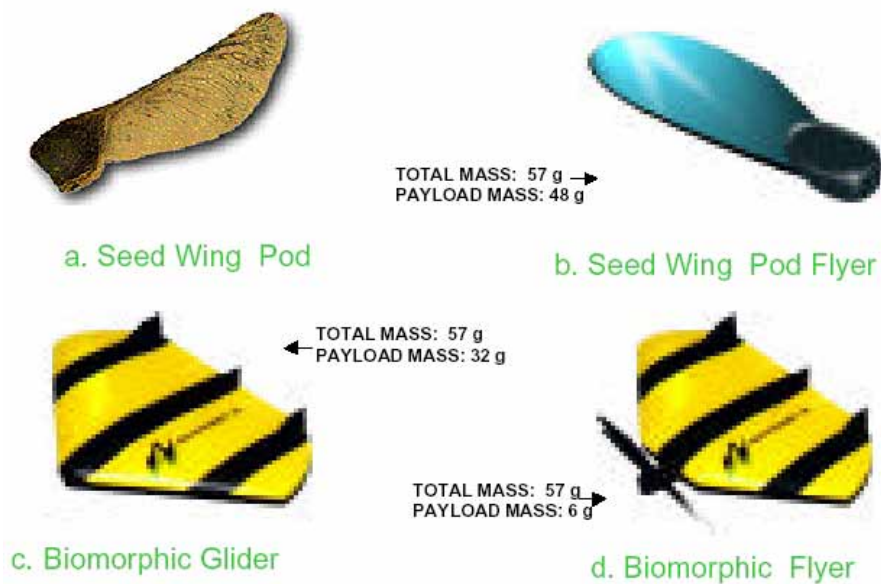


Figure 3-41 Biomorphic explorers

In strict mass/area terms, these are likely to be less efficient than deployable structures such as parachutes. However, their vastly reduced complexity (since they are monolithic, with no deployables, actuators etc. - or the onerous testing and qualification requirements for the same) makes them highly attractive.

Additionally, for atmospheric studies (e.g. net flux radiometry, all-sky cameras etc.) they have the added advantage that by avoiding a parachute, the full 2π steradian of open, unobstructed sky is available for study.

This advantage may also play double if solar power is contemplated: a flat-bladed design allows easy integration of a solar cell.

3.4.5.4 Miniature Helicopters

Conventional helicopters can now be miniaturized to a remarkable extent. Amateur hobbyists have succeeded in developing fully-functional radio controlled helicopters capable of free-flight under battery power, with a mass of 48 grams!

Such a vehicle would clearly be overkill for a simple descent probe measurement, but could be highly attractive for detailed investigation of specific surface sites, or even for surface sample acquisition and return to the 'mothership' balloon (see also www.planetinternet.be/pixel/)



Figure 3-42 Miniature helicopter Pixel 2000

3.4.5.5 *Unconventional Vehicles*

Various vehicles, designed around the low-Reynolds number paradigm of insect aerodynamics on Earth, have been proposed for the low-Reynolds number regime of the Martian surface. Flapping-wing designs (entomopters) and miniaturized wide-blade helicopters (mesicopters) have been explored, supported by NIAC.

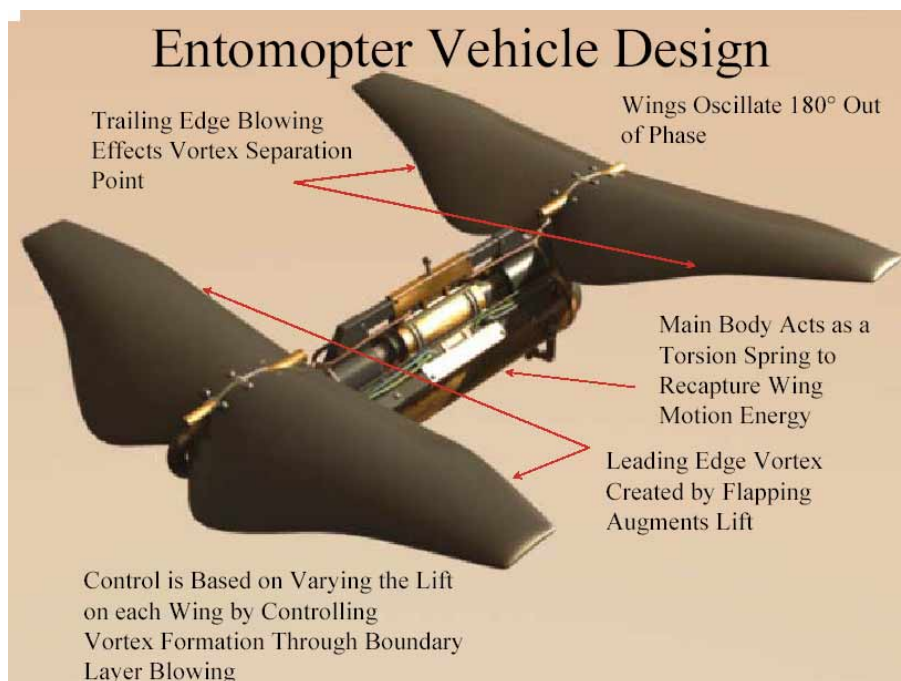


Figure 3-43 Entomopter Vehicle (A. Colozza, Northland Scientific/Ohio Aerospace Institute)

3.4.6 Tracking of Microprobes

3.4.6.1 Doppler Tracking

Radio tracking of microprobes might be expected to rely on the Doppler effect, which in turn relies on a precisely-known transmission frequency: the received frequency (i.e. the observed parameter) will differ from that by an amount called the Doppler shift. The accuracy with which this can be measured depends on the accuracy with which the transmit frequency can be predicted, i.e., its stability.

As an example, the stability exhibited by the quartz crystal oscillator in a digital watch (where the temperature is not regulated except perhaps by body heat) might be a few seconds per month, or about 1 part in one million. Controlling a radio signal to this precision would only allow velocity estimation of $c\Delta f/f \sim 300$ m/s - grossly inadequate for measuring planetary winds.

Ultrastable Oscillators (USOs) used on spacecraft for precision tracking use a variety of oscillators (e.g. Rubidium, as used in atomic clocks) although most typically are TCXO - temperature controlled crystal oscillators. Here the quartz crystal is in an insulated and temperature-controlled box, which increases the stability significantly. It should be noted that there is a basic long-term stability (as that of wristwatches above), which may be modest, but can be calibrated, e.g. by taking a frequency measurement before releasing the microprobe. There is also drift, which may occur over a variety of timescales - this, expressed as $\Delta f/f$ (often called the Allen Variance), has different values depending on the timescale τ considered. Typically the Allen Variance has a dependence on τ of the form $\tau^{-0.5}$ to τ^1 . As an example, to detect wind speeds of 1 m/s over a typical microprobe drop time of 3000 s requires $\Delta f/f$ of $(1/c)=3 \times 10^{-9}$. On the other hand, detecting the cm/s motions due to aerodynamic buffeting on second timescales, requiring $\Delta f/f$ of $(.01/c)=3 \times 10^{-11}$.

Note that Doppler measurements only give the line-of-sight motion - one cannot detect motion orthogonal to it, nor distinguish motion along the line of sight by the receiver from the transmitter (e.g. the balloon experiencing an updraft from the microprobe experiencing a downdraft.)

Precise frequency measurement of the received signal also requires a precision frequency reference on the receiving platform (which may be in this instance the balloon 'mother ship'.) That reference could be supplied internally by a separate USO.

Rubidium oscillators - more or less the present standard - have masses of around 1 kg and so cannot be realistically considered for microprobe application. Oven-controlled quartz oscillators can be modest in cost (<\$1000) and mass (<150g). It might be that a quartz oscillator that is not in an oven (and therefore cheaper, lower power and much lower mass) could be adequate, especially if its temperature were monitored. (The temperature coefficient of stability is -0.035 ppm/C².)

3.4.6.2 Ranging

A measurement that indicates some promise is ranging between the balloon and microprobe. This could be performed entirely passively on the part of the microprobe, simply by ensuring a strong radar backscatter, e.g. with a cube-corner reflector. However, this may interfere with the aerodynamic performance needed for a rapid descent, so a transponder may be required. This can be a very simple piece of equipment, to simply return a pulse signal when the interrogation pulse is received from the balloon. The return pulse may be tagged (e.g. by a modulated frequency) to uniquely identify the microprobe. This type of equipment is routinely used on aircraft for air traffic control, although for a microprobe, could be considerably miniaturized.

The time for the return pulse to be received by the balloon gives an instantaneous distance measurement between the balloon and the microprobe. If performed often enough (e.g. 1 or more times per second) motions due to wind gusts can be detected.

Again ranging only provides one-dimensional information - for a fixed balloon location, the microprobe may lie anywhere on a spherical shell defined by the range and movement on that shell cannot be detected.

Much more valuable than a single ranging measurement is a set of ranges to different microprobes - ideally one on the ground, known not to be moving. The simultaneous data would allow one to eliminate some of the balloon motion from the analysis. Similarly, multiple ranging measurements (e.g. from two or more balloons) to a microprobe would allow the three-dimensional descent path to be reconstructed.

3.4.6.3 Angle-Sensitive Links

To get around the nonuniqueness of a set of ranges in defining the descent path of a microprobe, one could also consider angular information recovered from the balloon. One possibility is a mechanically or electronically scanned directional antenna (like in old-fashioned radars) where the time an echo (or transponded signal) is received, indicates the target's azimuth or elevation. Another, more likely possibility is to use phase information from several antennas to determine interferometrically the angle to the source. This interferometric technique is straightforward to implement with no moving parts.

Even angle information with modest resolution would be useful - from 60km during a 1 hour descent, a 1 m/s wind will cause a drift of 3.6km, subtending an angle of 3 degrees or so. Such an angle would be trivial to detect, but the measured angle would be with reference to the vehicle (gondola) itself - additional, perhaps optical, measurements would be needed to reference that in turn to celestial or geographical directions.

3.4.6.4 VLBI

Interferometry can provide even the supreme angular resolution to track motion on Venus from Earth. The very small angles required to sense this in turn require large (continental-scale) separation distances between the receiving antennas - hence VLBI or Very Long Baseline Interferometry. VLBI using the Deep Space Network, plus other radio telescopes, allows

tracking from Earth with only modest on-board capabilities. It is however a very large commitment of valuable and oversubscribed DSN assets, and is thus unlikely to be sanctioned without a very strong scientific case (and an engineering case of why this technique must be used). It was used on the VEGA balloons, but this represented a one-off mission of only 2 days duration, and did so at a time when there were fewer demands on the DSN. In the 2008- time frame the DSN will be busy with several high-bandwidth Mars missions, as well as Cassini and other spacecraft. It seems unpromising to baseline VLBI for a set of dozens of microprobes, although augmenting some of them with VLBI might merit exploration on an experimental basis.

3.4.7 Conclusions

A variety of configurations of vehicle are possible, able to transmit ~1 Mbit of data over an hour or so over several tens to one or two hundred km, to the balloon, with masses of 0.1-1kg. The scale involved suggests scope for imaginative thinking.

An investigation of the frequency stability of radio links for miniaturized hardware, potentially with large temperature excursions as might be expected on a microprobe, would be an important part of assessing the scientific potential of microprobe Doppler tracking measurements. Ranging transponders on the microprobes, coupled with an interferometric antenna array on the balloon, may offer the best performance for realistic costs and robust implementation.

4 DARE Architecture Potential Applications

4.1 Introduction

Based on the review of the scientific objectives published by the National Academy of Science (“An Integrated Strategy for the Planetary Sciences 1995-2010”, Space Studies Board, National Research Council, Washington, DC, 1994; “The Future of Solar System Exploration 2003-2013” The Astronomical Society of the Pacific, San Francisco, CA, 2002; “New Frontiers in the Solar System: An Integrated Exploration Strategy”, National Research Council, Washington, DC, 2002) and input from planetary science experts participating in the study, we identified potential science and engineering objectives for DARE planetary exploration architecture.

4.2 Venus

4.2.1 Science Requirements and Priorities

The Magellan spacecraft provided detailed radar imaging of the surface of Venus, while Venera, VEGA and Pioneer probes, as well as telescopic observations provided a wealth of information on atmospheric structure and circulation and composition of the surface. However, many questions pertaining to atmospheric composition, circulation and evolution, interaction between the atmosphere and surface, chemical and mineralogical make-up of the surface, and processes in the interior remain unanswered. The objectives and measurements for future exploration of Venus are:

- Measure longitudinal distribution of atmospheric constituents (H_2 , O_2 , sulfur, and halogen compounds) and properties to determine the chemical processes that maintain stability of the CO_2 atmosphere.
- Measure the isotopic ratios of the reactive elements H, C, N, and O and of the noble gases to a minimum accuracy of 10% in the atmosphere to enable meaningful comparisons with elemental compositions observed in the Sun, in meteorites, and in other planets. In the case of $^{13}C/^{12}C$, $^{18}O/^{16}O$, $^{15}N/^{14}N$, and D/H-ratios for isotopes in the major molecular species-the requirement increases to an accuracy of 1%.
- Measurements of seismic waves as a way to probe the planet interior (will be complicated by survivability of surface stations under high surface temperatures and pressures).
- *In situ* surface heat flow measurements.
- Identify elemental and mineral composition of the crust (regional analyses on scales of a few to a hundred kilometers).
- Measurements of atmospheric flow properties within the lowest two scale heights of the atmosphere (between the surface and about 30 to 40 km elevation) to study the momentum transport processes that can maintain the atmospheric rotation. The required velocity precision is 0.1 m/s, (an order of magnitude better than previous measurements), and a horizontal sampling interval smaller than the planetary radius.

- Measure upward and downward radiation fields as a function of height and frequency. Determine the concentrations of radiatively important trace gases.
- Simultaneous determinations of atmospheric temperature (relative temperatures to better than 0.1 K near the surface) and velocity in order to establish heat fluxes.

4.2.2 Model Atmosphere

Venus GCMs have difficulties in simulating the superrotation of the atmosphere of Venus, thus we developed a simplified engineering model of Venus circulation. The atmosphere of Venus is much less chaotic than the atmospheres of fast rotating planets like Earth and Mars, which allows for the development of a simple model of atmospheric circulation. The model is based on available observations and the model of Newman and Leovy, 1992. Figure 4-1 shows time average velocity fields in solar-fixed reference frame, at cloud top (from Gierasch et al, 1997). Contours of constant zonal winds (in m/s) are on the left and contours of constant poleward winds (in m/s) are on the right. Panels (A) and (B) show calculated results from Newman and Leovy, 1992, and panels (C) and (D) give the zonal and meridional components from measurements by Del Genio and Rossow, 1990.

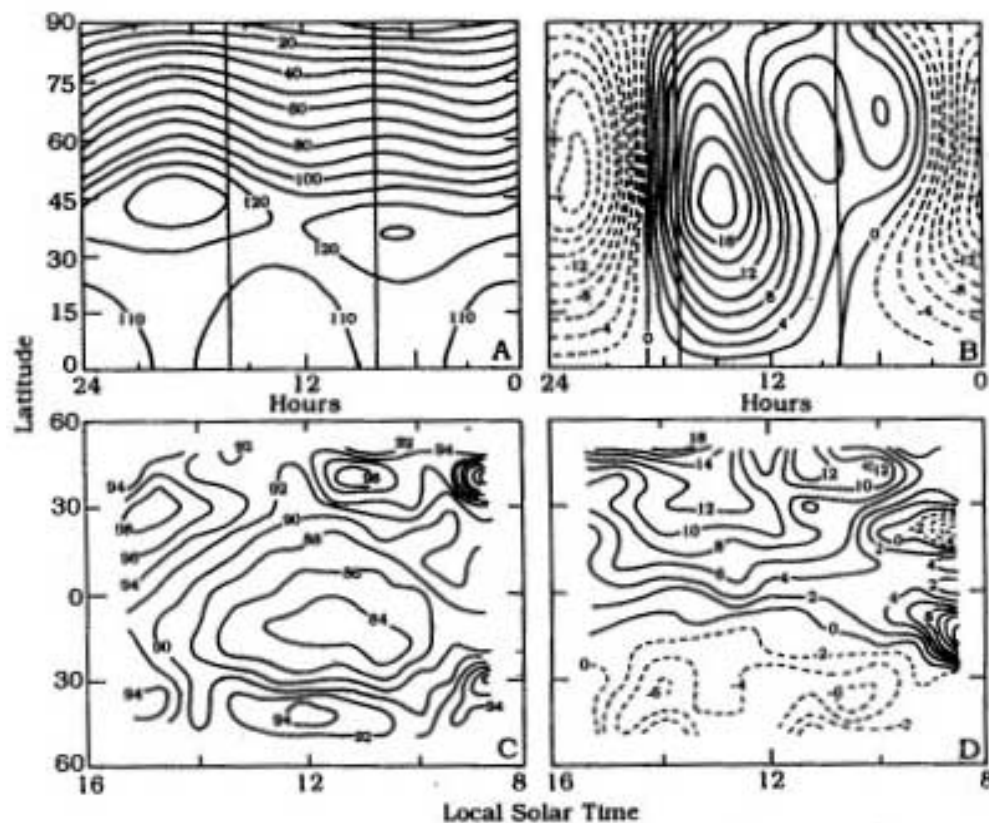


Figure 4-1 Time average velocity fields (m/s) in solar-fixed reference frame, at cloud top (from Gierasch et al, 1997).

We assume that the zonal winds are constant from -45 to 45 latitude and decrease to 0 m/s from 45 degrees poleward (see Figure 4-2). Vertically, the zonal winds change from 0 m/s at 10 km

and below to -80 m/s at 60 km (cloud top) (based on Venera probes descent profiles). The meridional wind pattern (panels B and D on Figure 4-1) is modeled with a product of cosine of latitude and sine of longitude (see Figure 4-3, dotted lines indicated negative (southward) winds). The meridional pattern rotates relative to the longitude with Venus sidereal period of ~116 d). Vertically, the meridional winds increase as $\rho^{-0.5}$, where ρ is density of the atmosphere, in accordance with the Venus probes measurements (Figure 3-14).

Meridional winds calculated by Newman and Leovy are dominated by solar tides with a small contribution from Hadley circulation. The observed meridional winds at cloud tops are theoretically consistent with both the Hadley circulation and the tidal winds. There is little evidence for Hadley cell in vertical profiles of meridional winds (Figure 3-14). There are, however, no doubts that the tidal component exists. The Hadley circulation adds poleward component to meridional winds on both day and night side of the planet. If the Hadley component were strong, there would be no reversal from poleward to equatorward motion in meridional wind flow. To answer the question of the relative strength of Hadley and tidal parts of the meridional circulation, the meridional winds on the night side of Venus need to be observed in detail.

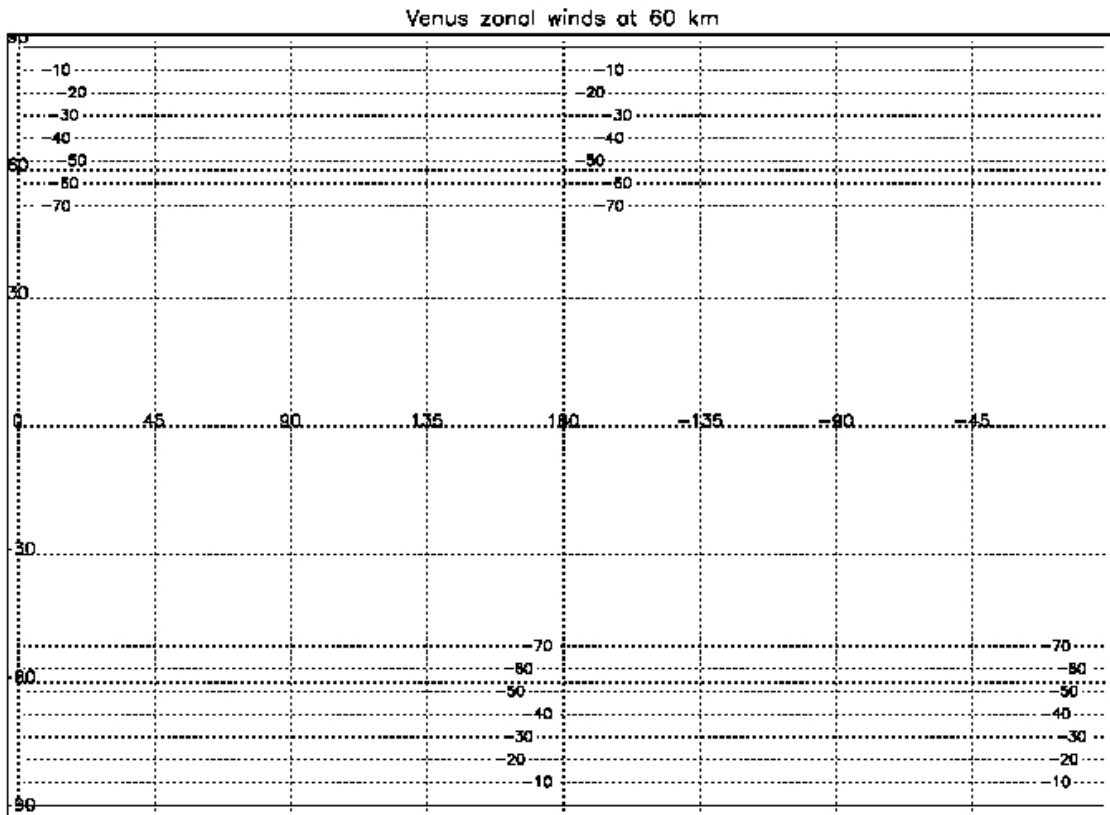


Figure 4-2 Model Venus zonal winds at 60 km (m/s) on a latitude-longitude grid

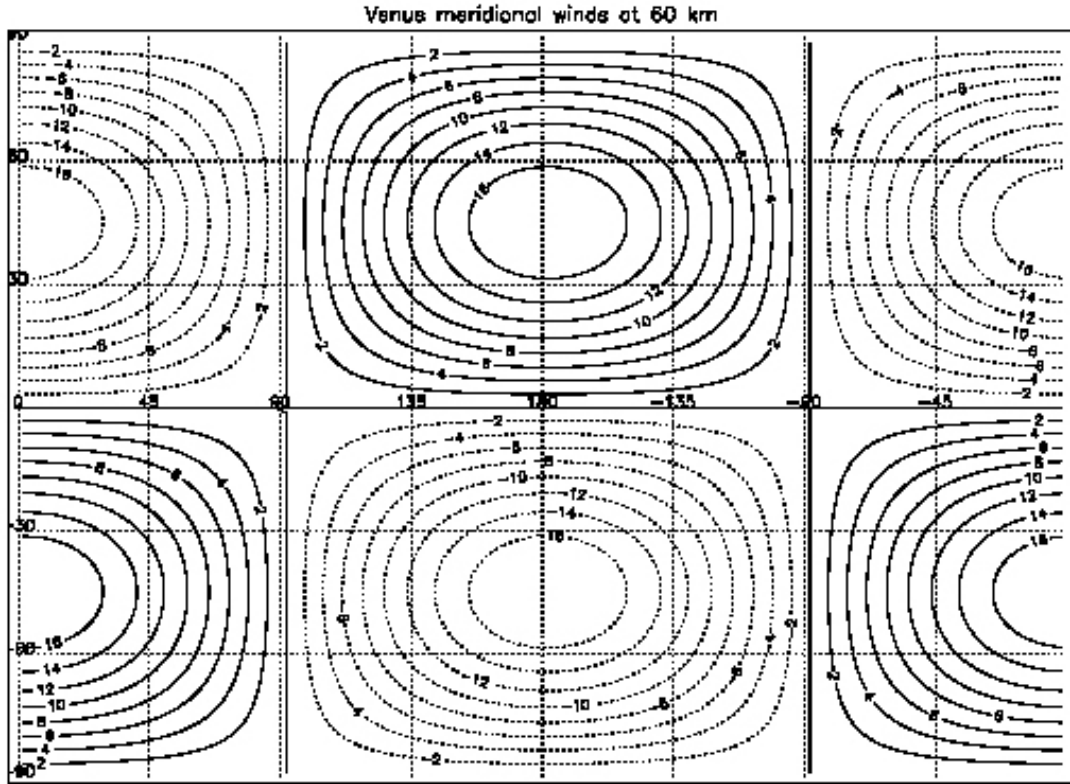


Figure 4-3 Model Venus meridional winds at 60 km (m/s) on a latitude-longitude grid

The question of the relative strength of Hadley and tidal parts of the meridional circulation has direct implications for balloon trajectories on Venus. If the meridional wind pattern is dominated by tides, as shown on Figure 4-3, the balloon's path can be effectively controlled with limited available control (see Section 4.2.3). If Hadley circulation dominates the meridional winds, the available limited control capabilities of the TCS (1 to 2 m/s) would not be sufficient to control the balloon above 30-40 km (see Figure 3-14), because the winds would steadily pull the balloon towards the poles. There are, however, other options to control the balloon in this case (see discussion in Section 4.6).

Our model does not take into consideration the propagation of thermal tide through the atmosphere. Because of the finite time that it takes for the heat to propagate through the atmosphere, the general wind patterns at different atmospheric levels look like the one shown on Figure 4-3, but are "shifted" relative to each other. This "phase shift" manifests itself as oscillations in the vertical winds profile (see Figure 3-14). This fact, however, does not affect our results at this preliminary analysis stage, because the available control velocity in balloon trajectory simulations is treated as being constant and primarily defined by the difference in zonal winds at the balloon altitude and the TCS altitude. In reality, the control velocity is dependent on the magnitude and direction of the relative wind at the wing altitude. The tide propagation changes the angle between the winds at the balloon and wing altitudes (angle α in 3.3.4.4) and thus affects the TCS performance. This effect will be taken into account in future analysis.

4.2.3 Potential Applications

Based on science and engineering objectives outlined in Section 4.2.1 we envision the following possible scenarios.

4.2.3.1 In Situ Atmospheric Sampling

A DARE platform with onboard mass spectrometers and UV and IR spectrometers for trace gas profiling visits various regions of the atmosphere and constructs complete inventory of the atmospheric constituents.

4.2.3.2 Surface Seismological and Meteorological Station Network

A DARE platform delivers several surface stations (15 to 20 for meteorology, 8 or more for seismology) to the locations that span latitude, longitude, and elevation contrasts. DARE platform overflies the stations to collect the data and relay it to Earth or to the orbiter. The goals here are to deliver the probes to preset target locations (that could be sufficiently large) and then to overfly these locations several times within a short distance.

4.2.3.3 Surface and Subsurface Probes

A DARE platform delivers probes that perform elemental, compositional, chemical and chronological studies to selected sites. This application might not require a subsequent overfly, depending on how fast the measurements are made and how long the DARE platform can stay within a communication range.

To analyze these types of scenarios one can randomly choose several points on the planetary surface (to represent the sites of interest) and test the DARE platform's ability to fly within a certain radius from those locations. One then can test how many times DARE can revisit these sites assuming a 100-day mission

4.2.3.4 Potential Landing Site Reconnaissance

DARE platform visits several pre-selected potential spacecraft landing sites for high-resolution imagery. An onboard high-resolution camera or a gliding probe provide images revealing 1 to 10 cm scale objects on the surface.

4.2.3.5 Monitoring Global Circulation

Several DARE platforms simultaneously monitor winds and atmospheric parameters in different regions of the atmosphere (equatorial, midlatitude, polar). Another approach is to have one platform visiting different atmospheric regions. Single platform approach is suitable for Venus because a platform would be able to sample both day and night sides of the planet during one Venus day. The platforms can carry suites of in situ instruments at the gondola or along the TCS tether, and deploy meteorological dropsondes.

To test this scenario a small constellation (3 or 4) of DARE platforms maintaining their respective “patrol zones” (40° to 60° wide latitudinal corridors) throughout a 100-day mission or a single platform achieving global coverage can be simulated.

4.2.3.6 *Monitoring Volcanic Activity*

A DARE platform can float over the regions of potential volcanic activity and monitor atmospheric chemistry or thermal radiation from below to detect signs of active volcanism. Trajectory analysis of such application would test how quickly and accurately the DARE platform can be maneuvered towards randomly appearing extended target.

4.2.4 Trajectories

We performed numerical simulation of balloon trajectories on Venus. For these simulations we assumed that the balloon speed is the sum of the wind speed and the prescribed control velocity.

Trajectories of two uncontrolled balloons at 60 km are shown on Figure 4-4. The trajectories start at 180° E and 15° and 45° N respectively. The zonal winds carry balloons westward – to the left. The balloons circumnavigate the planet several times and thus there are many overlaps between the successive trajectories of the balloons. The sinusoidal pattern of the trajectories is due to the meridional winds changing direction on the night and day side of the planet. The successive trajectories are shifted relative to one another because of the slow rotation of the solar-fixed wind pattern.

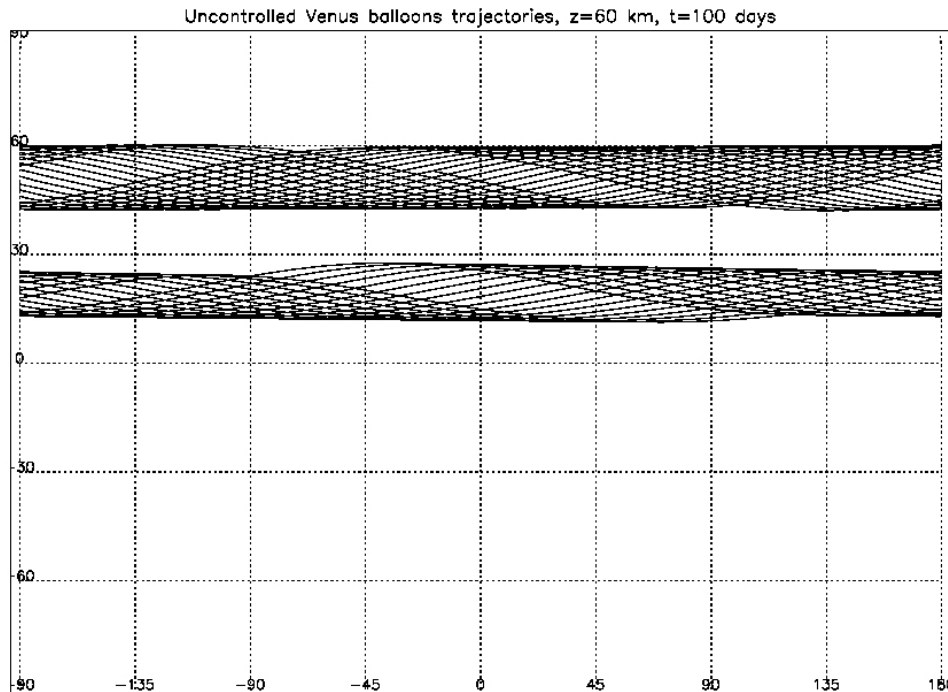


Figure 4-4 Trajectories of 2 uncontrolled balloons at 60 km at Venus

Figure 4-4 shows that uncontrolled balloons would sweep a corridor about 15° wide during a 100-day mission.

The controlled balloons, on the contrary, have much more "freedom". Figure 4-5 shows trajectory of a controlled balloon at 55 km. The objective of the simulation is to analyze the coverage that can be achieved with the controlled balloon at Venus. The maximum control velocity is 1 m/s and can only be directed sideways relative to the wind direction. The balloon starts at 180° E and 30° N and is directed south. During a 100-day simulation the balloon is able to visit latitudes between 45° N and 45° S. The balloon completes almost 18 circumnavigations.

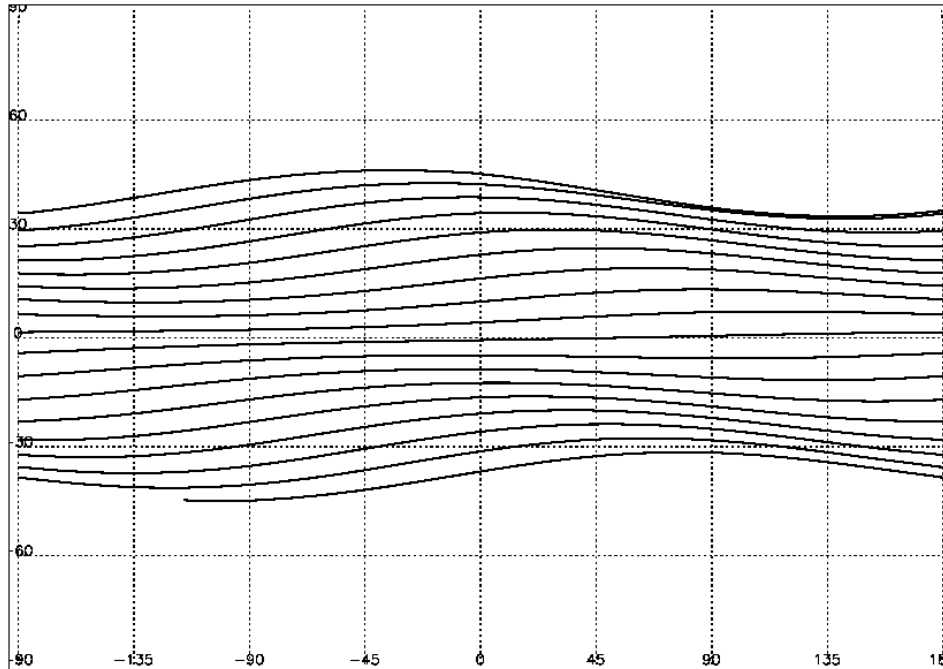


Figure 4-5 Venus DARE balloon trajectory at 55 km

We also performed simulations of a target overflight. In this simulation the DARE balloon is directed to fly over the surface target. As soon as the DARE balloon flies over a target, the next target is "turned on". We use a simple algorithm to perform targeted simulations. The algorithm does not assume knowledge of the flow field to target the balloon. The only assumption we make is that the flow field within certain latitudinal band does not change significantly for a period of one circumnavigation. We then direct the balloon towards the latitude of the target and calculate the range to the target when the balloon crosses the longitude of the target. Control velocity in latitudinal direction is calculated by dividing this distance by the period of circumnavigation. We vary the size of the targets to see how close to the target the balloon can be directed.

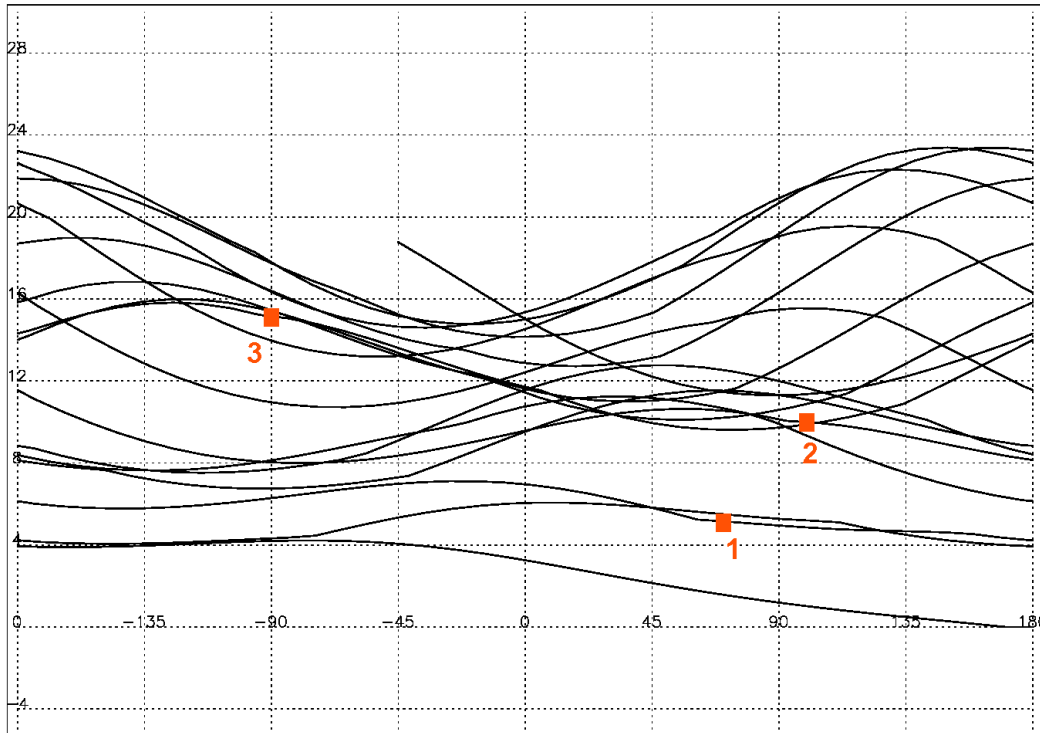


Figure 4-6 Venus DARE multiple target overfly

The result of these simulations is shown on Figure 4-6. Even with such a simple algorithm a balloon can be directed to fly very close to a target. In this example there are three targets indicated on the plot as 1, 2 and 3. Target 1 is “turned on” first, when the balloon flies over it, target 2 is “turned on”, and so on. In this simulation the balloon is directed to fly within 26 km from the targets. The balloon is started from the equator at 180° E and is able to fly over 3 targets during the 100-day simulation. It takes 3, 4 and 8 circumnavigations to fly over target 1, 2 and 3, respectively. It is easier to perform targeting closer to the equator (target 1), where meridional winds are weak and comparable to the cross-track velocity provided by the TCS. In the midlatitudes (target 3) the meridional velocity is the largest and thus control is the weakest. Four point targets in midlatitudes (not shown) can be overflown within 150 km (horizontal distance) during 100-day simulation.

The targeting can be probably significantly improved with the Advanced TCS. Employing the ATCS can reduce the number of circumnavigations required to fly over a target site and allow to fly over smaller targets.

4.3 Titan

4.3.1 Science Requirements and Priorities

Three sets of objectives may be defined, considering three altitude regions. Various balloon concepts may be able to operate in one or more of these regions. Deployable sensors may allow to achieve objectives in several altitude regions.

50-80km altitudes

This is the lower stratosphere of Titan, situated beneath most of the organic haze. The region is characterized by strong zonal winds, in excess of 50 m/s (see Figure 3-23, corresponding pressure levels are from 7.6 mbar to 1.7 mbar), so circumnavigation takes about 3.5 days at the equator, less at higher latitudes. This region features steep temperature gradient, from around 72 K at 50 km to 120 K at 80 km (see Figure 3-20). Condensation of many organic species occurs in this altitude range. These are the altitudes above which most cosmic rays are absorbed.

Objectives and measurements:

- Measure winds at high altitudes via autonomous navigation and/or tracking from ground or orbiter.
- Measure gas abundances of major species as a function of the altitude (using TDL absorption spectrometer or other compact instrument - full GCMS (Gas Chromatograph - Mass Spectrometer) not required).
- Investigate condensation processes via side/up-looking radiometer (to measure light scattering by condensate mist layers - see DISR instrument on Huygens) or/and a nephelometer.
- Investigate cosmic ray absorption via simple, compact radiation detector.
- Wide-area down-looking imager for broad mapping, weather monitoring and change detection, i.e. simple webcam type optics. (This region is below most of the haze, although Rayleigh scattering and methane absorption beneath will compromise image contrast and resolution at some wavelengths).

14-40 km altitudes

The case for operation in the 14-40 km altitude range is less obvious - there is likely to be convective activity in this range (as also below this altitude), but icing presents a potential hazard and most science goals are better addressed either higher or lower than this range.

1-14 km altitudes

This is the region of the lower troposphere. The region is characterized by modest zonal winds, with some meridional component due to tides, topography interaction with zonal flow, etc. Occasional convective events are also possible within the region.

Objectives and measurements:

- Detailed geomorphological studies via side- and down-looking imagers, possibly with some spectral capability to aid in classifying surface composition units.
- Ethane lake depth measurement, and subsurface structure profiling via simple radar sounder.
- Meteorological monitoring - autonavigation wind measurement, pressure, temperature and methane humidity measurement (simple sensor). Cloud and mist studies via side/up-looking imager.

1-0 km altitudes

The near-surface region of the Titan atmosphere is characterized by generally weak winds. Tidal winds and boundary layer effects could be significant. No strongly preferred wind direction.

Objectives and measurements:

- Same as for 1-14 km plus:
- Surface chemistry analyzer (and sample acquisition system) (Instrument technology still TBD, but surface chemistry has been identified as a major goal by Prebiotic Material in the Solar System CSWG).
- Radiation sensor to carbon-date surface deposits.
- Deployable surface instrumentation (e.g. seismometer).

4.3.2 Model Atmosphere

Titan and Venus atmospheres are considered to be similar, as it appears that both atmospheres are in a cyclostrophic flow regime, characteristic of slowly rotating planets. In a cyclostrophic flow the gradient of geopotential in the atmosphere is balanced by the centrifugal force acting on the zonal wind, rather than by the Coriolis force, as in the geostrophic flow. The model of the Titan atmosphere is based on the model of the zonal circulation by Flasar et al. (1997), to which we add the model of tidal winds (caused by gravitational pull of Saturn) by Takano and Neubauer (“Tidal winds on Titan caused by Saturn”, *Icarus* **158**, 2002, henceforth TN). The Hadley circulation is thought to be nonexistent on Titan so that the tidal winds are solely responsible for the meridional component of the general circulation in our model. Zonal winds in the TN model are much weaker than the zonal winds suggested by temperature gradient measurements (i.e. Flasar model), thus we decided to combine the zonal winds from the Flasar model with the tidal winds from the TN model.

We use analytical approximation for the zonal winds. The Flasar model gives zonal winds for the case when the observed horizontal temperature gradient is doubled. Flasar model thus gives an envelope of zonal winds. We recalculate the zonal winds in the Flasar model back to the case of the observed temperature gradient. Since the zonal winds are approximately proportional to the square of the temperature gradient, we simply divide the Flasar winds by the square root of 2. The model zonal winds are shown on Figure 4-7.

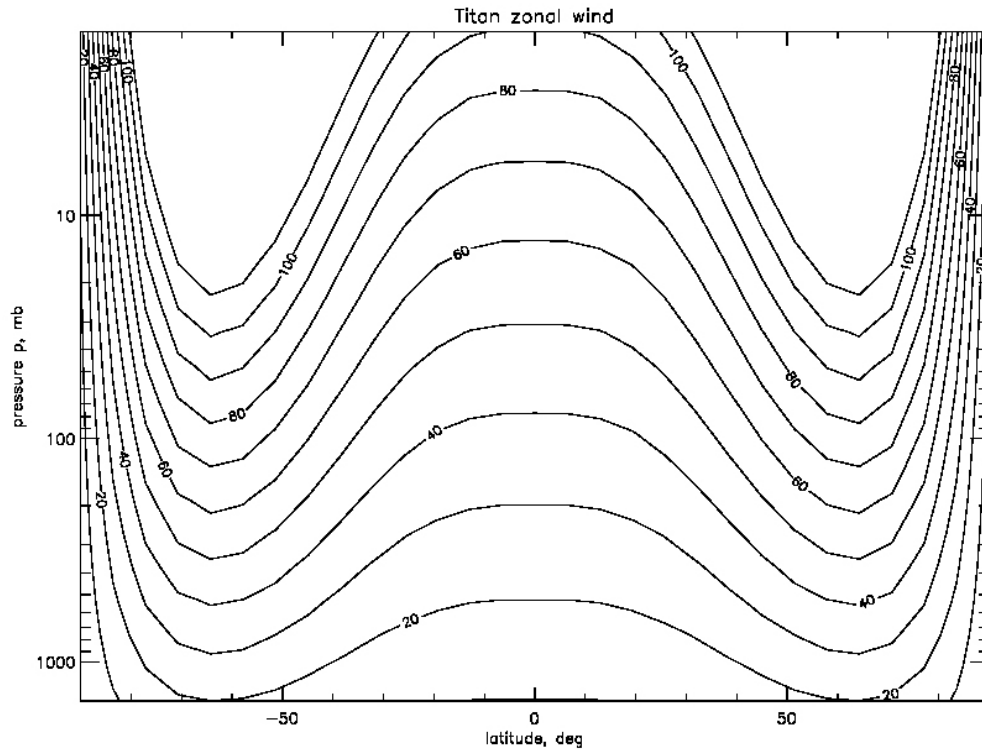


Figure 4-7 Model Titan zonal winds

Figure 4-7 shows the meridional cross-section of the Titan atmosphere with the contours of the constant zonal winds.

We approximate the tidal winds with a product of trigonometric functions, in a manner similar to that of Venus solar tide wind model. This approach gives a very good agreement with the TN data. Figure 4-8 illustrates the agreement between the simple model and the model of TN (Figure 4-9). The zonal winds in this simple model test were not those derived from Flasar model, but the much weaker winds chosen to match the zonal winds in TN. The biggest arrows on Figure 4-8 and Figure 4-9 correspond to wind speeds of the order of 14 m/s. The tidal wind pattern rotates around the planet with a period of 32 Earth days.

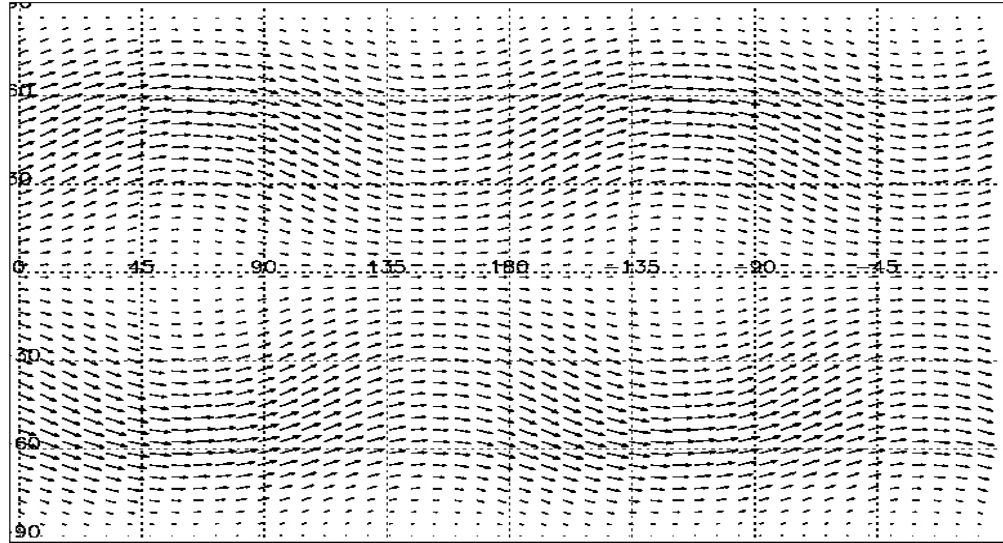


Figure 4-8 Model Titan winds at 40 km

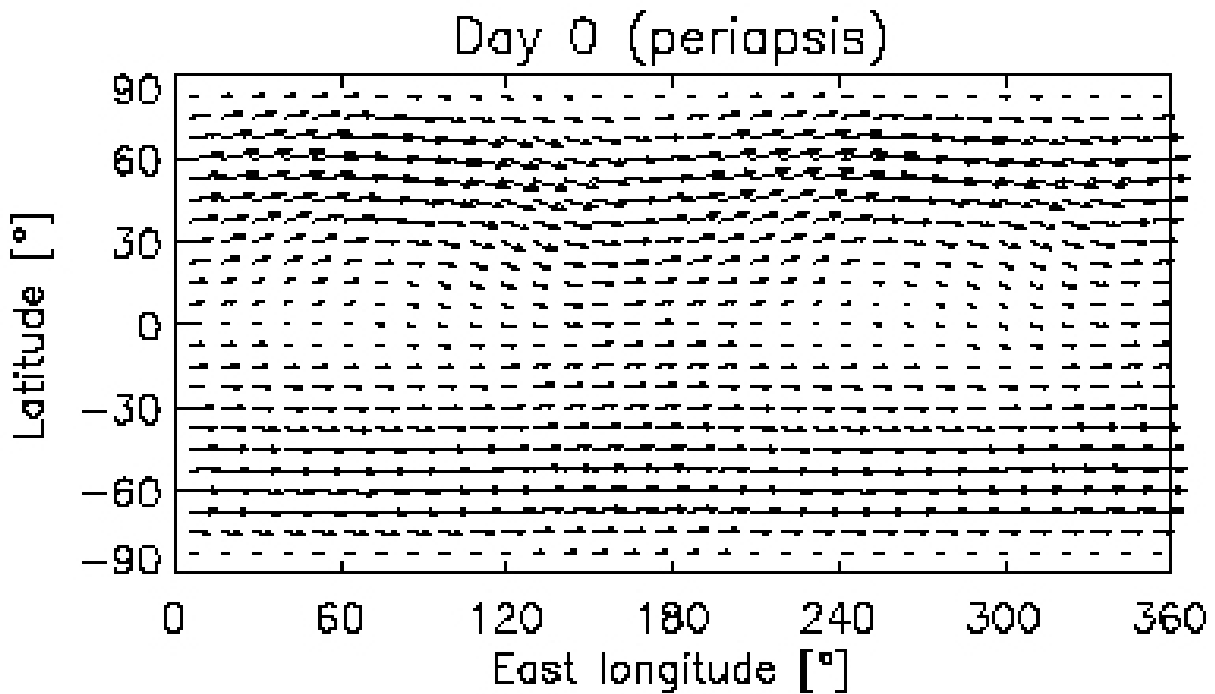


Figure 4-9 Titan winds at 40 km from TN

We approximate the vertical variations of the tidal winds in TN (Figure 4-10) with the linear dependences between 40 and 60 km, and between 60 and 100 km. The maximum meridional winds in this region on Titan are at about 40 km – 4 m/s. The minimum winds are at 60-70 km altitude – about 1 m/s. The control velocity calculated for Titan is comparable with the strength of the meridional winds at 60-70 km altitude, which means that the balloon at this altitude on Titan can “fight” the meridional winds.

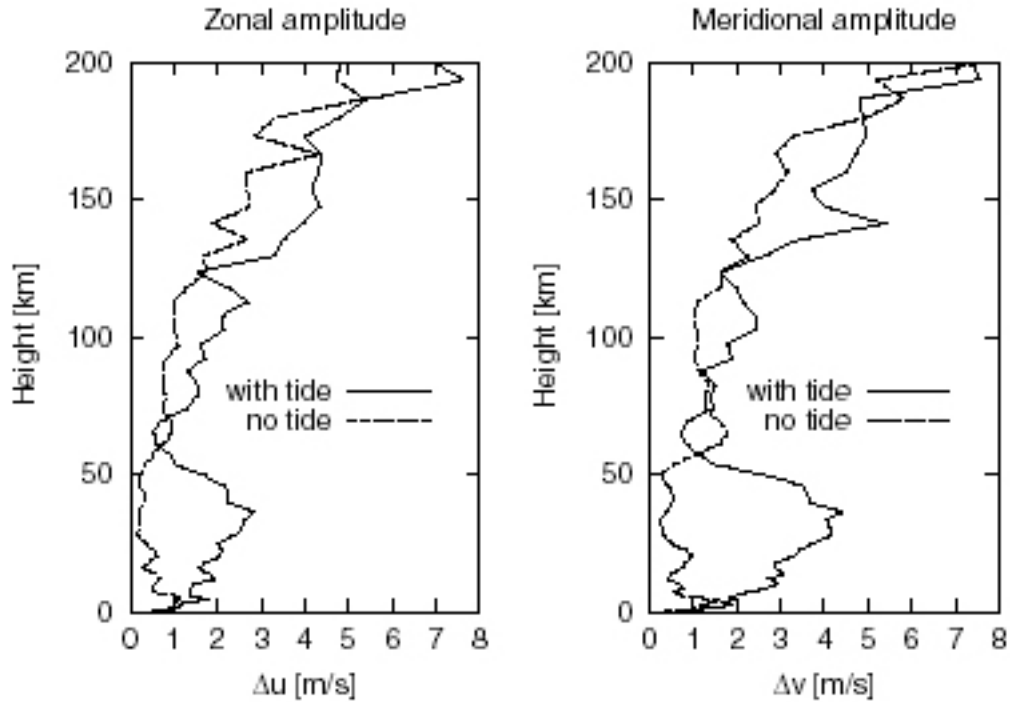


Figure 4-10 Vertical profile of the longitudinal amplitude of zonal and meridional wind at 60° N simulated by the GCM (from Takano and Neubauer, 2002)

4.3.3 Application Scenarios

It seems that the majority of measurement identified for Titan (Section 4.3.1) can be made from a DARE platform above 50 km altitude deploying surface and atmospheric probes.

The application scenarios for Titan are essentially the same as for Venus, except that volcanic activity monitoring scenario is not applicable.

4.3.4 Trajectories

Trajectory of an uncontrolled balloon at 80 km is shown on Figure 4-11. The trajectories start at 180° E and 45° N. The zonal winds carry the balloon eastward – to the right. The balloon circumnavigates the planet several times. Because the meridional winds are very weak, all trajectories collapse into one on Figure 4-11. The uncontrolled balloon at Titan would observe a very narrow latitudinal band.

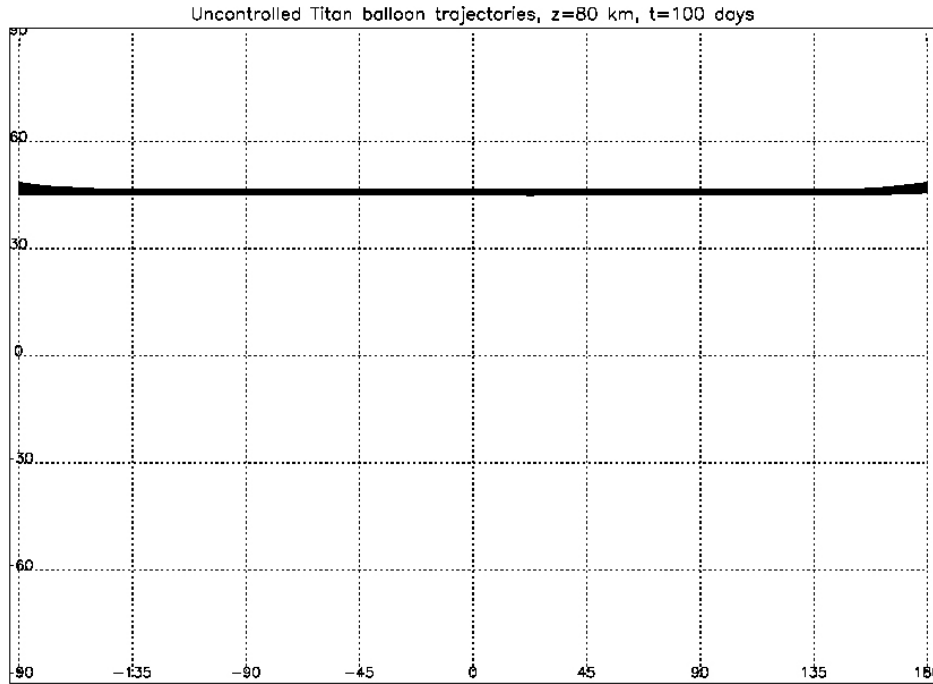


Figure 4-11 Uncontrolled balloon at Titan

Figure 4-12 shows the trajectory of the controlled balloon at Titan. The red arrow indicates the direction of motion. Start and Finish indicate locations of the balloon at the start and at the end of the simulation.

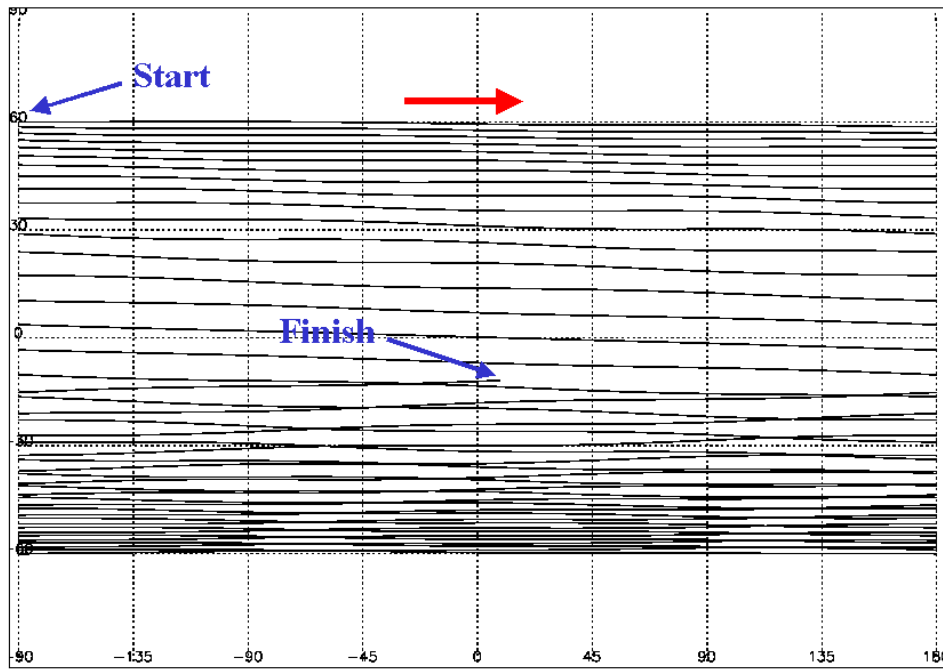


Figure 4-12 Titan DARE trajectory at 60 km

The maximum control velocity in this simulation is 0.9 m/s and it can only be directed sideways relative to the wind direction. The balloon is started at 180° E and 60° N. The balloon is directed to “sweep” the corridor between 60° N and 60° S. After touching 60° N it is directed south. After reaching 60° S it is directed north again. By the end of the 100-day mission the balloon is able to reach the 60° S and to return to about 10° S. This analysis shows that balloon control with the proposed TCS is sufficient to observe most of the planet and greatly expands the capabilities of a single balloon.

4.4 Jupiter

4.4.1 Science Requirements and Priorities

In defining the science objectives, it is useful to review the results of the Galileo probe, which is the only terrestrial spacecraft to have entered the atmosphere of Jupiter or any giant planet. The probe carried instruments to measure temperature, pressure, composition, clouds, sunlight, infrared radiation, radio emissions from lightning, and winds, all as functions of depth. The Doppler shift of the probe’s radio signal determined both the mean wind and the turbulent fluctuations. The probe was designed to operate and transmit data to a pressure of 10 bars. It exceeded its design specifications and operated at least to 24 bars, when the probe signal was lost (Young et al. 1996, Young 1998 and 14 accompanying articles).

Like any successful planetary mission, the Galileo probe produced several big surprises. The winds increased with depth in the 1 to 5-bar range and then remained constant. The expected water cloud, with base at 6 ± 1 bar, was absent. Water vapor, which was expected to be the third most abundant molecule after hydrogen and helium, was present at 1% of the expected concentration above the 6 bar level but was gradually increasing with depth when the probe signal was lost. Other condensable gases NH_3 and H_2S behaved similarly, but their elemental abundance ratios N/H and S/H leveled off to values about 3 times the solar ratios. Carbon as CH_4 and the noble gases Ar, Kr, and Xe also were present at ~ 3 times the solar values. These results may be peculiar to the spot that the probe went in, which was known from Earth-based observations to be the crest of an equatorial wave and an unusual cloud-free zone. Knowing the winds below the clouds is essential if we are to understand the longevity of the Jupiter’s weather patterns, including the Great Red Spot (GRS), which is at least 300 years old. Knowing the water abundance of the deep atmosphere is essential if we are to understand how Jupiter and the other giant planets formed, since water ice is the vehicle that delivered volatile elements to Jupiter and the inner planets, including Earth. Yet the atypical nature of the Galileo probe site may have frustrated our efforts to answer these questions.

The solution, therefore, is to send probes to a variety of sites, including cloudy zones and cloud-free zones, turbulent regions and quiescent regions, jet streams, storm centers, and regions in between. Even 2 or 3 probes that avoided the latitude of the Galileo probe would be valuable. The DARE platforms would be an ideal delivery vehicle for these probes. They could change latitude by hitching a ride on one of the circulating currents (Smith and Hunt 1976, Rogers 1995), which connect an eastward jet at one latitude with a westward jet nearby. For instance, the GRS blocks the eastward flow impinging on it from the east at 19°S to recirculate westward at latitude 23°. The GRS itself extends from 17°S to 23°S and carries material around its periphery

in 7-10 days. A balloon with the ability to tack at an angle of a few degrees off the wind direction could use these currents to visit most of the major types of weather systems on the planet.

Thus, the goals of the DARE platforms are the same as those of the Galileo probe, but to repeat the measurements at a variety of sites (2 or 3 minimum) that represent the major types of weather systems. Winds and water are the highest priority. The DARE platforms can serve as a data relay for the relatively weak probe signals. Assume that the balloon drops off a probe that descends 200 km in one hour to the ~ 30 bar level. Even if the horizontal wind increased by 100 m s^{-1} , so that the balloon and the probe were drifting apart at this speed, the probe would only be 360 km away from the probe in the horizontal direction and 200 km away from the probe in the vertical direction. This is much better than when the relay is an orbiting satellite that quickly gets out of range or goes over the horizon. This is what happened to the Galileo probe when its signal was lost at 24 bars.

The prioritized objectives and measurements are:

- Probe the atmosphere to 100 bars at three locations - a belt (cyclonic band), a zone (anticyclonic band), and a large anticyclonic oval like the Great Red Spot;
- Determine the abundance of water and ammonia with a factor of 2 uncertainty, e.g., O/H in the range 2-4 times the solar value;
- Measure the zonal winds as a function of depth with $\pm 10 \text{ m/s}$ uncertainty;
- Measure the temperature profile to an accuracy sufficient to distinguish between moist and dry adiabats;
- Determine the location and optical thickness of cloud layers;
- Measure sunlight and infrared fluxes.
- Measure the profiles of the vertical mixing ratios of trace chemical species (e.g., CO and N_2) that can be used to infer both vertical mixing and convection rates and the relative importance of photochemistry to thermochemistry in the troposphere. Also measure the C/H, N/H, and O/H ratios as a function of altitude to understand the cosmochemical origins of the Jupiter atmosphere.

4.4.2 Model Atmosphere

The Jupiter model atmosphere is based on the meridional profile of the zonal winds (see Figure 3-29) and superimposed vortices. For this model we are considering just one vortex – the Great Red Spot (GRS). The wind velocities around the vortex are calculated based on the synthetic velocity field for GRS from “Potential Vorticity and Thickness Variations in the Flow around Jupiter Great Red Spot and White Oval BC” by Dowling and Ingersoll (Journal of Atmospheric Science, vol. 45, #8, 1988, p.1380).

The vertical variations of the winds are calculated based on the observations of the thermal wind shear. Thermal wind shear is anti-correlated with jets in the Jupiter atmosphere. The winds decay with height with the decay scale height h of the order of 2-3 scale heights. We assume that the

atmospheric scale height at 0.1 bar (day flight altitude) and at 0.2 bar (night flight altitude) is the same and is $H \sim 20$ km. We also assume for simplicity that the decay scale height h is the same for all latitudes (for all jets). We assume $h=3$, because it corresponds to small observed change between those 2 pressure levels, and it also corresponds to du/dz at this levels 12 and 14 per scale height which is not far from measured $du/dz=30$.

The zonal wind and vortex winds are calculated at $p=0.6$ bar level and then recalculated for the 0.1 bar or 0.2 bar level.

4.4.3 Application Scenarios

Based on science and engineering objectives outlined in Section 4.3.1 we envision the following possible scenario.

4.4.3.1 Deployment of Dropsondes at three Locations

A DARE platform visits three locations - a belt (cyclonic band), a zone (anticyclonic band), and a large anticyclonic oval like the Great Red Spot, - to deploy dropsondes. These regions represent major types of the atmospheric flows at Jupiter and are visibly distinct from each other. This application would reveal if the differences exist in radiative, dynamic and compositional environments at these sites.

To analyze this scenario we simulate DARE trajectories in the atmosphere of Jupiter and test the feasibility of maneuvering the DARE platform to these regions

4.4.4 Trajectories

The figures below show examples of the DARE platform trajectories at Jupiter in support of the application described in Section 4.4.3. The balloon is as described in Table 3-9; the control velocity is 0.9 m/s. The trajectories shown are for a 100-day simulation of the balloon at 0.1 bar pressure level. In reality, the balloon would oscillate between the 0.1 and 0.2 bar levels and experience different zonal winds at these pressure levels. Taking into account this complex behavior requires a more complex trajectory simulation model. Such a model can be developed in the Phase II of the study. Comparison of the simulations for constant 0.1 bar and 0.2 bar pressure level floating altitude show qualitative similarity. Thus, analysis of the trajectories at the constant pressure level is adequate for the initial assessment of the DARE capabilities at Jupiter.

We also assume that the vertical wind shear is constant everywhere, while observations suggest that it varies across the planet (see Figure 3-29). A more detailed model of the atmosphere that addresses this observation can be developed in Phase II.

Figure 4-13 shows the DARE platform trajectory plotted on the image of the disc of Jupiter for context. The goal of the simulation was to attempt and observe large parts of the neighboring belt and zone. In this simulation the TCS directs the DARE balloon towards the Great Red Spot (GRS) in an attempt to use strong winds inside the GRS to significantly change the balloon trajectory. The meridional winds inside the GRS are much stronger (100 m/s) than the velocity provided by the TCS, thus, if the balloon can enter the northward or southward branch of the

GRS and quickly exit it, the traveled latitudinal distance can be much greater than without the GRS assistance.

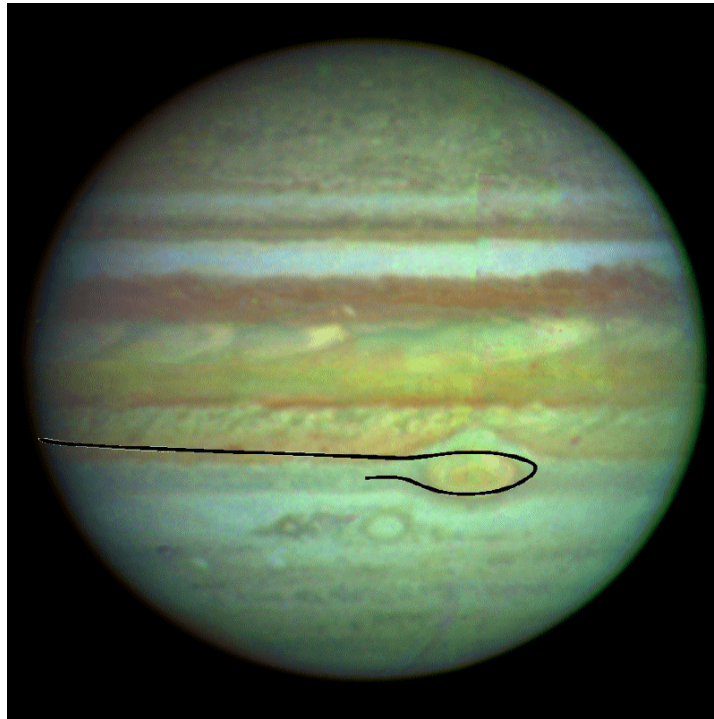


Figure 4-13 DARE trajectories at Jupiter

The balloon on Figure 4-13 is started to the west from the GRS and is pushed by the TCS northward. The atmospheric winds carry the balloon eastward, then around the GRS and then westward. The total traveled latitudinal distance is about 8° . The DARE balloon is able to travel from about middle of the zone to the middle of the belt, thus accomplishing the simulation objective.

The starting latitude to perform the “GRS maneuver” has to be chosen quite carefully. If the balloon was started several degrees further south from the shown location it would just “graze” the GRS and continue to travel eastward. If the balloon was started several degrees further north, it would get trapped in the GRS winds for longer period of time, so that the traveled latitudinal distance would be smaller.

It is possible to cross from the belt into a zone (or visa versa) using the TCS without the assistance of the GRS, but the traveled latitudinal distance would be smaller (by about 25%). The latitudinal distance traveled with the assistance of the GRS would be greater with more efficient TCS.

Figure 4-14 shows the trajectory of the DARE balloon spiraling into the GRS. The horizontal axis here is longitude; the vertical axis is latitude. The TCS pushes the balloon towards the center of the GRS. The balloon is able to reach the center of the GRS after about 4 revolutions around the GRS. The DARE balloon deploys probes in the process, thus sampling different regions of the GRS.

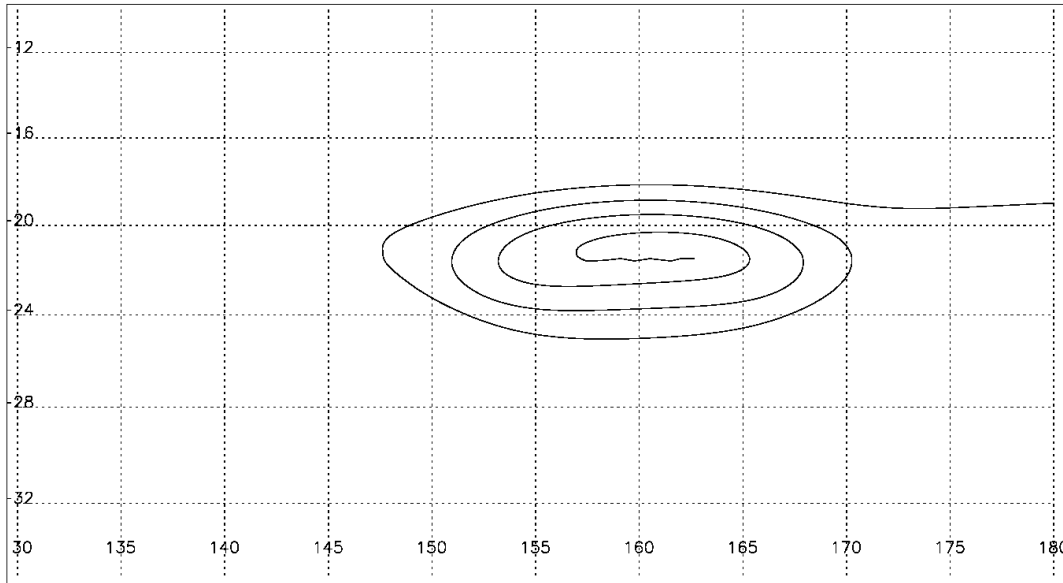


Figure 4-14 DARE trajectory spiraling into GRS

Figure 4-15 shows the trajectory shown on Figure 4-14 in the context of the Jupiter disc.

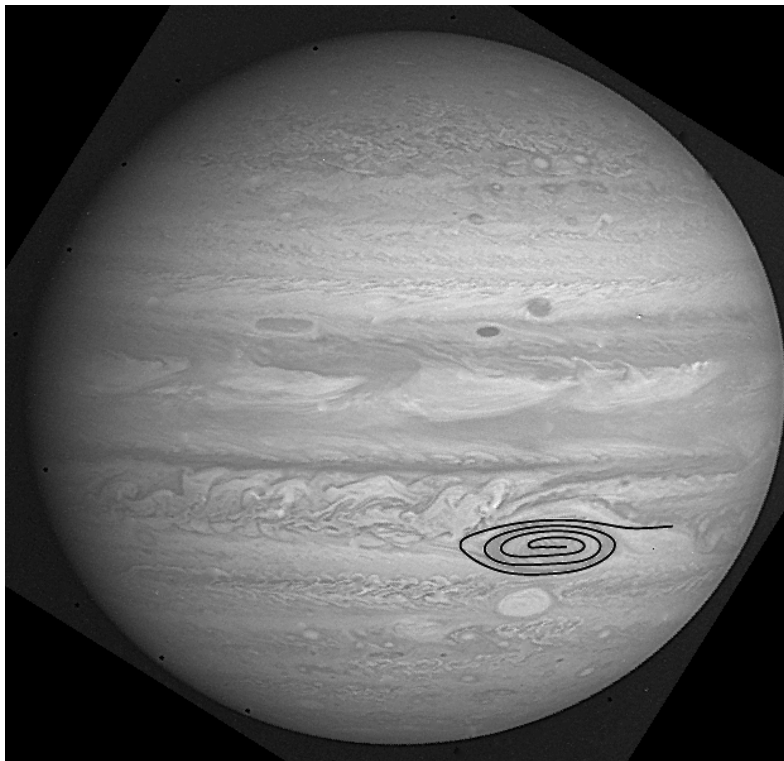


Figure 4-15 DARE spiraling into GRS plotted on the Jupiter disc

This analysis shows that controlled balloon on Jupiter can sample a belt and a zone or the interior of the GRS during a 100-day mission. However, the required TCS is relatively large – with the estimated wing mass of 50 kg and wing area of 10 m².

4.5 Mars

4.5.1 Science Requirements and Priorities

The objectives and measurements are:

- High-resolution (20 cm/pixel) imaging of future landing sites.
- Measurements of crustal magnetic field anomalies.
- Measurements of seismic waves as a way to probe the planet interior.
- Measure longitudinal distribution of atmospheric constituents (H₂O, O₃, dust) and properties to differentiate the relative importance of the HO_x and dust cycles and to determine the chemical processes that maintain stability of the CO₂ atmosphere.
- Determine the seasonal variation of Martian surface winds. At least 15 to 20 stations are required to simultaneously sample equatorial, mid, and polar latitudes over a range of longitudes, with some coverage of altitude.
- Measure the isotopic ratios of the reactive elements H, C, N, and O and of the noble gases to a minimum accuracy of 10% in the atmosphere to enable meaningful comparisons with elemental compositions observed in the Sun, in meteorites, and in other planets. In the case of ¹³C/¹²C, ¹⁸O/¹⁶O, ¹⁵N/¹⁴N, and D/H-ratios for isotopes in the major molecular species-the requirement increases to an accuracy of 1%.
- Study the episodic nature of martian dust storms. Monitor the global circulation of Mars for at least a full martian year at a horizontal resolution greater than 10% of the planetary radius and with vertical resolution of a pressure- scale height or better.
- *In situ* surface heat flow measurements.
- Elemental and mineral composition of the crust, determination of absolute ages, isotopic measurements. Surface materials that are important targets for analysis include the soil (with depth profiles), volcanic rocks, impact ejecta, and the polar ices. Sampling of identifiable stratigraphic units.
- Search for volatiles and monitoring of the volatiles cycling between atmosphere and surface.
- Measure the microphysical and chemical structure of the laminated terrains and/or permanent caps of the Polar Regions to a depth of at least 1 m.

4.5.2 Model Atmosphere

Even though simplified models of Martian general circulation were developed before, we chose to use the available Mars GCM (MGCM) data for balloon trajectory analysis. There are several reasons for doing so. First, previously developed simplified models (like the truncated spectral models by Haberle *et al.* 1997, Moriyama and Iwashima 1980) are not simple enough to permit quick incorporation into the available trajectory simulation code within the time and funding limits of the Phase I study. Other models are zonally symmetric (like Haberle *et al.* 1982,

Murphy *et al.* 1993, Pankine and Ingersoll, 2002) and don't resolve atmospheric vortices explicitly. Large-scale vortices that can significantly affect balloon trajectories are observed in the Martian atmosphere and in the GCMs. Thus we chose to use the available Mars GCM data for trajectory simulations.

The MGCM data available to us constitute the Run 98.04 of the MGCM with the pre-MOLA topography. The data consist of a series of data files that span one Martian year. This is sufficient to study seasonal variations of balloon trajectories. Examples of the data are shown in Section 3.3.7.1.

4.5.3 Application Scenarios

Based on science and engineering objectives outlined in Section 4.5.1 the application scenarios for Mars are essentially the same as for Venus, except that a volcanic activity monitoring scenario is not applicable. In addition, there is the dust storm monitoring application.

4.5.3.1 Monitoring Dust Storm Activity

DARE platform monitors regions of known dust storm activity (edges of the polar caps in spring, southern hemisphere). Dust storms on Mars extend upward to altitudes of 50 km. Thus, the DARE platform observing the storm from above would be in the storm. This may present an opportunity to sample the Martian dust *in situ* without deploying a surface probe. At the initial stage of the storm development DARE platform can provide high-resolution visible and thermal imaging of the core of the storm providing insight into the storm genesis.

4.5.4 Trajectories

Here we present the results of the numerical simulations of the uncontrolled and controlled balloon trajectories on Mars. The trajectory analysis here is based on the MABS-MGA-like balloon. The balloon would float at the density level of about 0.008 kg/m^3 . The pressure level of the floating altitude is between 2.4 and 3.4 mbars. The altitude of the balloon system above the surface would vary depending on geography and season from 6 km (summer over Southern highlands) to 12 km (winter over Northern lowlands).

The cross-track velocity due to TCS is constant during the simulation. The values for the cross-track velocity are chosen based on the analysis of Section 3.3.7.3. A more sophisticated approach would consider the variation of the relative winds at the wing altitude and calculate the cross-track velocity "on-line". Such an approach can be developed in Phase II of the study.

Figure 4-16 compares trajectories of the free-floating balloon and the controlled balloon. The plot shows trajectories plotted over MOLA topography image of Mars for reference.

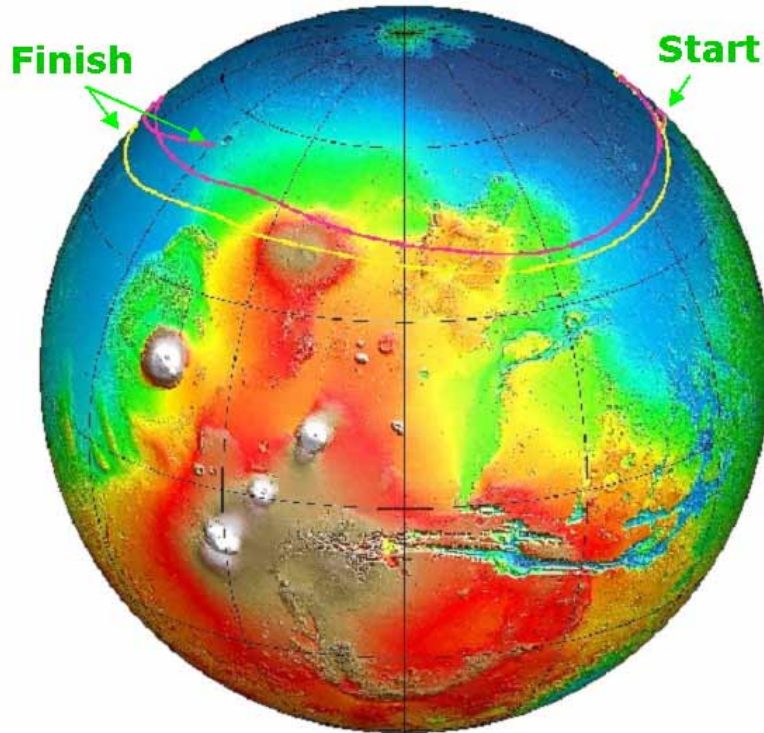


Figure 4-16 Comparison of 5-day trajectories of the free-floating and controlled balloon on Mars.

The simulation starts at $L_s=270^\circ$ at 45° N latitude and 180° E longitude and continues for 5-days. The winds for this period are shown on Figure 3-33 and Figure 3-34. The yellow trajectory marks the path of the free-floating balloon, and the purple trajectory marks the path of the controlled balloon. Available cross-track velocity for the controlled balloon is 1 m/s. The controlled balloon is pushed north.

This simulation shows that trajectory control can significantly modify balloon trajectories on Mars over a 5-day period. Over longer periods of time (90 days) the difference between the controlled and uncontrolled trajectories is less pronounced due to the strong winds in the Polar Region at this season.

Figure 4-17 and Figure 4-18 show the trajectories of the free-floating and controlled balloon, respectively, in southern hemisphere at $L_s=0^\circ$. This season corresponds to vernal equinox (spring in Northern hemisphere). Moderate atmospheric winds are present in both hemispheres similar to the situation during northern spring shown on Figure 3-36. The goal of the simulation is to see how well the balloon can be controlled in the moderate spring/autumn winds in Polar Regions.

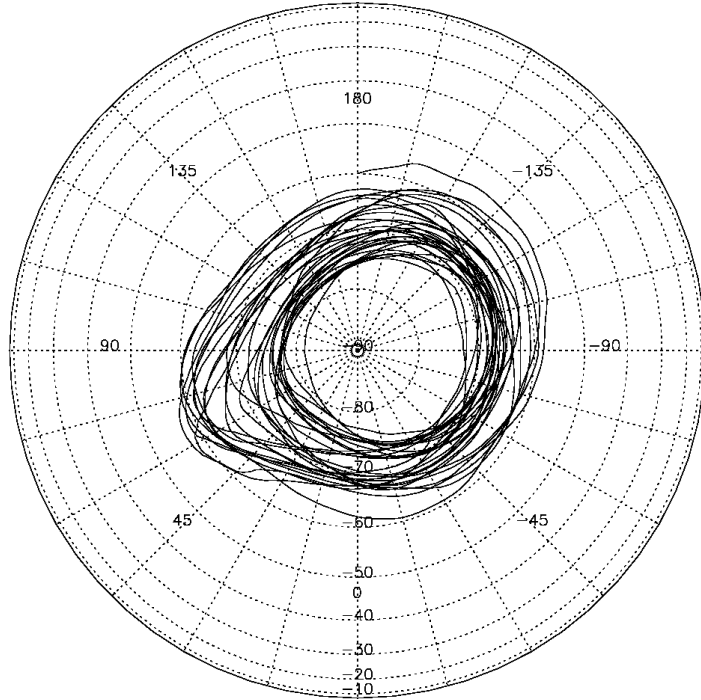


Figure 4-17 Mars free-floating balloon in southern hemisphere, $L_s=0^\circ$

Figure 4-17 shows the satellite projection centered on the South Pole of the free-floating balloon trajectory. The simulation is started at 60° S latitude and 180° E longitude and continues for 90 days. The balloon covers the region between 60° to 80° S during the simulation.

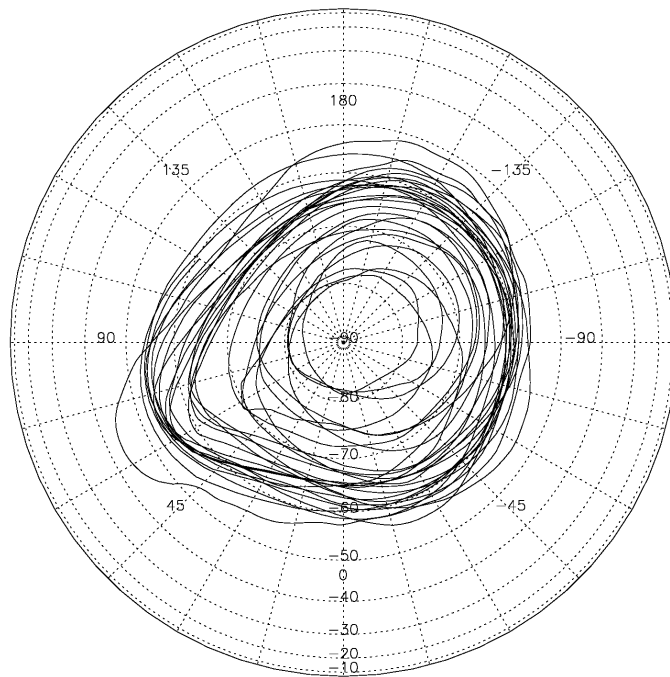


Figure 4-18 Mars DARE balloon in southern hemisphere, $L_s=0^\circ$

Figure 4-18 shows the trajectory of the controlled DARE balloon. The control velocity is 0.5 m/s. The control objective here is to keep the balloon floating along the 60° S latitude. As can be seen from the figure the TCS is unable to keep the balloon at the desired latitude all the time. However, the subsequent loops of trajectory are more “spread out” than the loops of the trajectory of the free-floating balloon. A detailed look at the coverage shows that there are significant statistical differences between the two trajectories.

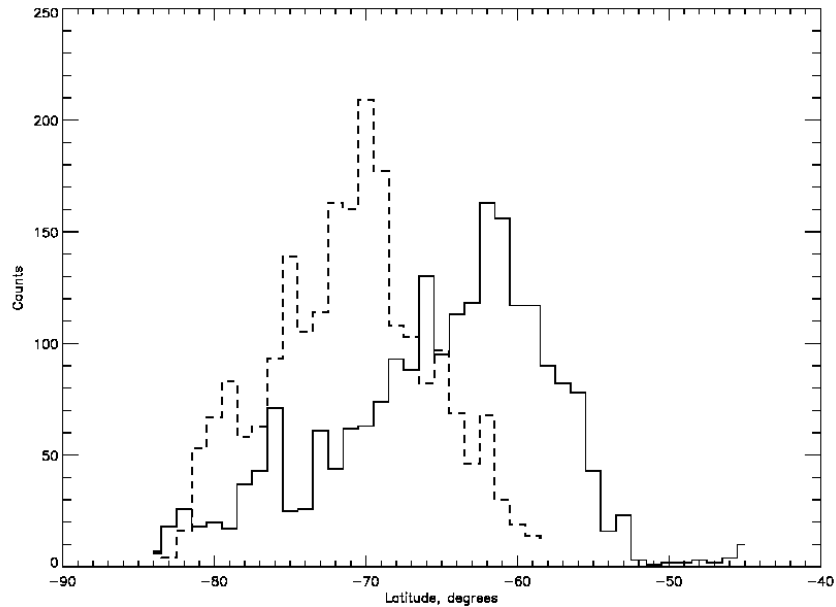


Figure 4-19 Histogram of the Mars balloon locations

Figure 4-19 shows the histogram of the latitudinal locations for the two trajectories. The horizontal axis is latitude, the vertical axis indicates how many times the balloon was seen within a latitudinal band. Solid line is for the controlled balloon and the dashed line is for the free-floating balloon. As can be seen from the figure the controlled balloon spends much more time in the vicinity of the 60° S latitude than the free-floating balloon. As a result, the controlled balloon provides more latitudinal coverage – from 53° to 85° S, than the free-floating balloon – from 50° to 85°. The uncontrolled balloon spends more time in the vicinity of 70° S.

This analysis can be used to design trajectories for observation of crustal magnetic anomalies in the southern hemisphere.

Similar analysis for the summer season in the Northern hemisphere is shown on Figure 4-20 and Figure 4-21. The projection is the same as on Figure 4-17 and Figure 4-18 but it is centered on the North Pole. The goal here is to see how well the balloon can be controlled in relatively weak summer winds in Polar Regions.

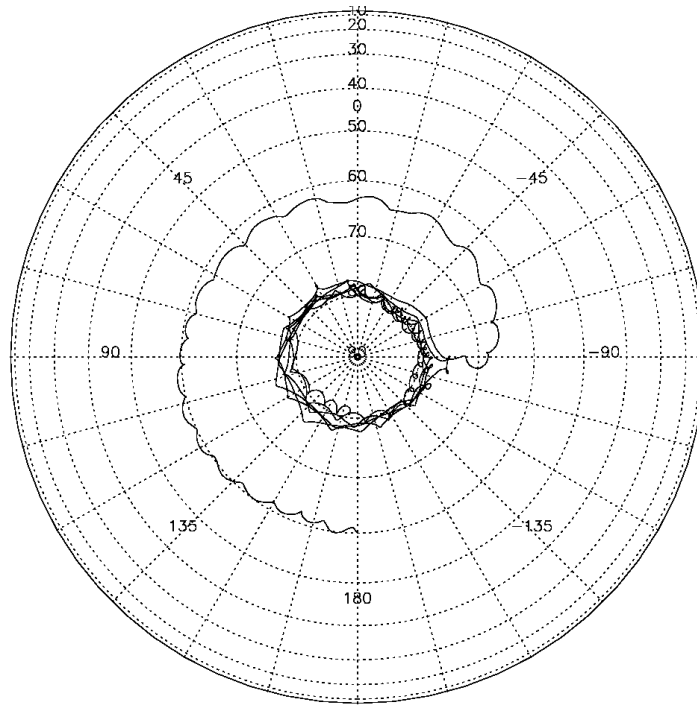


Figure 4-20 Mars free-floating balloon in Northern Hemisphere, Ls=90°

Figure 4-20 shows the trajectory of the free-floating balloon. The balloon slowly drifts along the starting latitude of 60° N at the beginning of the simulation, but then drifts north to the 80° N latitudes and stays there for the rest of the simulation.

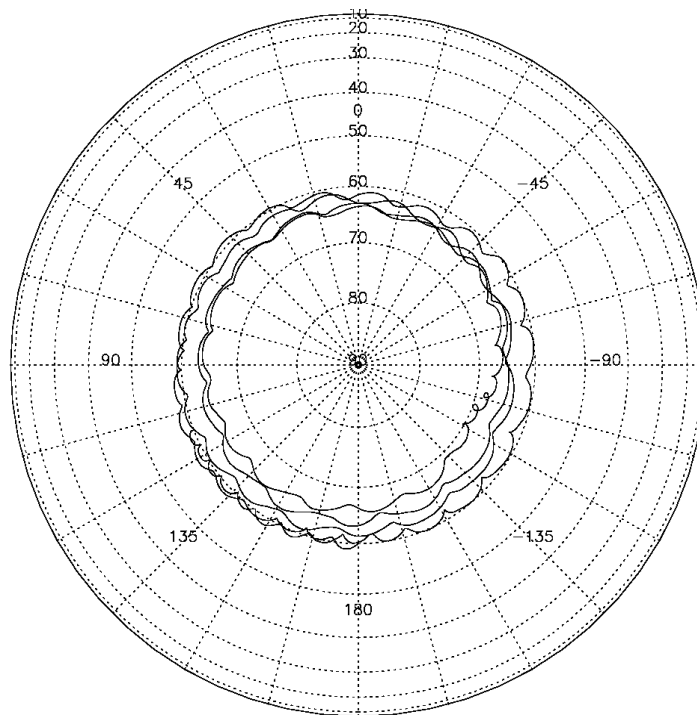


Figure 4-21 Mars DARE balloon in Northern Hemisphere, Ls=90°

Figure 4-21 shows the trajectory of the controlled balloon. The control velocity is 0.1 m/s, corresponding to the weak vertical wind gradient at this location. The control objective is to keep the balloon at 60° N. As can be seen from the figure, the control is quite efficient – the balloon remains within the 60° – 70° N corridor during the 90-day simulation, but spends a lot of time in the vicinity of the 60° N.

Simulations of balloon trajectories initiated closer to the equatorial regions indicate that TC available with the small 1 m² wing is not sufficient to effectively maneuver the balloon and avoid topography. Most of the time the balloons crash into the Tharsis bulge. Only on one occasion were we able to successfully maneuver the balloon from the southern to northern hemisphere. The result of this simulation is shown on Figure 4-22.

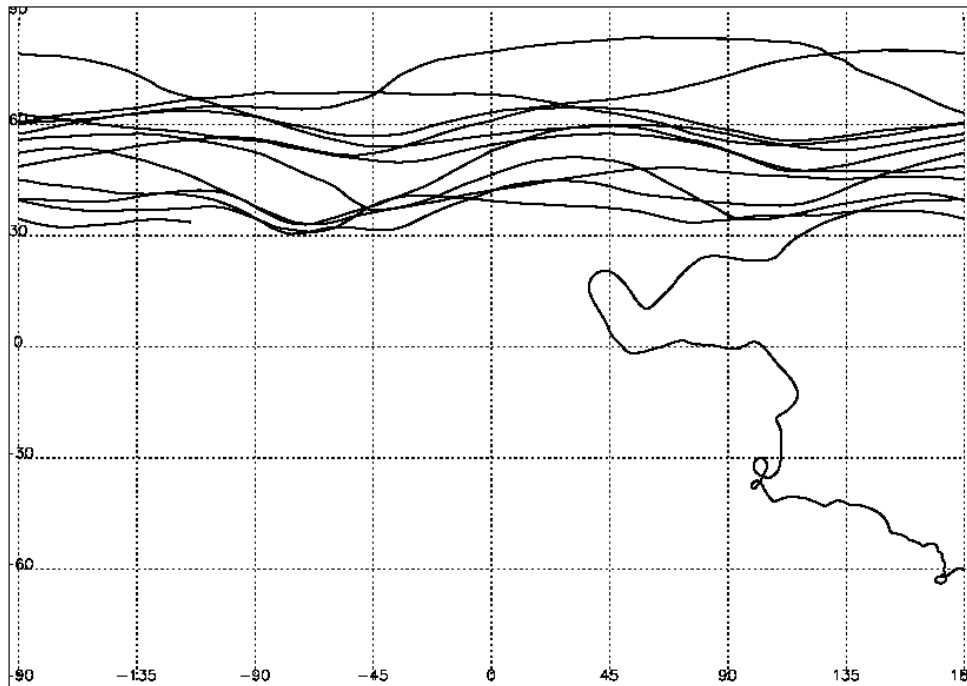


Figure 4-22 Mars DARE cross equatorial trajectory

Figure 4-22 shows the trajectory of the controlled balloon crossing from the southern hemisphere into the northern hemisphere. The control velocity is 1 m/s and the season is $L_s=255^\circ$, corresponding to late spring in the southern hemisphere. The balloon attempts to reach latitude of 80° N and then return back into the southern hemisphere. The balloon is able to avoid crashing into the elevated Tharsis region by crossing the equatorial region before it gets pulled into the zonal equatorial flow. However, it is not clear how robust this trajectory is, in other words, how the change in starting date and location would affect it.

This analysis shows that the TCS can significantly affect the balloon trajectories on Mars, especially in relatively calm summer season winds. However, it is not yet clear if the science objectives can be accomplished with the considered TCS. A larger system may be needed to achieve targeting and expand coverage.

4.6 Venus is chosen for design analysis

We came to the conclusion that Venus is the most promising planet for the application of the DARE planetary exploration architecture in the near term. The reasons for this are:

a) Most of the science objectives identified for Venus can be accomplished with DARE architecture.

DARE platforms are very well suited for the atmospheric studies, because they can be navigated throughout the atmosphere. Analysis in this study relied on the assumption (supported by available observations) that meridional circulation on Venus is dominated by thermal tidal winds. If Hadley circulation dominates the meridional component of the circulation at cloud tops (55-60 km) the platforms would need to be placed lower in the atmosphere, at the level between the upper poleward (at 50-60 km) and lower equatorward (at 20-25 km) branches of the hypothetical Hadley cell, where Hadley cell winds would be much weaker (less than 0.1 m/s at 40 km). Meridional winds at this altitude (40 km) may be dominated by waves with amplitudes of the order of 2-4 m/s (see Figure 3-14). The platforms would face challenging thermal and corrosive chemical environments at this altitude. Another solution would be to control platform's altitude, rather than sideways velocity. By switching between the poleward and equatorward branches of the Hadley cell it would be possible to control platform velocity in meridional direction to some extent.

The atmosphere can be sampled by repositioning DARE platforms geographically and either deploying dropsondes or changing platform's altitude. Altitude changing techniques based on the use of the phase changing fluids and small internal balloons were studied before and shown to be feasible. Altitude changing balloons have the advantage of not being limited by the number of dropsondes they can carry to do science. This advantage comes at a price of a much heavier system. The major deficiency of the approach is the fact that currently existing balloon materials cannot survive more than ten descents/ascents (even theoretically).

It does not seem to be feasible to do some surface science with deployable sondes, since surface measurements require spending significant time at the surface. Probes would be heavy because of the thermal protection, which prohibits carrying many of them on a balloon. Heavy seismological or surface thermal flux measuring stations can be deployed independently and DARE platforms used to overfly them and relay data to Earth or an orbiter.

There are, however, approaches that may allow surface chemistry, mineralogy and other experiments with balloon platforms. One approach is to deploy a small sonde that would grab surface material and then ascend to the altitude of the main platform to deposit the material into flying laboratory. The balloon laboratory can then analyze the sample for a longer period of time. Another approach is again to use an altitude-changing balloon descending periodically to the surface to get a sample of the surface and then ascend to higher (colder) altitudes to perform sample analysis.

From these considerations it seems that both approaches – balloon at constant altitude deploying sondes and altitude-changing balloon – need to be pursued as complimentary platforms.

b) Even though the trajectory control would be more efficient on Titan, Venus is much easier (and cheaper) to reach.

c) The recently published Solar System Exploration Survey (“New Frontier in the Solar System”, National Research Council, 2002) makes a detailed exploration and study of the composition of Venus’ atmosphere and surface, including sample return, a highest priority for inner planets. In fact, the Survey outlines a combined lander/balloon Venus mission – VISE (Venus In Situ Explorer) as the highest ranked mission for the Inner Planet exploration for the next decade. The DARE architecture for Venus atmosphere and surface exploration fits very well into Venus exploration strategy. The DARE Venus concept supports Venus exploration by developing new options for Venus balloon mobility, atmospheric and surface measurements, by developing concepts for Venus microprobes.

d) Mars has a very thin atmosphere, so that the DARE platforms would need to float in the atmosphere at low altitudes (6-12 km). At these altitudes the platforms will face challenges of avoiding topography and very turbulent atmosphere with dust devils extending up to 8 km high into the atmosphere. Future developments to reduce system mass and improve TCS performance will make Mars a more attractive DARE candidate.

e) Jupiter requires a very large balloon and a large wing for control. Even with a very large wing the control may not be sufficient to sample several zonal wind bands, as required by science objectives.

f) The only flights of the planetary balloon technology to date were the successful Venus Venera-Vega missions. The technologies developed for those missions can be leveraged for DARE architecture development.

5 Key Conceptual Design Requirements

This section contains a brief description of the preliminary design and technology requirements for the DARE planetary exploration architecture. The conceptual design requirements are levied on the design of the operational system. This section serves to provide conceptual design requirements for use in the preliminary design phase of Phase 1 of the NIAC DARE study. A revised version of this section, taking benefit of the understanding of user requirements and the conceptual design details developed during Phase I, will be developed during the Phase II effort.

5.1 Performance Requirements

Preliminary requirements on the various components of the VENUS DARE architecture are delineated below. Where a “TBD” is used, estimated requirements are shown in brackets “[estimated]”.

5.1.1 Flight duration

DARE shall be able to operate in planetary atmosphere for the duration sufficient to achieve science objectives.

5.1.2 Flight altitude

Balloon altitude must be consistent with the gondola’s and dropsondes’ thermal design and balloon material structural strength.

5.1.3 Suspended mass

Buoyancy system must provide lift for a TBD [100 kg] payload of dropsondes, and TBD [40 kg] mass of the gondola and TCS.

5.1.4 TCS Tether

The tether of the TCS shall be capable of surviving for the duration of the mission TBD [100 days] in harsh environments (Venus clouds).

5.1.5 Trajectory control capabilities

The TCS shall be capable to provide sufficient trajectory control to achieve the objectives.

5.1.6 Materials longevity

Balloon material, the TCS and TCS tether must survive in the Venus clouds.

5.1.7 Balloon envelope stress

Balloon must accommodate altitude changes due to dropsonde release and gas leaks.

5.1.8 Communications

The DARE platform shall be capable to maintain radio contact with the deployed probes over line-of-sight.

5.1.9 Data storage

DARE platform shall be capable to store the science and engineering data until an opportunity to upload it to Earth or to the orbiter arises.

5.1.10 Power generation and storage

DARE platform shall have means to generate and/or store energy to support engineering and science activities on board for the duration of the mission.

5.1.11 Navigation

DARE platform shall be able to operate (and navigate) autonomously.

5.1.12 Dropsonde measurements

Dropsonde instruments must be able to measure pressure, temperature, and radiative fields with the required accuracy.

5.1.13 Dropsonde lifetime

Dropsonde instruments must perform for the whole duration of the dropsonde descent.

5.1.14 Dropsonde power

Dropsonde instruments must be power efficient to allow for small dropsonde battery.

5.2 Technology Requirements

5.2.1 Balloon material

Lightweight and strong balloon material with small gas permeability and resistant to sulfuric acid needs to be developed

5.2.2 Dropsonde thermal control

Passive or active lightweight thermal control for dropsondes needs to be developed.

5.2.3 Deployable instruments

Lightweight dropsondes for surface chemistry/mineralogy analysis need to be developed.

5.2.4 High temperature electronics

High temperature electronics allowing operation of instruments in the deeper and hotter regions of the Venus atmosphere needs to be developed.

5.2.5 Balloon thermal control

Balloon thermal control systems and models need to be developed to assure stable and reliable balloon operation.

5.2.6 Power storage

Lightweight high capacity batteries for dropsonde and gondola systems need to be developed.

5.2.7 Lightweight inflation systems

Lightweight inflation systems need to be developed to reduce the weight of the spacecraft.

5.2.8 Venus Balloon TCS

Venus Balloon TCS needs to be developed to provide the TC capabilities at Venus.

6 VENUS DARE Conceptual Architecture Design Description

6.1 Introduction

We developed a preliminary concept for a Venus DARE mission. The objective of the mission is to obtain profiles of atmospheric properties (pressure, temperature, winds, etc.) from top of the clouds level to the surface at multiple locations. These measurements would allow comprehensive understanding of the dynamics of the Venus atmosphere and pave the way for future Venus exploration with balloons. DARE platforms are well suited for this mission since they can carry multiple meteorological dropsondes and can be repositioned in the atmosphere. Long mission duration allows sampling at different solar times. We envision a DARE platform floating in the atmosphere of Venus at 54 km altitude for 100-days. The DARE platform would carry multiple (100), small (less than 1 kg) dropsondes that would be deployed throughout the atmosphere to provide atmospheric profiles at different latitudes, longitudes and times of day. The DARE platform can also carry fixed instrumentation on the gondola for other experiments. The DARE platform would be maneuvered to provide measurements at multiple latitudes across the planet and at the day and night sides. TC resulting in the trajectory shown on Figure 4-5 can be used. The design of the mission is loosely based on the Venus Discovery mission. (Venus Discovery mission envisioned 3 balloon probes delivered to Venus by a single spacecraft. Each balloon was a 5.6 m diameter helium superpressure balloon. Each balloon carried a 34 kg gondola that had 4 dropsondes weighing 2.5 kg each. The total floating mass of each system was about 69 kg. The floating altitude was 57 km.) Dropsondes would transmit data to the gondola on descent after which data would be later relayed directly to Earth. The horizontal atmospheric winds throughout the atmosphere would be determined from Doppler measurements of the probe signal received at the gondola and on Earth by the Deep Space Network (DSN) using the techniques of the Very Large Base Interferometry (VLBI). Horizontal winds at the float level would be determined from the DARE platform tracking by DSN.

6.2 Conceptual Architecture Description

6.2.1 DARE Venus System Parameters and Components

We have started work on DARE conceptual design. We base our design on the Venus Discovery design. DARE design requires a larger balloon than Venus Discovery design because of the much heavier payload and the inclusion of the TCS system (total estimated payload 134 kg compared to 34 kg for Venus Discovery). The Venus DARE design also requires provisions for dropsonde and TCS storage and deployment mechanisms.

We have made a preliminary estimate of the DARE system parameters for an initial 54 km flight altitude:

Table 6-1 Preliminary DARE system parameters

T_{gas}	300 K
P_{gas}	51000 Pa
ρ_{gas}	0.08179 kg/m ³
ρ_{atm}	0.89964 kg/m ³
m_{gas}	18.855 kg
m_{envelope}	54.547 kg
m_{tot}	207.401 kg
m_{dry}	188.547 kg
Diameter	7.6 m
Surface area	182 m ²

A 1 m² TCS wing on a 10 km tether would provide a cross-track control velocity in excess of 1 m/s for this system. A schematic view of the deployed DARE platform is shown in Figure 6-1

6.2.2 Balloon

The balloon would be a spherical superpressure balloon. The balloon material used for Venera-VEGA missions (i.e. Teflon fabric) seems to satisfy (according to preliminary analysis) the balloon system performance requirements. Other candidate materials with lower densities and higher strength can be studied in the future. The thickness of the VEGA envelope material may need to be increased in future (from 180 μm) to provide higher strength. This would increase the balloon envelope mass and overall system mass if the payload mass is held constant. Pumpkin shaped balloons can provide an alternative to an increase of the thickness of the balloon film.

The balloon will be coated with silverized Teflon to reduce the superpressure jump during the day. An overpressure check valve would be needed to relieve high superpressure during the day.

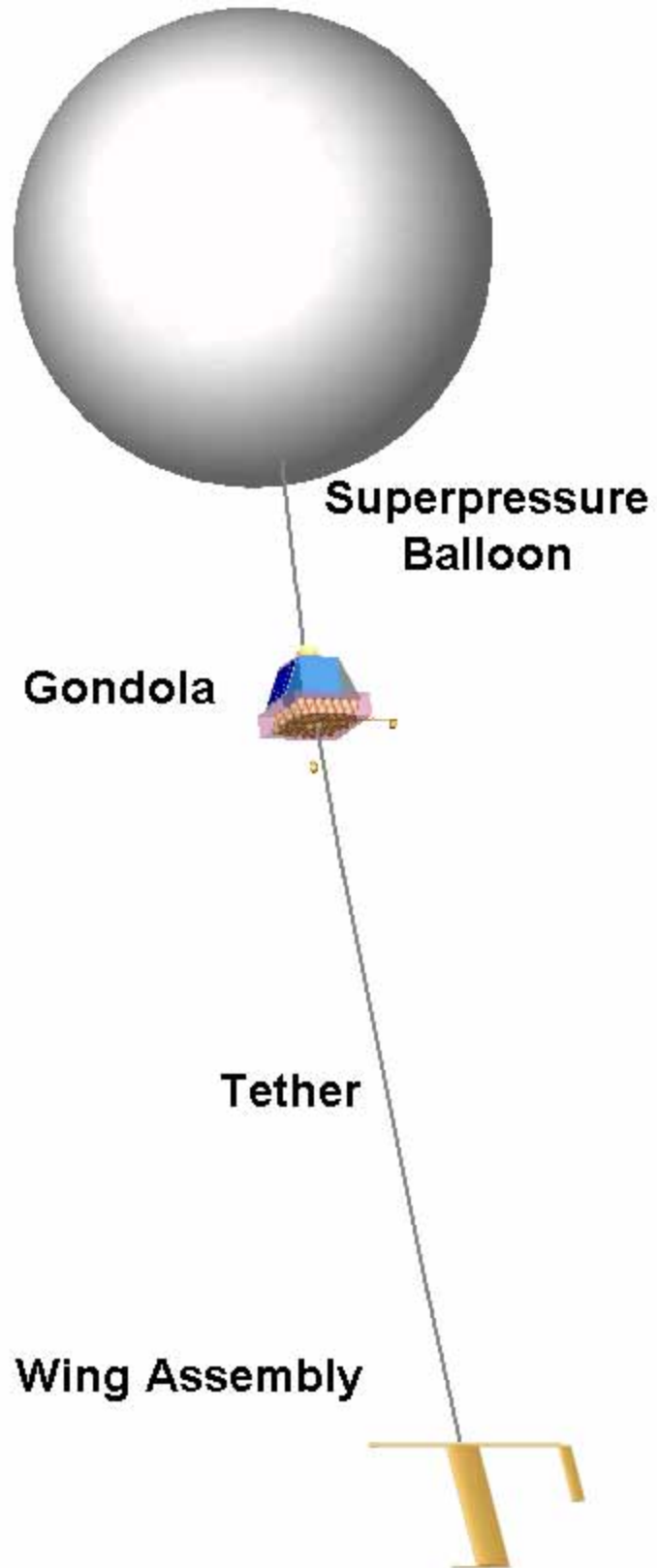


Figure 6-1 Conceptual drawing of the deployed VENUS DARE platform

6.2.3 Gondola

The gondola carries scientific and engineering equipment and the dropsonde magazine. The TCS is attached to the gondola via the 10 km long tether. Figure 6-2 shows the deployed gondola with one dropsonde being released and falling to the surface. The gondola carries scientific and engineering equipment.

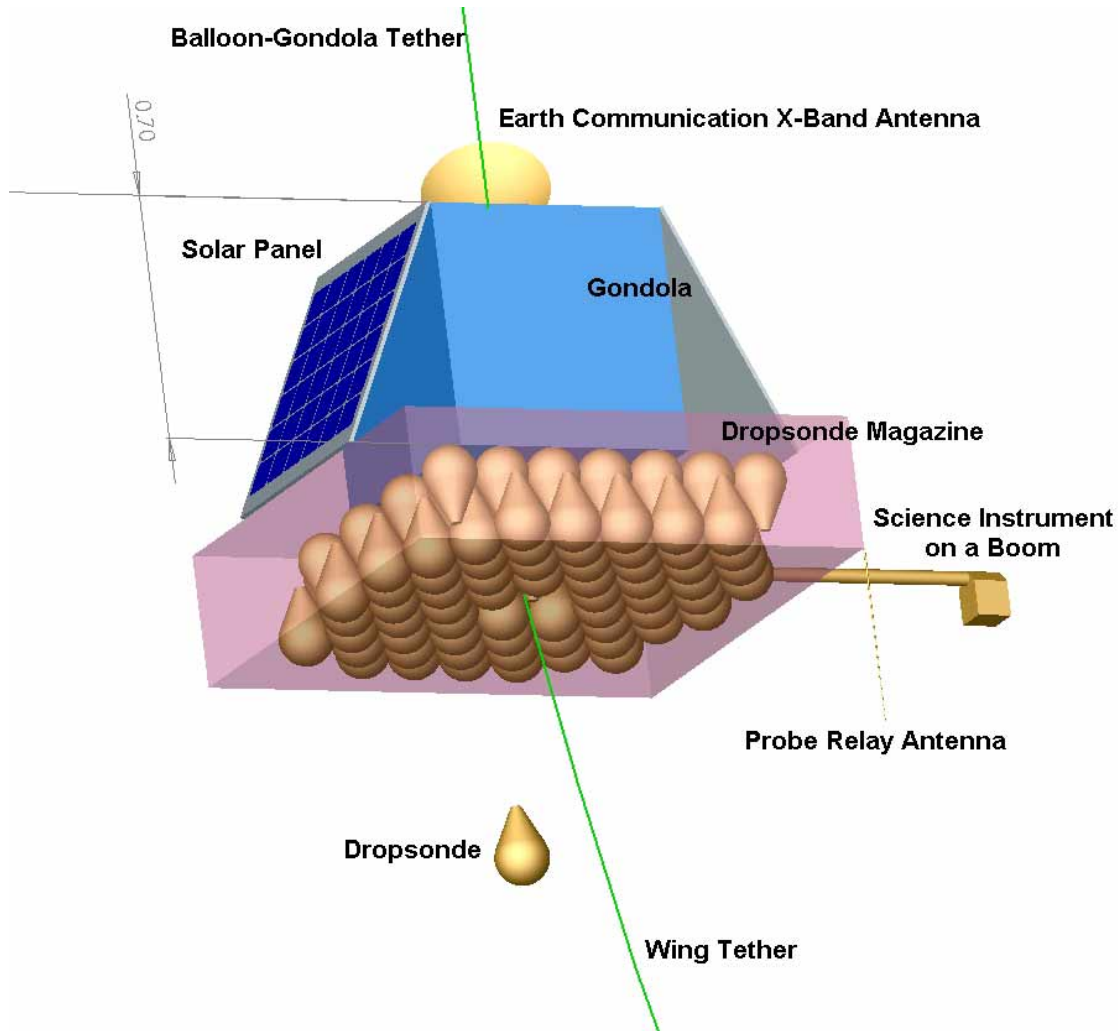


Figure 6-2 Conceptual drawing of the VENUS DARE gondola with dropsonde magazine

The gondola design is based on the design of the Venus Discovery gondola. The platform communicates with earth directly through the X-Band antenna, seen on Figure 6-2 at the top of the gondola. Two solar panels 0.5 m^2 each provide power for the payload. The gondola communicates with the deployed probes via the S-Band antenna seen at the bottom of the gondola.

The detailed mass and power analysis of the gondola components would be done in Phase II of the study.

6.2.4 Trajectory Control System

Figure 6-3 shows preliminary design of the TCS consisting of a wing, rudder and a boom. The TCS is attached to the gondola via 10 km tether.

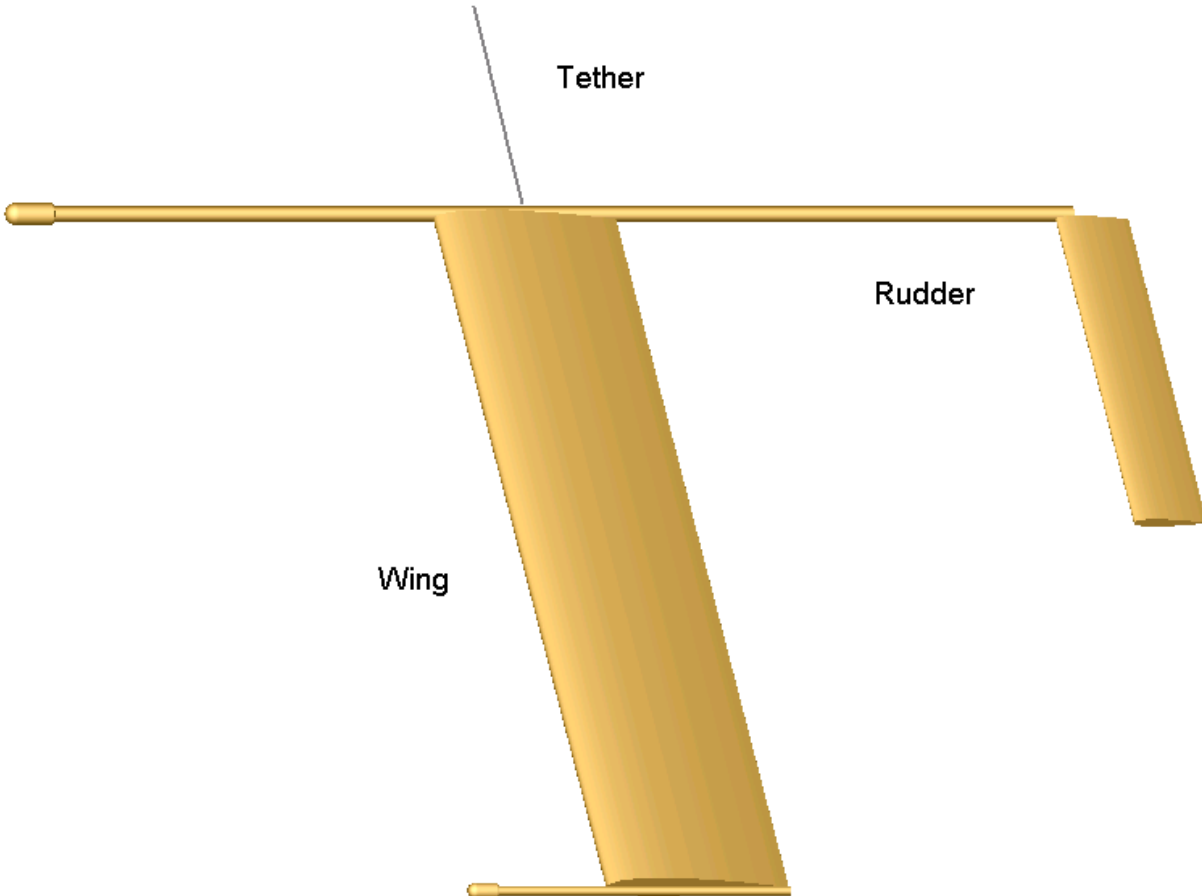


Figure 6-3 Conceptual drawing of the deployed VENUS DARE TCS

The wing on Figure 6-3 has area of 1 m². The lifting force is controlled via rudder. The commands to the TCS are sent from the gondola. The electronic equipment, possible meteorological sensors and motors can be placed inside the boom and the wing.

In developing the preliminary design for the TCS we relied on the design of the Earth StratoSail®. We used simplified geometrical scaling approach to arrive at the preliminary design. The optimum wing design requires development of complex scaling models that take into account the gravity of the planet, atmospheric density at the altitude of the operation, the stresses on the boom and the wing due to lift and drag forces, and other parameters. These more complex scaling relationships and optimal design would be considered in the Phase II of the effort.

Figure 6-4 illustrates how the TCS can be folded into a more compact shape for packaging into an aeroshell for interplanetary flight.



Figure 6-4 Potential TCS wing assembly foldings

The folded TCS wing assembly would be released and unfolded upon the completion of the balloon inflation process and upon reaching the floating altitude at the start of the mission. The falling wing assembly would pull out the tether through the opening in the dropsonde magazine from the package on the gondola.

6.2.5 Dropsonde

We base the dropsonde design on the Venus microprobes design study by R. Lorenz (R. D. Lorenz, “Design Considerations for Venus Microprobes”, *Journal of Spacecraft and Rockets*, v. 35(2), pp.228-230, 1998). Figure 6-5 schematically shows the Venus dropsonde.

Pressure, temperature and water humidity (COTS sensors discussed in Section 3.4.3.1 would be adequate over a useful altitude range) sensors would be carried, and simple photodiode-based up- and down-looking photometers would record the cloud opacity and short-wave radiation balance. These could be modestly augmented to spectrometers, perhaps combining detector electronics with a camera.

A possible low-resource but speculative payload element would be a magnetometer.

Some means of tracking the microprobe after its release from the balloon will be desired - exploiting Doppler tracking, ranging via a small transponder and/or radio direction finding.

Assuming 1-hour descent duration, the electrical power requirements are very modest. We will pessimistically assume a 10 W power requirement. The energy needs can be met with a 10 Whr battery - only 50 g assuming the typical 200 W-hr/kg specific energy of modern lithium sulfur-dioxide or lithium thionyl chloride batteries. Conservatively, we assume a mass of 100 g to take into account mounting hardware and capacity derating at higher temperatures.

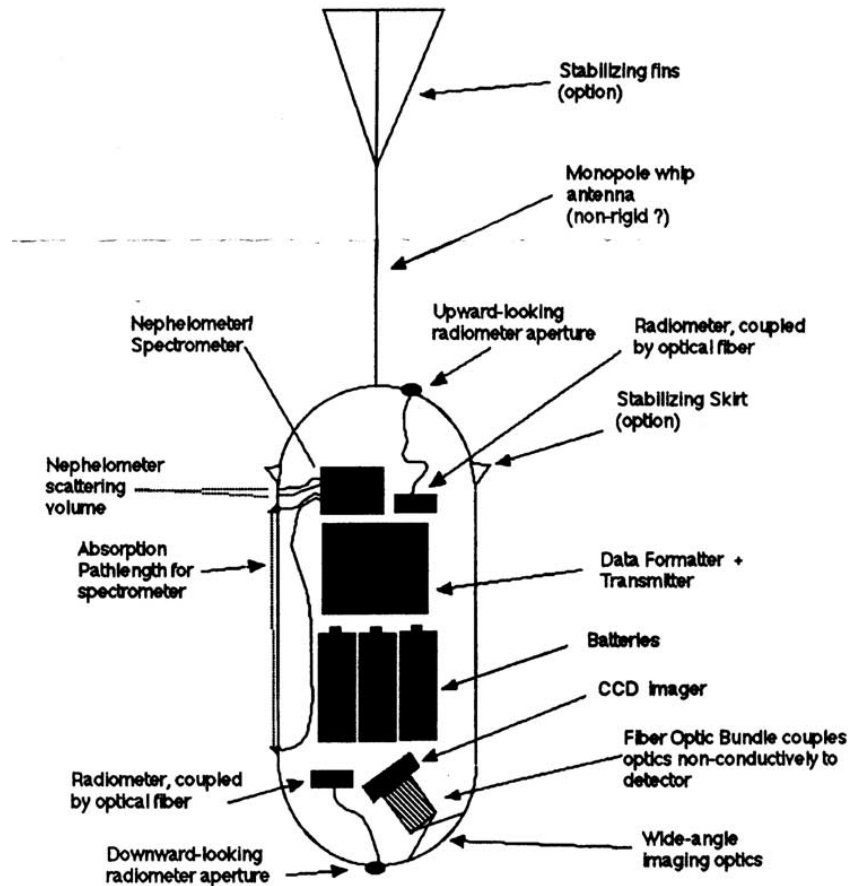


Figure 6-5 Conceptual drawing of the Venus dropsonde

The payload mass is very small - the pressure, temperature, humidity and light sensors trivially so, the camera probably only a few tens of grams depending on the mounting hardware and optics chosen.

The radio transmitter can be small - comparable with beacon transmitters or even cellphones (compare to the DS-2 Mars microprobe UHF radios, which were able to transmit 7 kbps with an RF output power of 300 mW)

A Mars microballoon study by Pioneer Aerospace (http://www.pioneerastro.com/Mmb/MMBP_Final_Report.doc) developed a prototype balloon payload with capabilities very similar to that of our microprobe (computer-controlled digital camera with radio telemetry) and using commercial-off-the-shelf components could achieve a mass of less than 600 g. It is likely that incorporating higher-integration techniques (e.g. flexible interconnects, surface mount components etc.) as employed in modern consumer electronics or the DS-2 probes would result in a substantial reduction.

Moroz (Moroz, I, "Estimates of visibility of the surface of Venus from descent probes and balloons", *Planetary and Space Science*, vol. 50, 287-297, 2002) suggests that a wavelength of 1.02 micron is most favorable for surface imaging of Venus, this wavelength lying between water absorption bands at 0.95 micron and 1.13 micron, while also being within the range of

silicon CCD cameras. He suggests that for additional surface information, the wavelengths 0.65 and 0.85 μm would be most appropriate, although the atmosphere is less transparent at these short wavelengths.

It should be noted that even at noon at the equator, about 10% of the upwelling flux from the surface at this wavelength is from thermal emission, rather than reflected sunlight.

Moroz computes a visibility factor (essentially a contrast ratio) as a function of altitude for the three wavelengths using Venera 14 data (a slightly more optimistic set of factors result from using Venera 13 data). The visibility factors at the 0.65, 0.85 and 1.02 μm are denoted as $V(0.65)$, $V(0.85)$ and $V(1.02)$ respectively in Table 6-2.

Table 6-2 Altitude visibility factor dependence

Height, km	Pressure, bar	$V(0.65)$	$V(0.85)$	$V(1.02)$
0	92	1.0	1.0	1.0
2	81	0.078	0.24	0.36
4	71	0.01	0.09	0.20
8	54	0.002	0.03	0.10

Note that visibility factors improve significantly over elevated topography (e.g. over a highland region, 6 km above the datum, $V(1.02)$ is >0.1 for altitudes 20 km above the ground. Also, contrast is improved (although signal is lower) for the nightside, where only thermal emission from the ground is seen.

Note that it may not be necessary to cool the entire camera for the entire descent - the principal requirement is to reduce the dark current during the exposure itself. One could imagine a Joule-Thomson or thermoelectric cooler operated only for a few seconds prior and during an exposure, while several minutes may elapse between exposures. The optimization of this strategy, and the attendant reliability implications, would require more detailed study.

A parametric study (Lorenz, 1998) determined that the performance of small balloon-dropped microprobes as in fact only weakly sensitive to shape - more slender (and thus faster-falling) probes had larger wetted areas and thus higher insulation mass requirements, such that spherical vehicles were in fact optimal. The vehicle mass is highly sensitive to the insulation performance (taking into account heat leaks through penetrations such as instrument ports).

Figure 6-6 shows a table with the calculated Venus dropsonde properties from Lorenz, 1998. The probe geometry is defined by a radius and a slenderness ratio r with the length/radius equal to $1+r$, i.e., a sphere has $r=1$.

Although the vehicle would be spherical in overall shape, maintaining a nominal orientation offers important advantages for telemetry performance (the balloon typically remains within the toroidal pattern of a monopole probe antenna) and for science data acquisition (e.g. downlooking camera, up- and down-looking photometers.) Thus some sort of stabilizing skirt or vanes would be used.

Table 1 Selected configuration cases

Case ^a	Payload mass, kg	Slenderness ratio	Vehicle radius, cm	Insulation thickness, mm	Ballistic coefficient, kg/m ²	Descent time, h	Internal temperature at impact, K	Vehicle mass, kg
A1	0.2	1	6.4	20	182	0.76	368	1.28
A2	0.2	3	5.5	18.5	293	0.57	362	1.56
A3	0.2	5	4.5	17	409	0.49	360	1.56
A4	0.2	10	3.7	15	655	0.39	361	1.69
A5	0.6	1	8.3	19	179	0.74	367	2.23
A6	0.6	3	6.3	16	304	0.56	373	2.27
A7	0.6	5	5.5	15	420	0.48	369	2.39
A8	0.6	10	4.6	14	689	0.38	362	2.75
A9	2.0	1	11.2	17	203	0.69	364	4.80
A10	2.0	3	8.5	15	356	0.52	362	4.86
A11	2.0	5	7.4	14	487	0.45	362	5.03
A12	2.0	10	6.0	12.5	771	0.38	364	5.32
B1	0.2	1	6.5	20	51	1.40	374	0.40
B3	0.2	5	4.4	16	118	0.93	368	0.44
B4	0.2	10	3.7	15	187	0.75	366	0.48
B5	0.6	1	7.7	13	371	1.19	371	0.79
B8	0.6	10	4.2	10	253	0.64	369	0.84
B9	2.0	1	10.2	7	111	0.94	367	2.18
B12	2.0	10	5.3	5	414	0.49	370	2.19
AP1	0.2	1	5.6	20	173	0.75	366	1.02
AP4	0.2	10	3.3	15	676	0.38	357	1.38
AP5	0.6	1	7.0	18	195	0.71	366	1.76
AP8	0.6	10	3.9	13	710	0.37	369	2.03
AP12	2.0	10	4.2	11	848	0.34	367	4.00
BP1	0.2	1	5.4	18	60	1.28	372	0.33
BP4	0.2	10	3.1	13	207	0.70	371	0.38
BP5	0.6	1	6.2	10	96	1.01	360	0.70
BP8	0.6	10	3.4	8	335	0.54	358	0.73
BP12	2.0	10	5.0	11	624	0.39	362	2.08
AG5	0.6	1	8.1	16	209	0.68	370	2.58
AG8	0.6	10	4.5	12	776	0.35	368	2.96
BG5	0.6	1	7.0	5	136	0.85	376	1.26
BG8	0.6	10	3.7	4	495	0.44	370	1.28
AL5	0.6	1	8.4	14	188	0.71	356	2.50
AL8	0.6	10	4.8	12	738	0.36	339	3.20
BL5	0.6	1	7.4	3	120	0.90	338	1.24
BL8	0.6	10	3.8	3	462	0.46	302	1.26

^aAx denotes polystyrene insulation, no phase-change material, and payload density of 560 kg/m³; Bx denotes advanced (Dewar) insulation, no phase-change material, and payload density of 560 kg/m³; APx, BPx are the same as Ax, Bx but with payload densities of 1000 kg/m³; ALx, BLx are the same as Ax, Bx but with lithium nitrate trihydrate equal to the payload mass added; AGx, BGx are the same as Ax, Bx but with gallium equal to the payload mass added.

Figure 6-6 Venus dropsonde parameters

That study found that a vehicle with a 0.6 kg payload would be able to reach the surface with an internal temperature of less than 373 K and could be constructed with a total (payload plus insulation) mass of 0.8 to 2.3 kg. This wide range depends on the insulation performance achievable (the high end corresponding to simple solid plastic, the low end assuming a Dewar with aerogel radiation blocking.) Note that for such a small vehicle, the instrument penetrations are likely to cause significant heat leaks - these, and the internal power dissipation, are likely to compromise the apparent gains from using high-performance insulation. A significant performance advantage derives from being able to package the payload at a high density (1000 kg/m³ vs. the 560 kg/m³ typical for many probes.) This should be readily achievable with a compact modern design.

Assuming a compact payload, Dewar insulation, and a spherical vehicle (configuration BP5 in Lorenz, 1998) gives a total probe mass of 0.8 kg, with a descent time of 1.19 hrs.

A more slender, rapidly descending, vehicle could be made with a modest (~10%) mass increase.

No advantage in using phase-change materials as internal heat sinks was apparent (although that result depends on the internal power dissipation).

(Note that this design does not assume a pressure vessel - the hot atmosphere is excluded by the elimination of any void space by potting compound, oil, or insulation).

7 Future Work

7.1 Introduction

Although we have achieved considerable progress in developing the DARE planetary exploration architecture, there is much additional work remaining to refine the capabilities and to define the optimum configuration of the architecture. Additional work is suggested in:

- 7.2 Study of DARE architecture performance advantages
- 7.3 Research and development of the trajectory control and observational techniques
- 7.4 Further development of the deployable microsondes concepts
- 7.5 Further development of the balloon concepts
- 7.6 Development of the DARE Architecture engineering and life cycle cost model
- 7.7 Identification and pursuit of pathways to DARE architecture development

7.2 DARE Architecture Performance Advantages

Some of the advantages of the DARE architecture were outlined in Phase I as the justification for the study. A more detailed and substantiated analysis is required to support the claims of advantageous performance. The detailed analysis would include the assessment of unique observations that can be performed with the DARE architecture and comparison with the observations that are possible from other platforms or with other means.

7.3 Trajectory Control and Observational Techniques

In Phase I a preliminary analysis of the trajectory control capabilities and possible observations was made. In Phase II this analysis would be further developed. The atmospheric models need to be refined to include realistic small-scale turbulence and medium and large-scale vorticity, possibly based on the GCM simulations. The Advanced TCS aerodynamics analysis needs to be developed. The TCS model needs to be fully incorporated into the trajectory simulation code to provide realistic changes in the control velocity consistent with the changing environment. Trajectory control techniques enabling targeting and desired coverage with specific science goals in mind need to be developed too. Innovative observational techniques need to be studied, including observations from multiple platforms, from balloon altitudes and from microprobes, and concerted observations from the balloon and the orbiter (a GPS-like atmospheric profiling), from the balloon and the microprobe(s), from the orbiter and the microprobe(s), together with the related issues of intercommunication, data handling, and navigation.

7.4 Deployable Microsondes Concepts

Development of concepts for deployable microprobes need to be continued, including atmospheric profilers, tethered probes, landers, rovers, penetrators, flyers, and floaters. Sample

return and in situ analysis capabilities need to be studied, as well as miniaturization and payload packaging approaches, and innovative data analysis techniques.

7.5 Balloon Concepts

The designs of the DARE architecture subsystems need further development and definition. During Phase I we developed preliminary conceptual designs for the Venus DARE components such as the balloon, the TCS, dropsonde and dropsonde magazine. Design and interface requirements for these and other systems need to be identified; also, computer-aided designs developed. Preliminary designs for DARE architecture on other planets need to be developed.

7.6 DARE Architecture Engineering Cost Analysis

The cost of the DARE architecture for different planets needs to be assessed. This analysis will highlight the costliest elements, subsystem and technologies and serve to identify technological requirements to enable the architecture.

7.7 Pathways to DARE Architecture Development

In the future, guided balloons will float by Olympus Mons sniffing for water and releasing sophisticated micro robots into vents on its volcanic flanks, photograph future human Mars landing sites, open the hostile surface of Venus to scientifically targeted surface and atmospheric measurements, explore the Red Spot of Jupiter, and search for biological precursors in the frigid atmosphere of Titan. The pathways to this future implementation of the DARE architecture and its potential impact on near-term planetary exploration should be explored with NASA robotic and human Mars program planners and managers. DARE systems can advance Mars exploration by exploring the surfaces of planets in enough detail to enable more ambitious and expensive robotic landing and rover missions leading to the return of samples or to the safe arrival of astronauts from Earth. DARE systems are probably essential to Venus surface sample return by targeting sample collection systems with the precision of a bombsight and then enabling atmospheric rendezvous of these samples with return vehicles. At Titan, DARE systems will offer a vantage point below the dense organic haze from which a survey of the detailed geology can be carried out. Jupiter's enormous Red Spot, banded zonal wind structure and the depth of the atmosphere below the clouds could be explored by DARE-deployed dropsondes to provide a snapshot of these features that would require a hundred Galileo probes to create with the conventional exploration architecture.

Pathways to DARE will include several steps including identification of technology development required to enable DARE systems including balloons qualified for flight in planetary atmospheres, miniaturized microprobes for planetary atmosphere surface and subsurface exploration, and lightweight, deployable trajectory control devices optimized to operate in a variety of planetary atmospheres.

Planetary scientists will need to be informed on the potential of DARE systems and encouraged to identify new scientific applications in order to broaden and deepen the interest and need for DARE technology development. This can be accomplished by presenting the DARE concept at

relevant science meetings where it will be of most interest, i.e., low-cost planetary mission, lunar and planetary and other science related conferences.

The potential contributions from the study of DARE architecture should be explored with NASA SSE and HEDS planners and program managers in order to make them aware of the benefits to their programs.

8 Summary

This report describes the work accomplished and results obtained during Phase I of the development of an innovative and new concept for Direct Aerial Robot Explorers in support of the NASA Institute for Advanced Concepts. During Phase I, we demonstrated feasibility of the new planetary exploration architecture that is designed to provide new capabilities in observing planetary atmospheres and surfaces. During Phase I, we achieved our objective by:

- Demonstrating the validity of the proposed system architecture for long-term exploration of planetary atmospheres and surfaces, which focuses on long-duration balloons low-energy trajectory control technology, and the use of small deployable probes.

Features of the new architecture include:

- Low-cost, low-energy, long-duration (100 days) autonomous balloon systems,
- Balloon trajectory control capability,
- Lightweight and efficient power generation and energy storage,
- Deployable micro sensors for *in situ* atmospheric profiling or surface exploration, and
- Communications relay orbiter.

There were four tasks during Phase I:

This new architecture provides a new vantage point for observations of the planetary atmospheres and surfaces; enables unique observations; supports objectives of the NASA SSE and HEDS Enterprises by enabling understanding of the formation and evolution of planetary bodies in the Solar System, by searching for life on other planets, by enabling investigation of the compositions and resources of the planetary bodies, by enabling new technical approaches and capabilities, by helping to create 21st century scientific and technical workforce (all SSE), and by enabling human exploration through cooperative robotic missions (HEDS).

- 1) Task 1 Develop Application Scenarios
- 2) Task 2 Define Preliminary System Requirements
- 3) Task 3 Conceptual System Architecture Design
- 4) Task 4 Planning and Reporting

During Phase I, we met 100% of the objectives by completing all the tasks. This document includes reports on the first four tasks. Its submission completes the fifth task.

9 Acronyms

ATCS	Advanced TCS
A_w	TCS Wing area
C_D	Aerodynamic drag coefficient
C_L	Aerodynamic lift coefficient
DARE	Direct Aerial Robot Explorer
HEDS	NASA Human Exploration and Development of Space Enterprise
HST	Hubble Space Telescope
IR	Infrared
L_s	Subsolar latitude
L_t	Tether length
MABS	Mars Aerobot/Balloon System
MAP	Mars Aerial Platform
MGA	Mars Geoscience Aerobot
MGCM	Mars General Circulation Model
MIP	Microprobe
MOLA	Mars Orbital Laser Altimeter
M_w	TCS Wing mass
PCF	Phase-change fluid
Re	Reynolds number
RTG	Radioisotope Thermoelectric Generator
SIRMA	Solar Infrared Montgolfier Balloon
SSE	NASA Space Science Enterprise
TC	Trajectory Control
TCS	Trajectory Control System
TWA	TCS Wing Assembly
VAMS	Venus Aerobot Multisonde
VEVA	Venus Exploration of Volcanoes and Atmospheres
VGCS	Venus Global Circulation Study
WISE	Venus In Situ Explorer
Z_B	Balloon altitude